

**CASE FILE**  
**COPY**

N 62 13877

NASA TN D-1019

NASA TN D-1019



**TECHNICAL NOTE**

D-1019

**GEOMAGNETIC- AND INTERPLANETARY-MAGNETIC-FIELD  
ENVIRONMENT OF AN EARTH SATELLITE**

By Edward W. Leyhe

Langley Research Center  
Langley Station, Hampton, Va.

**NATIONAL AERONAUTICS AND SPACE ADMINISTRATION**  
**WASHINGTON**

July 1962



## CONTENTS

	Page
SUMMARY . . . . .	1
INTRODUCTION . . . . .	1
SYMBOLS . . . . .	2
GENERAL DESCRIPTION . . . . .	7
MAGNETIC CLASSIFICATION . . . . .	11
THE EARTH'S MAIN MAGNETIC FIELD . . . . .	17
GEOMAGNETIC-FIELD VARIATIONS . . . . .	23
GEOMAGNETIC-FIELD FLUCTUATIONS . . . . .	27
CURRENT SYSTEMS . . . . .	29
CORRELATION WITH SOLAR ACTIVITY . . . . .	33
ROCKET AND SATELLITE MEASUREMENTS . . . . .	35
APPROXIMATIONS USED IN CALCULATING FIELD CHANGES IN PASSING THROUGH A CURRENT SYSTEM . . . . .	46
ALTITUDE EXTRAPOLATION OF MAGNETIC INTENSITY . . . . .	48
MAGNETOMETERS . . . . .	49
CONCLUDING REMARKS . . . . .	49
REFERENCES . . . . .	51
TABLES . . . . .	57
FIGURES . . . . .	74

1000 100 10 1

Figure 1. Schematic representation of the experimental design. The subjects were divided into two groups: the control group (CG) and the experimental group (EG). The CG was divided into two subgroups: the control group (CG) and the control group (CG). The EG was divided into two subgroups: the experimental group (EG) and the experimental group (EG). The CG was divided into two subgroups: the control group (CG) and the control group (CG). The EG was divided into two subgroups: the experimental group (EG) and the experimental group (EG).

NATIONAL AERONAUTICS AND SPACE ADMINISTRATION

---

TECHNICAL NOTE D-1019

---

GEOMAGNETIC- AND INTERPLANETARY-MAGNETIC-FIELD

ENVIRONMENT OF AN EARTH SATELLITE

By Edward W. Leyhe

SUMMARY

A general description of the geomagnetic field is presented to acquaint the reader with the various phases of this subject. This description consists of brief surveys of (1) the methods of classification of magnetic activity; (2) the earth's main magnetic field; (3) the solar, lunar, and disturbance variations in the geomagnetic field; (4) the short-period fluctuations and pulsations in the geomagnetic field; (5) the current systems responsible for these variations and fluctuations; and (6) the correlation of magnetic-field disturbances with solar activity.

Magnetic-field measurements obtained from recent rocket and satellite flights are presented and discussed. The measured magnetic field is compared with the theoretical field, evidence concerning current systems and magnetic storms at various altitudes is presented and discussed, the distant geomagnetic and interplanetary magnetic fields are examined, solar activity is correlated with interplanetary-magnetic-field disturbances, and the existence of a lunar magnetic field is investigated.

In addition, approximations used to calculate magnetic-field changes in passing through a current system are discussed together with altitude extrapolation of the magnetic-field intensity. A brief reference to magnetometers is included.

INTRODUCTION

The new frontier of space travel has tremendously broadened the concept of environment. One phenomenon of new-found importance is the geomagnetic field. The environmental effects of the geomagnetic field upon an earth satellite are both direct and indirect.

The geomagnetic field directly affects the drag, the direction of motion, and the attitude of a satellite. These effects are a consequence of the interaction of the geomagnetic field with the electric charge that accumulates on a satellite, with currents that are induced on a satellite by the geomagnetic field as a result of the motion of the satellite, and with currents that result from the operation of instruments, and so forth, within the satellite. These direct effects are small but may be significant for a satellite that is to be in orbit for an extensive period of time.

Indirectly, the geomagnetic field affects a satellite by its interaction with other environmental phenomena. Thus, the geomagnetic field determines the trajectories of cosmic rays and is the agent through which charged particles become trapped in orbits around the earth to form the Van Allen radiation belts. There is also a direct correlation between the geomagnetic field and auroras, ionic motions within the ionosphere, and radio-wave interference.

In addition, the geomagnetic field can be used to determine the spin rate and orientation of rockets and satellites by means of aspect magnetometers.

The primary purpose of this paper, therefore, is to present a brief description of the geomagnetic field for engineers and scientists with little or no previous knowledge of the subject who may be engaged in the design, operation, and utilization of earth satellites. As a result, the material presented herein is mainly concerned with the distributions in time and space and the magnitudes of the various constituent fields. Also, recent rocket and satellite data are discussed and evaluated.

## SYMBOLS

$A_k$	daily local equivalent amplitude
$A_n^m, B_n^m$	spherical harmonic coefficients
$A_n^m, B_n^m$	modified spherical harmonic coefficients
$A_p$	daily planetary equivalent amplitude
$a$	radius of current volume cylinder
$a_k$	3-hour local equivalent amplitude

$a_m, b_m$	Fourier coefficients
$a_p$	3-hour planetary equivalent amplitude
B	north magnetic pole
C	magnetic character figure
$C_1$	international magnetic character figure
$c_n^m, s_n^m$	numbers lying between zero and 1
D	disturbance magnetic field; also, magnetic declination
$D_1$	irregular disturbance variation
$D_m$	daily mean of disturbance
$D_{mi}$	daily mean of disturbance for international disturbed days
$D_{st}$	storm-time variation
d	distance between poles of magnetic dipole
F	total magnetic-field intensity
$F_0$	main magnetic-field intensity
$F'$	total magnetic-field intensity minus local external variable-magnetic field intensity
f	variable magnetic-field intensity
$f'$	nonlocal part of variable-magnetic-field intensity
$g_n^m, h_n^m$	Gaussian coefficients
H	horizontal component of magnetic-field intensity
$H_0$	horizontal component of magnetic-field intensity at geomagnetic equator
h	height above earth's surface
I	magnetic inclination

$i$	line current
$J$	volume current intensity
$j$	sheet current intensity
$j'$	sheet current intensity when current vector has been rotated through $90^\circ$
$K$	magnetic 3-hour index
$K_p$	magnetic 3-hour planetary index
$K_s$	magnetic 3-hour standardized index
$L$	lunar daily variation
$l$	perpendicular distance from a current-carrying line to a point $P$
$M$	magnetic moment
$m$	order of terms in spherical harmonic series; also, magnetic pole strength
$N$	north geographic pole
$N_s$	sunspot numbers per year
$n$	degree of terms in spherical harmonic series
$O$	center of earth or of dipole
$P, P_1$	points in space
$P_o$	a point on a current-carrying line
$P_n(\cos \theta)$	Legendre function
$P_{n,m}(\cos \theta)$	associated Legendre function
$P_n^m(\cos \theta)$	quasi-normalized associated Legendre function
$P_+, P_-$	positive and negative magnetic poles of a dipole

R	range
$R_E$	radius of earth
r	distance measured from center of earth or from center of dipole
$r_0$	distance from center of earth to center of ring current
S	solar daily variation
$S_D$	disturbance daily variation
$S_d$	disturbed-day solar daily variation
$S_q$	quiet-day solar daily variation
t	time
$t_0$	initial time
U	mean interdiurnal variability
u, $u_1$	magnetic-activity measures
V	magnetic potential
$V_1$	potential of dipole
$V_n$	sum of terms having degree n in the spherical harmonic expression of potential
X	geographic north component of magnetic-field intensity
$X'$	geomagnetic north component of magnetic-field intensity

$$X_n^m = \frac{dP_n^m(\cos \theta)}{n d\theta}$$

Y      geographic east component of magnetic-field intensity

$Y'$       geomagnetic east component of magnetic-field intensity

$$Y_n^m = \frac{mP_n^m(\cos \theta)}{n \sin \theta}$$

$Z$	vertical component of magnetic-field intensity, $Z = Z'$
$\alpha$	unipolar sunspot group
$\alpha_n^m, \beta_n^m$	coefficients defined by equations (17) and (18)
$\beta$	bipolar sunspot group
$\beta\gamma$	semicomplex sunspot group
$\gamma = 10^{-5} \Gamma$	also, complex sunspot group
$\Delta$	departure from a specified base
$\zeta$	angle between magnetic axis and horizontal intensity $\bar{H}$ projected to intersect axis
$\Theta$	geomagnetic colatitude
$\theta$	geographic colatitude
$\theta_0$	geographic colatitude of the geomagnetic poles
$\kappa = \text{arc } NP_1$	
$\Lambda$	geomagnetic longitude
$\lambda$	geographic longitude; also wavelength
$\lambda_0$	geographic longitude of geomagnetic poles
$\sigma$	angle between $\bar{F}'$ and $\bar{j}'$
$\Phi$	geomagnetic latitude
$\phi$	geographic latitude
$\phi_0$	geographic latitude of geomagnetic poles
$\psi$	angle between geographic and geomagnetic meridians at point P
Subscripts:	
av	average
e	external source

i	internal source
j	index
m	order of terms in spherical harmonic series where m = 1, 2, . . .
max	maximum
n	degree of terms in spherical harmonic series where n = 1, 2, . . .
s	surface value
$\perp$	perpendicular to spin axis of vehicle

Superscripts:

e	external source
h	designates hours
i	internal source
m	order of terms in spherical harmonic series where m = 1, 2, . . .

A bar over a symbol designates a vectorial quantity.

## GENERAL DESCRIPTION

The material concerning the general description of the geomagnetic field is based on information obtained from references 1, 2, and 3.

The geomagnetic field is produced by sources both internal and external to the solid envelope of the earth. The largest part of the geomagnetic field is of internal origin with a small, less than 1 percent, portion of the field being of external origin. For descriptive purposes, the geomagnetic field is assumed to be a permanent field upon which are superposed fields that change with time. That part of the geomagnetic field that can be represented as a uniformly magnetized sphere, or similarly, a magnetic dipole, is called the regular field. The remaining part is called the irregular field of which the permanent part is called the residual field.

The geomagnetic field of internal origin is primarily ascribed to electric currents in the form of eddies in the earth's metallic fluid core which, when rotated by the earth, give an aggregate effect of a

single current flowing in a large circle around the earth's core. The process resembles that occurring in a self-excited dynamo. Overall, the field is fairly stable but the individual eddies, which start, grow, and decay, produce continental and regional anomalies. These anomalies are the nonpermanent part of the irregular field of internal origin, and their change with time is called the secular variation which is a slow variation that is measured in years or decades. (See fig. 1 which is from ref. 1.) The permanent part of the irregular field of internal origin is composed of local anomalies due to large deposits of ferromagnetic material.

The external sources of the geomagnetic field are also electric currents but these currents are located in and above the atmosphere. The fields produced by these electric currents are, within the limits of observational data, entirely variable and nonpermanent in nature. The currents are a direct result of solar radiation, both electromagnetic and corpuscular.

The effective high-frequency part of the electromagnetic radiation from the sun, such as ultraviolet and X-ray radiation, ionizes the atmosphere and produces the layers known collectively as the ionosphere. In this layer, the ion-density distribution about the earth is a function of the intensity of the ionizing radiation, which falls only on the sunlit hemisphere, and of the recombination time of the ions. Movement of these ions with respect to a fixed point on the earth results in a current. The ion movement is due to potential differences, tidal motion, and thermal expansion. However, the apparent motion of the ions due to the earth's rotation produces the major effect. Thus, the resultant magnetic-field variation is primarily a function of local (that is, solar) time. In addition, tidal motions associated with the moon produce a variable magnetic field that is a function of lunar time.

During periods of intense solar activity, corpuscular radiation spews out from the sun in the form of a plasma. When this plasma encounters the earth's magnetic field, many of the charged particles are trapped in orbits about the earth and produce currents. These currents are thought to be in the form of a ring encircling the earth at distances of several earth radii from the earth. The currents gradually decrease as the particles are either absorbed by the atmosphere or escape into space. The departure of the magnetic field from normal field values during such an encounter commences almost simultaneously over the whole earth. Such magnetic disturbances are characterized by a notable decrease in the average value of the horizontal magnetic-field intensity with a gradual recovery over several days. Magnetic-field changes such as these are called magnetic storms and are not related to solar or lunar time.

Because of the manner in which they arise, the variable magnetic fields have been given the following general designations: (1) those related to the solar day are denoted by S; (2) those related to the lunar day are indicated by L; and (3) those that exhibit significant or irregular departures from the expected daily variation are designated by D and are referred to as disturbances. These general designations permit some overlapping of the classes as will be seen in the section entitled "Magnetic Classification." Many authors refer to these variable magnetic fields as "transient magnetic variations." However, most authors prefer to group the variations having a 24-hour period under the name "temporal variations" and to refer to the rest as "transient variations."

Two additional currents that affect the geomagnetic field are that which is induced within the earth by the atmospheric currents and that which proceeds from the air into the earth or from the earth into the air. The former has a magnitude of about one-third that of the upper atmospheric system, whereas the latter, which is of a nonpotential nature, is usually ignored.

The cgs system of units is universally used in geomagnetic work. The unit of magnetic-field intensity is a gauss and is denoted by the symbol  $\Gamma$ . A smaller unit that is extensively used is the gamma  $\gamma$ , where  $1\gamma = 10^{-5}\Gamma$ .

The total magnetic-field intensity  $F$  at any point is specified by the rectangular components  $X$ ,  $Y$ , and  $Z$  or by the magnetic elements  $H$ ,  $D$ , and  $I$  which are defined as follows (fig. 2 which is from ref. 2):

$F$	total magnetic-field intensity
$H$	horizontal component of $F$ , always positive
$X$	component of $H$ in geographic meridian, positive if northward
$Y$	component of $H$ transverse to geographic meridian, positive if to eastward
$Z$	vertical component of $F$ , positive if downward
$D$	azimuth of horizontal component, or magnetic declination, positive when measured from geographic north toward east
$I$	angle made by direction of $F$ with $H$ , or magnetic dip or magnetic inclination, positive if force is directed downward

The rectangular components and the magnetic elements are related to each other by the following equations:

L  
1  
6  
9  
2

$$\left. \begin{aligned}
 H &= F \cos I \\
 X &= H \cos D \\
 X^2 + Y^2 &= H^2 \\
 Z &= F \sin I = H \tan I \\
 Y &= H \sin D \\
 X^2 + Y^2 + Z^2 &= H^2 + Z^2 = F^2
 \end{aligned} \right\} \quad (1)$$

The vertical plane through the magnetic intensity, or through its horizontal element, is called the local magnetic meridian. The magnetic meridian makes the angle  $D$  with the geographic meridian. At a fixed altitude, the line on which  $Z$  (or  $I$ ) vanishes is referred to as the magnetic equator. The line on which  $Z$  (or  $I$ ) of the earth-centered dipole vanishes is called the geomagnetic equator.

At times it is convenient to use a geomagnetic coordinate system based on the polar axis of the centered dipole. The geomagnetic coordinates  $\Theta$ , or  $\Phi = 90^\circ - \Theta$ , and  $\Lambda$  of a point  $P$  whose geographic coordinates are  $\theta$ , or  $\phi = 90^\circ - \theta$ , and  $\lambda$ , where the coordinates are the colatitude, latitude, and the longitude, respectively, are calculated in the following manner.

Figure 3 (from ref. 1) shows a spherical triangle on which  $B$  is the north magnetic pole of the centered dipole and  $N$  is the north geographic pole. The colatitude  $\Theta$  is measured from the direction of  $OB$ , where  $O$  is the center of the earth. The geomagnetic longitude  $\Lambda$  is measured eastward from the meridian half-plane bounded by the dipole axis and containing the geographic south pole. The magnetic declination corresponding to the centered dipole field, at any point  $P$ , is the angle  $NPB$  or  $\psi$  measured eastward from the geographic north direction  $PN$ . From the spherical triangle,  $NB = \theta_0$ ,  $NP = \theta$ ,  $BP = \Theta$ ,  $NBP = 180^\circ - \Lambda$ ,  $NPB = -\psi$ , and  $BNP = \lambda - \lambda_0$ . Let  $PP_1$  be the perpendicular on the surface from  $P$  to the line  $NB$  and  $\kappa = NP_1$ . Then, on the spherical triangles  $NPP_1$ ,  $NPB$ , and  $BPP_1$

$$\tan \kappa = \tan \theta \cos(\lambda - \lambda_0) \quad (2)$$

$$\tan \Lambda = \frac{\tan(\lambda - \lambda_0) \sin \kappa}{\sin(\kappa - \theta_0)} \quad (3)$$

$$\cot \Theta = \cos \Lambda \cot(\kappa - \theta_0) \quad (4)$$

$$\sin \psi = - \frac{\sin \theta_0 \sin(\lambda - \lambda_0)}{\sin \theta} = - \frac{\sin \theta_0 \sin \Lambda}{\sin \theta} \quad (5)$$

The magnetic north and east components based on the geomagnetic axes are designated  $X'$  and  $Y'$ .

### MAGNETIC CLASSIFICATION

From extensive analyses (refs. 1 and 2) of the variable magnetic field that is produced by electric currents located in and above the atmosphere, a number of characteristic patterns with time and latitude have been discerned. The variable magnetic field at any instant and location is considered to be the sum of the individual fields that produce these patterns plus any irregularities that are present. Each constituent field results from solar radiation, as previously discussed. Graphs of the magnetic elements (or components) as a function of time for a particular constituent field taken over an appropriate time interval are called the variation of that constituent field.

The variation of each constituent field is denoted by an appropriate name and symbol, which is also used to indicate the instantaneous value of that field. These constituent-field variations are as follows: (1) The quiet-day solar daily variation  $S_q$  which has a period of 24 hours and results from electromagnetic radiation during so-called normal solar activity; (2) the disturbance daily variation  $S_p$  which also has a period of 24 hours but is primarily the result of enhanced electromagnetic radiation caused by abnormal solar activity such as flares; (3) the storm-time variation  $D_{st}$  which is a result of solar corpuscular radiation and is measured from the onset of the storm; and (4) the lunar daily variation  $L$  which is a result of the moon's tidal effect on the ionosphere. The rest of the field exhibits no regular pattern and has no singular source; it is referred to as the irregular variation  $D_i$ .

In order to obtain some estimate of the magnitude of these variations, averaging procedures have been devised to separate these constituents from each other and from the permanent field. These procedures, however, are imperfect and the elements (or components) of each of the variations so obtained include contributions from all the other variations. This imperfection is particularly true for  $S_p$ . Nevertheless, these averaged values are considered to represent the actual variations, and the same designations are applied as are used for the idealized concepts. In addition, various magnetic indices for determining the relative magnet activity of disturbances over various periods have been

evolved. These averaging procedures and magnetic indices are essentially quotations from reference 2 and are summarized as follows:

**Hourly values:** Hourly values are the mean values of any magnetic element (or component) for 1-hour intervals which extend either from one exact hour to the next or are centered at each exact hour.

**Daily mean values:** The mean of the 24 hourly values of any magnetic element (or component) from midnight (0<sup>h</sup>) to the following midnight (24<sup>h</sup>) is called the daily mean value of that element (or component).

**Monthly (or annual) mean value:** The daily mean value of any magnetic element (or component) may be averaged over a month (or year) to obtain the monthly (or annual) mean value of the element (or component). In the same way, the group mean value for a group of selected days may be obtained from the daily means.

**Mean hourly values:** The mean of the hourly values of any magnetic element (or component) for a particular hour of the day taken over the days of the month (or year) is referred to as the mean hourly value for the month (or year) of that particular hour and element (or component). The mean hourly value is obtained for all 24 hours. Similarly, mean hourly values may be obtained for a selected group of days.

**Mean daily inequality:** The difference between the mean hourly values for the month (or the year) and the monthly (or yearly) mean value for any magnetic element (or component) gives a sequence of hourly departures which is known as the mean daily inequality for the month (or year). Similarly, the mean daily inequality may be obtained for a particular group of days.

**Daily-variation curve:** The variation with time of the 24 values of the mean daily inequality for any magnetic element (or component) is called the daily-variation curve of that element (or component) for the month (or the selected group of days).

**Solar daily variation S:** The daily-variation curves for the three elements (or components) derived from all the days of the month are designated the solar daily variation S.

**Quiet-day solar daily variation  $S_q$ :** The daily-variation curves for the three elements (or components) obtained from the five most quiet days of the month are known as the quiet-day solar daily variation  $S_q$ .

**Disturbed-day solar daily variation  $S_d$ :** The daily-variation curves for the three elements (or components) obtained from the five most disturbed days of the month are called the disturbed-day solar daily variation  $S_d$ .

Lunar daily variation L: The magnitude of the lunar daily variation L is very small, about one-tenth of that of the solar daily variation S, and cannot be detected by mere visual inspection of the records of a single day as can be done with the solar daily variation S. The lunar daily variation is obtained as follows.

Subtract the monthly mean value and the values for the appropriate hours of the solar daily variation S from the 24 hourly values of the day for each magnetic element (or component). This operation is performed for each day of the month for many months. The differences will vary over the 24 hours of each day because they contain the lunar daily variation L and the magnetic disturbances. These 24 successive values for each day are now arranged in rows, one row for each day and each row commencing with the hour nearest to that of the lunar transit. If the means of the values in each column are taken, the variations due to the magnetic disturbances cancel out, as they are not related to lunar time. The row of averages thus gives only that part of the variation of the earth's magnetic field which is related to the lunar time, that is, the lunar daily variation L. Similarly, the lunar daily variation can be obtained for a particular phase of the moon by choosing appropriate days of the month for many months.

Disturbance variations: The disturbance field D is defined as the instantaneous value obtained from the difference between the total field and the average field with due allowance for  $S_q$  and L, which are now thought of as instantaneous values. Thus,

$$D = F - \frac{1}{t - t_0} \int_{t_0}^t F dt - S_q - L \quad (6)$$

where the integral is over an interval of, say, 1 month and the magnitudes of  $S_q$  and L for the same time of day as F are used. The magnetic elements (or components) rather than the total field may be similarly obtained. The disturbance field is the resultant of three types of disturbances whose variations are referred to as the disturbance daily variation  $S_D$ , the storm-time variation  $D_{st}$ , and the irregular variation  $D_i$ .

The disturbance daily variation  $S_D$  arises from a systematic difference, particularly noticeable in higher latitudes, between S or  $S_d$  and  $S_q$ . The distribution over the earth of the field representing this difference is very different from that of the  $S_q$  field. As the  $S_D$  field is still related to solar time, either difference  $S - S_q$  or  $S_d - S_q$  is called the disturbance daily variation. The intensity of  $S_D$  is obviously

greater for the latter difference but the distributions over the earth are similar for the two differences.

The average time history of the storm-time variation  $D_{st}$  is obtained as follows. At a particular station, a number of magnetic storms of roughly similar intensity are chosen so that the times of commencement of the storms are fairly evenly distributed over the 24 hours of Greenwich time. A particular magnetic element (or component) is now chosen and its successive hourly values are written out in rows, one row for each storm and each row commencing with the value of the element for the hour preceding the commencement of the storm. The hourly values in the vertical columns are added and the means are then taken. In the hourly means thus obtained, all periodic changes of the magnetic element (or component) which depend on the local time evidently cancel out owing to the fact that the hours of commencement are almost uniformly distributed over the solar day. The mean of the first column, which is the mean value of the element (or component) for the hour preceding the commencement of the storm, is subtracted from the row of means and the difference is plotted as a function of time. This plot represents the storm-time variation  $D_{st}$ .

The irregular disturbance variation has no statistical meaning inasmuch as the average over a period of, say, a month of the values of the elements (or components) for each particular hour of the irregular disturbances would be zero. As a concept, however, it may be thought of as being the variation obtained by subtracting the instantaneous values of  $S_D$  and  $D_{st}$  from  $D$ .

Daily mean disturbance  $D_m$ : The daily mean disturbance is the mean of the disturbance daily variation  $S_D$  taken over the day and is denoted by  $D_m$ . Because of the way in which the values for  $S_D$  are obtained, the average value over the day is not zero as would be expected if it were the true disturbance daily variation. Furthermore, the average value over the day is obviously greater when  $S_D$  is taken as  $S_d - S_q$  than when it is taken as  $S - S_q$ . It is evident, therefore, that the value of  $D_m$  is related to the storm-time variation  $D_{st}$ . In addition, an international daily mean disturbance  $D_{mi}$  is obtained by using in the term  $S_d$  only selected disturbed days that occur over the entire earth.

Range  $R$ : The range  $R$  is the difference between the highest value and the lowest value within a specified period of any curve generated from magnetic-field data. When the range is obtained from the magnetic elements (or components), it affords a fairly good classification of days according to their relative degree of disturbance. However, on

some days the range may depend on a single brief disturbance in the magnetic field.

Magnetic character figure  $C$ : The magnetic character figure  $C$  is a rough indication of magnetic activity for the day. It is so defined that days of quiet magnetic condition are identified by the character figure  $C = 0$ , days of moderate disturbances by the character figure  $C = 1$ , and days of intense disturbances by the character figure  $C = 2$ . The exact method of assigning these character figures is left to the discretion of each observatory. The magnetic character figure averaged over all observatories, to one decimal place, is called the international magnetic character figure  $C_1$  for the day and characterizes the worldwide magnetic condition. The five most quiet and the five most disturbed days of a month are called the international quiet and the international disturbed days of the month, respectively.

Magnetic-activity measures  $u$  and  $u_1$ : As previously noted, one feature of a magnetic storm is that the average value of the horizontal component of the magnetic-field intensity  $H$  is decreased immediately after the incidence of the disturbance. The intensity then gradually recovers to its normal value. The change in the average value of  $H$  from one day to the next can be used to obtain a universal measure of the magnetic activity  $u$  for the period under consideration. The computation of  $u$  is made as follows.

To each day is assigned the difference obtained by subtracting the mean value of  $H$  for that day from the mean value of  $H$  for the preceding day. The average of the absolute values of these differences over a month may be called the mean interdiurnal variability of the month  $U$  and is expressed in gammas. A worldwide magnetic disturbance may be considered to be due to circular current systems in space encircling the earth parallel to the magnetic latitudes. The magnetic field of such a current system is directed along the magnetic axis but only the element  $H$  is effective in producing the prominent observed change during a magnetic storm. Hence, the universal magnetic-activity measure  $u$  is introduced and is given by  $u = (U \times 10^{-1}) / \cos \zeta$ , where  $\zeta$  is the angle in space between the magnetic axis and  $\vec{H}$  projected to intersect the axis.

Another measure of the magnetic activity is  $u_1$  which is a function of  $u$ . Since the value of the daily magnetic character figure  $C$  cannot exceed 2, it follows that the great magnetic storms get less weight in the monthly means of the character figure  $C$  than in the monthly value of  $u$  which has no upper limit. It is desirable to have a measure of magnetic activity which is just as well defined as  $u$  but at the same time reduces somewhat the influence of exceptionally great

disturbances. Such a measure is  $u_1$  which was introduced by Bartels (ref. 1) and is related to the  $u$ -measure by the curve generated by plotting the values given in table I.

**K-indices:** In order to provide a homogeneous running record of disturbances, a magnetic K-index for each 3-hour interval has been introduced, with the first 3-hour interval beginning at the Greenwich mean time 0<sup>h</sup>. These K-indices are based on a range  $R$  which in this instance is applied to the curve generated by plotting the disturbance  $D$  as a function of time for each 3-hour period for the most disturbed element. The K-indices are assigned integers from 0 to 9 which are obtained from permanent scales that are essentially logarithmic and are adjusted for each observatory. These scales give the limits for which the range defines the K-index for each integer. Table II lists such scales for a number of observatories. (See ref. 4.)

This K-index, however, is only a regional index. A magnetic planetary index  $K_p$  is defined as a measure of the disturbances for the earth as a whole and is based on standardized  $K_s$ -indices which are freed from the local features insofar as possible. Conversion tables different for each observatory, which assign a  $K_s$ -index to every K-index, have been derived for 11 observatories and are determined in such a way that each observatory has within a year, for example, approximately the same number of intervals with  $K_s = 0$ ,  $K_s = 1$ , and so forth. These conversion tables are not presented herein. The average of the  $K_s$ -indices for the 11 observatories is the  $K_p$ -index given to the nearest third. For example, the interval 1.5 to 2.5 is divided equally into three parts designated by 2-, 2o, and 2+. These intervals provide 28 grades of  $K_p$ . The daily value of  $K_p$  is also used and it is simply the sum of the eight values of  $K_p$  for each day.

**Equivalent amplitude indices:** For some investigations, it is convenient to have the homogeneous running records of the disturbances in the form of an amplitude (ref. 5) of the disturbances rather than as the logarithmic K-indices. A direct reversion from the K-indices is ambiguous, however, as each value of  $K$  defines a range of amplitudes. An equivalent amplitude is thus defined as follows.

To each 3-hour local K-index, a 3-hour local equivalent amplitude  $a_k$  is assigned for which the functional relationship is shown in table III (from ref. 5). The daily equivalent amplitude  $A_k$  is simply the average of the eight values of  $a_k$  per day. Similarly, to each 3-hour planetary index  $K_p$  a 3-hour planetary equivalent amplitude  $a_p$  is assigned for which the functional relationship is shown in table IV

(from ref. 5). The daily planetary equivalent amplitude  $A_p$  is the average of the eight values of  $a_p$  per day. An approximate value of  $A_p$  may also be obtained from  $C_1$  by using the relations of table V (from ref. 5).

These equivalent amplitudes are expressed in the unit  $2\gamma$  in order to indicate their approximate nature. For example, if  $a_p$  has a value of, say, 48, the range of the most disturbed of the three magnetic elements (or components) for the 3-hour interval has an equivalent value of  $96\gamma$ .

### THE EARTH'S MAIN MAGNETIC FIELD

The main magnetic field of the earth (refs. 1, 4, and 6) is composed of the fields of internal origin and any permanent fields of external origin. This main field is described by the method of spherical harmonic analysis, the coefficients of which are determined from observatory measurements at the earth's surface. Because of the scatter of the observatories, the resultant field is smoothed out and does not show local anomalies.

A magnetic potential  $V$  over the earth's surface can be expressed in terms of the series

$$V = R_E \sum_{n=0}^{\infty} \sum_{m=0}^n P_n^m(\cos \theta) \left\{ \left[ c_n^m \left( \frac{r}{R_E} \right)^n + \left( 1 - c_n^m \right) \left( \frac{R_E}{r} \right)^{n+1} \right] \underline{A}_n^m \cos m\lambda \right. \\ \left. + \left[ s_n^m \left( \frac{r}{R_E} \right)^n + \left( 1 - s_n^m \right) \left( \frac{R_E}{r} \right)^{n+1} \right] \underline{B}_n^m \sin m\lambda \right\} \quad (7)$$

where  $R_E$  is the radius of the earth,  $r$  is the distance measured from the earth's center,  $\theta$  is the colatitude, and  $\lambda$  is the east longitude,  $c_n^m$  and  $s_n^m$  are numbers lying between zero and 1, representing the fraction of the harmonic terms  $P_n^m \cos m\lambda$  and  $P_n^m \sin m\lambda$ , respectively, in  $V$  which, at  $r = R_E$ , is due to matter outside the earth, and  $\underline{A}_n^m$  and  $\underline{B}_n^m$  are spherical harmonic coefficients usually sought in analysis.

For the order  $m$  and degree  $n$  with  $m \leq n \leq 0$ , when  $m > 0$

$$P_n^m(\cos \theta) = \left[ \frac{2(n-m)!}{(n+m)!} \right]^{1/2} P_{n,m}(\cos \theta) \quad (8)$$

and when  $m = 0$

$$P_n^m(\cos \theta) = P_{n,m}(\cos \theta) \quad (9)$$

The function

$$P_{n,m}(\cos \theta) = \frac{\sin^m \theta \, d^m P_n(\cos \theta)}{d(\cos \theta)^m} \quad (10)$$

may be written

$$P_{n,m}(\cos \theta) = \frac{(2n)!}{2^n n! (n-m)!} \sin^m \theta \left[ \cos^{n-m} \theta - \frac{(n-m)(n-m-1)}{2(2n-1)} \cos^{n-m-2} \theta \right. \\ \left. + \frac{(n-m)(n-m-1)(n-m-2)(n-m-3)}{2 \cdot 4(2n-1)(2n-3)} \cos^{n-m-4} \theta - \dots \right] \quad (11)$$

where  $P_n(\cos \theta)$  is the Legendre function and  $P_{n,m}(\cos \theta)$  is the associated Legendre function. The function  $P_n^m = P_n^m(\cos \theta)$ , together with the functions  $X_n^m = \frac{dP_n^m(\cos \theta)}{n d\theta}$  and  $Y_n^m = \frac{m P_n^m(\cos \theta)}{n \sin \theta}$ , has been tabulated by Schmidt (ref. 7).

The north, east, and vertical intensities are  $X = \partial V / r \partial \theta$ ,  $Y = -\partial V / r \sin \theta \partial \lambda$  and  $Z = \partial V / \partial r$ , respectively. By substituting the equivalencies  $nA_n^m = A_n^m$ ,  $nB_n^m = B_n^m$ , and  $r = R_E$  into equation (7), the X-, Y-, and Z-intensities become

$$X = \sum_{n=0}^{\infty} \sum_{m=0}^n X_n^m (A_n^m \cos m\lambda + B_n^m \sin m\lambda) \quad (12)$$

$$Y = \sum_{n=0}^{\infty} \sum_{m=0}^n Y_n^m (A_n^m \sin m\lambda - B_n^m \cos m\lambda) \quad (13)$$

$$Z = \sum_{n=0}^{\infty} \sum_{m=0}^n P_n^m \left\{ \left[ nc_n^m - (n+1)(1 - c_n^m) \right] \frac{A_n^m}{n} \cos m\lambda \right. \\ \left. + \left[ ns_n^m - (n+1)(1 - s_n^m) \right] \frac{B_n^m}{n} \sin m\lambda \right\} \quad (14)$$

If  $c_n^m$  and  $s_n^m$  are zero, the field is entirely of origin internal to the earth and

$$Z = - \sum_{n=0}^{\infty} \sum_{m=0}^n P_n^m \left( \frac{n+1}{n} A_n^m \cos m\lambda + \frac{n+1}{n} B_n^m \sin m\lambda \right) \quad (15)$$

If  $c_n^m$  and  $s_n^m$  are not zero, the vertical intensity  $Z$ , at  $r = R_E$ , may be analyzed in the form

$$Z = \sum_{n=0}^{\infty} \sum_{m=0}^n P_n^m \left( \alpha_n^m \cos m\lambda + \beta_n^m \sin m\lambda \right) \quad (16)$$

where

$$\alpha_n^m = \left[ nc_n^m - (n+1)(1 - c_n^m) \right] \frac{A_n^m}{n} \quad (17)$$

$$\beta_n^m = \left[ ns_n^m - (n+1)(1 - s_n^m) \right] \frac{B_n^m}{n} \quad (18)$$

from which  $c_n^m$  and  $s_n^m$  can be found.

The values of  $A_n^m$ ,  $B_n^m$ ,  $\alpha_n^m$ , and  $\beta_n^m$  are obtained from tables of  $X$ ,  $Y$ , and  $Z$  for various latitudes and longitudes (tables VI, VII,

and VIII, respectively, from ref. 4) which are in turn obtained from charts of the earth's main field. This procedure is conveniently carried out by first analyzing the observed values of  $X$ , say, along parallels of colatitude into Fourier coefficients  $a_m$  and  $b_m$  of the series  $a_m \cos m\lambda + b_m \sin m\lambda$ . The coefficients  $a_m$  and  $b_m$  are functions of colatitude only. These coefficients are next fitted by the functions  $X_n^m$ , say, for corresponding values of  $m$  where  $m \leq n$ , by solving sets of linear equations to obtain values of  $A_n^m$  and  $B_n^m$ . This operation is done independently for  $X$  and  $Y$ .

It may be noted that both  $X$  and  $Y$  contain  $A_n^m$  and  $B_n^m$  and, if the value of  $X$  is known over the earth, the value of  $Y$  can be deduced from it. If the results do not agree when  $A_n^m$  and  $B_n^m$  are found separately for  $X$  and  $Y$ , it means that the field is not completely derivable from a potential  $V$ . The values of  $A_n^m$  and  $B_n^m$  in  $Z$  are obtained by taking the mean of the values derived for  $X$  and  $Y$ .

The spherical harmonic coefficients for  $X$ ,  $Y$ , and  $Z$  are listed in table IX (from ref. 4) for the epoch 1945. The components  $X$ ,  $Y$ , and  $Z$  at any height,  $h = r - R_E$ , above the earth's surface can be computed from expressions obtained from the differentiation of the potential function, the use of the coefficients in table IX, and the assumption that  $c_n^m$  and  $s_n^m$  are zero inasmuch as they are negligible for this purpose.

A second useful way of writing the potential is

$$V = R_E \sum_{n=1}^{\infty} \left[ \left( \frac{r}{R_E} \right)^n T_n^e + \left( \frac{R_E}{r} \right)^{n+1} T_n^i \right] = V^e + V^i \quad (19)$$

where

$$T_n = \sum_{m=0}^n \left( g_n^m \cos m\lambda + h_n^m \sin m\lambda \right) P_n^m(\cos \theta) \quad (20)$$

and the superscripts  $e$  and  $i$  refer to the points which are, respectively, of external and internal origin. The coefficients  $g_n^m$  and  $h_n^m$  are called Gaussian coefficients. Their relation to the spherical harmonic coefficients is shown in the following expressions:

$$\left. \begin{aligned}
 g_n^{m,e} &= c_n^m \frac{A_n^m}{n} \\
 h_n^{m,e} &= s_n^m \frac{B_n^m}{n} \\
 g_n^{m,i} &= \left(1 - c_n^m\right) \frac{A_n^m}{n} \\
 h_n^{m,i} &= \left(1 - s_n^m\right) \frac{B_n^m}{n}
 \end{aligned} \right\} \quad (21)$$

Table X (from ref. 4) lists the first eight Gaussian coefficients for the internal field for various epochs up to epoch 1945.0.

The Gaussian coefficients for epoch 1955.0 were recently derived by H. F. Finch and B. R. Leaton and are given through order  $m = 6$  and degree  $n = 6$  in table XI (from ref. 8). The coefficients listed under the name Gauss were derived from two separate analyses in which X and Y were utilized in combination and are denoted as solution 1 and solution 2. In the second analysis, the coefficients were also derived from the values of Z and are listed under the name Schmidt inasmuch as this method is associated with the quasinormalized functions  $P_n^m$ . Further details of the analysis may be found in reference 8.

In addition to the analysis of reference 8, an independent spherical harmonic analysis of the geomagnetic field has been made; the method used and some results of this analysis are reported in reference 9. This analysis incorporates terms in the harmonic series up to order  $m = 17$  and degree  $n = 24$ . These coefficients are not presented herein since they are too numerous. A Fortran program (a copy of which has been obtained for use at the Langley Research Center) has been prepared by the Air Force Special Weapons Center (AFSWC) and utilizes these coefficients to compute the magnetic field at any altitude, latitude, and longitude.

The term in the magnetic potential series containing the coefficient  $g_1^0$  gives the potential of a dipole that is located at the earth's center and has a magnetic moment directed along the axis of rotation and toward the south geographic pole. The terms containing  $g_1^1$  and  $h_1^1$  give dipoles with moments lying in the plane of the geographic equator and directed, respectively, along the axes  $\lambda = 0^\circ$  and  $\lambda = 90^\circ$ . The superposition of these three orthogonal dipoles yields a single dipole located at the center of the earth and with an axis inclined to the axis of rotation, the so-called centered dipole. The sum of the first- and

second-degree terms is equivalent to the potential of a dipole located at a point displaced from the center of the earth plus the two quadrupole terms containing  $P_2^2$ . This eccentric dipole, the simplest model that characterizes the field as a whole, has the same vector moment as the centered dipole.

The simple dipole field is represented as follows. Figure 4 (from ref. 1) shows a magnetic dipole with axis  $P_+, P_-$  where  $P_+$  is the positive pole,  $P_-$  is the negative pole,  $m$  is the pole strength,  $d$  is the distance between poles, and  $r$  and  $\theta$  are the coordinates of a point  $P$  with the center of the dipole as origin. Thus,

$$\left. \begin{aligned} V_1 &= \frac{-m}{r - \frac{1}{2}d \cos \theta} + \frac{m}{r + \frac{1}{2}d \cos \theta} = \frac{-M \cos \theta}{r^2} \\ Z &= \frac{\partial V_1}{\partial r} = \frac{2M \cos \theta}{r^3} \\ H &= \frac{\partial V_1}{r \partial \theta} = \frac{M \sin \theta}{r^3} \end{aligned} \right\} \quad (22)$$

where  $M = md$  and is the magnetic moment. Terms in  $d^2$  are considered negligible.

The equation for the lines of force of a dipole is

$$\frac{r}{\sin^2 \theta} = \text{Constant} \quad (23)$$

The first-degree terms for internal source only of equation (19) can be put into the dipole form by the following transformations:

$$V_1 = R_E \left\{ \left( \frac{R_E}{r} \right)^2 \left[ g_1^0 \cos \theta + (g_1^1 \cos \lambda + h_1^1 \sin \lambda) \sin \theta \right] \right\} \quad (24)$$

Let

$$\left. \begin{aligned} (H_0)^2 &= (g_1^0)^2 + (g_1^1)^2 + (h_1^1)^2 \\ g_1^0 &= -H_0 \cos \theta_0 \end{aligned} \right\} \quad (25)$$

(Equations continued on next page)

$$\left. \begin{aligned} h_1^1 &= g_1^1 \tan \lambda_0 \\ \cos \Theta &= \cos \theta \cos \theta_0 + \sin \theta \sin \theta_0 \cos(\lambda - \lambda_0) \end{aligned} \right\} \quad (25)$$

then

$$V_1 = -R_E \left( \frac{R_E}{r} \right)^2 H_0 \cos \Theta = \frac{-M \cos \Theta}{r^2} \quad (26)$$

where  $H_0 = \frac{M}{R_E^3}$  and is the horizontal component at the geomagnetic equator and  $\theta_0$  and  $\lambda_0$  are the geographic coordinates of the geomagnetic poles.

For 1945,  $\phi_0 = 78.6^\circ$  N,  $\lambda_0 = 289.9^\circ$  E for the north magnetic pole and  $\phi_0 = 78.6^\circ$  S,  $\lambda_0 = 109.9^\circ$  E for the south magnetic pole. For 1955,  $\phi_0 = 78.3^\circ$  N,  $\lambda_0 = 291.0^\circ$  E for the north magnetic pole and  $\phi_0 = 78.3^\circ$  S,  $\lambda_0 = 111.0^\circ$  E for the south magnetic pole. The magnetic moment  $M$  was found to be  $8.06 \times 10^{25}$  cgs unit for both epochs.

#### GEOMAGNETIC-FIELD VARIATIONS

The information pertaining to the geomagnetic-field variations is obtained mainly from references 1, 2, and 4.

##### Geomagnetic Annual Variation

The geomagnetic annual variation is the departure of the monthly mean from the annual mean and is corrected for secular variation. Figure 5 (from ref. 4) shows the monthly departures from the annual means of the geomagnetic component  $\Delta X'$  for sunspot minimum and sunspot maximum years for various latitudes. The monthly averages show only a small annual variation with the extremes being near the equinoxes and the solstices.

The geomagnetic annual variation is similar to the annual variation of the monthly values of  $D_m$ . This annual variation of  $D_m$  can be divided into two parts with respect to latitude: one is symmetric about the equator; the other is antisymmetric about the equator. The antisymmetric part is also sinusoidal with respect to time over the year. For the special case of internationally disturbed days (ref. 4),

figure 6(a) presents the annual variation of  $D_{mi}$  for various latitudes in which the values for each month are averaged over the years 1922 to 1933. Figures 6(b) and 6(c) present the symmetric and antisymmetric parts, respectively. It has been found that an increase in magnitude of the symmetrical part with increased intensity of disturbance is not accompanied by a corresponding proportional increase in the magnitude of the antisymmetric part. The symmetrical part may be considered as that part which is due to the storm-time variation  $D_{st}$ ; the antisymmetrical part may be considered as that part which is due to the disturbance daily variation  $S_D$ .

#### Solar Daily Variation on Quiet Days $S_q$

The solar daily variation on quiet days  $S_q$ , averaged over the appropriate months of the years 1922 to 1933, is shown in figures 7(a) to 7(d) (from ref. 4) for winter, equinox, summer (corresponding to the northern hemisphere), and the entire year, respectively, at various latitudes. It can be seen from the figures that the departure of  $S_q$  from its daily mean value is greater during daylight hours than during the night hours. The departures of the components of  $S_q$  from their daily mean values show considerable variation with latitude and increase with increasing latitude except for the large enhancement of  $\Delta X'$  about the equator. There are also changes of phase with latitude;  $\Delta Y'$  and  $\Delta Z'$  are fairly constant in form but reverse direction at the equator, whereas  $\Delta X'$  maintains the same direction in both hemispheres except for two reversals occurring at about  $\pm 30^\circ$ . At latitudes above  $60^\circ$ , the effects of disturbances predominate even on international quiet days. These latitudes have not been included in the figures.

Figures 7(a) to 7(c) also show that the departure of  $S_q$  from its daily mean value changes with the seasons, being maximum at local summer and minimum at local winter.

Marked differences in the departure of  $S_q$  from its daily mean value on successive days that have been considered to be magnetically quiet have been noted, especially at the equator. These marked differences are the result of considerable shifts both to the north and to the south of the average position of the current system that generates the field. This day-to-day shift about the average position of the current system at the equator may be as much as several degrees in latitude.

#### Disturbance Daily Variation $S_D$

The nature of the  $S_D$  variation depends to a marked degree on the latitude. (See figs. 8(a) to 8(e) from ref. 4.) In the middle and

moderately high latitudes, the departure of  $S_D$  from its daily mean value is approximately the same during the day as during the night. As was noted for  $S_Q$ , the component  $\Delta X'$  maintains its direction in both hemispheres, whereas the components  $\Delta Y'$  and  $\Delta Z$  reverse directions at the equator. However, unlike  $S_Q$ , the departure of the  $\Delta X'$ -component of  $S_D$  from its daily mean value decreases from the equator up to the auroral region and then increases.

In the polar regions (fig. 8(b)), the  $S_D$ -variation is strongly associated with the auroral belts and its magnitude has a pronounced increase. The north component reverses sign near  $\phi = 55^\circ$ , attains its maximum range at the auroral zone, and again reverses sign near  $\phi = 72^\circ$ . In general, the magnitude of  $\Delta X'$  is largest in the early morning and early evening. The east component  $\Delta Y'$  is largest within the interior of the auroral zone, reverses sign at the auroral zone, and then remains small. The vertical component  $\Delta Z$  shows a large and pronounced morning maximum just inside the auroral zone and a small minimum just outside, both of which appear also in the evening but are reversed in sign.

The seasonal variation of  $S_D$  is presented in figures 8(c) to 8(e). It is noted that the seasonal variations are also most pronounced in the high latitudes.

#### Storm-Time Variation $D_{st}$

The storm-time variation  $D_{st}$  forms a characteristic feature of magnetic storms. (Additional information concerning magnetic storms may be found in refs. 10 to 15.) The course of the storm-time variation depends on the time reckoned from the commencement of disturbance. The horizontal-force variation exhibits a definite beginning. It at first increases above the normal undisturbed value, remains so for a few hours, and then rapidly decreases, the decrease being generally more than twice the initial increase. It then takes several days for the depressed value of  $H$  to regain its normal value. The recovery is at first rapid and then slows down considerably. The increase is called the initial phase of the storm. The decrease up to the point at which the rate of recovery begins to slow down is called the main phase. The period of slow recovery is called the last phase or the phase of recovery of the storm.

Figures 9(a) and 9(b) (from ref. 4) show the average storm-time weighted average of 11 storms for the polar year 1932-1933 for various latitudes. It can be clearly seen that the  $\Delta X'$ -component in  $D_{st}$  has an initial-phase duration on the order of 2 hours, decreases to a minimum in 20 to 24 hours, and reverses to a value near the initial value in about 70 hours.

Between the auroral belts (fig. 9(a)),  $\Delta X'$  attains a maximum near the equator about which the variation appears to be approximately symmetrical. The variation of  $\Delta Y'$  is small in all latitudes. The variation of  $\Delta Z'$  is, in general, positive throughout the low and middle latitudes in the northern hemisphere but becomes negative in the southern hemisphere.

In the polar regions (fig. 9(b)), the variation of  $\Delta X'$  exhibits the same general features as it does between the auroral belts but is less regular in character. In addition, as the geomagnetic pole is approached, the initial value of  $\Delta X'$  becomes zero and then negative in contrast to the positive initial value at lower latitudes. The  $\Delta Y'$ -component increases in magnitude as the geomagnetic pole is approached but it is still small compared with  $\Delta X'$  and  $\Delta Z'$ . The variation of  $\Delta Z'$  is positive in the polar region and has a magnitude that is of the same order as that of  $\Delta X'$ . The magnitude of  $\Delta Z'$  reaches a maximum about midway between the pole and the auroral belt. Within the auroral belt, the  $\Delta Z'$  variation becomes generally negative in sign but becomes positive in sign once again at the lower latitudes.

There is little doubt that geomagnetic storms are caused by streams of corpuscles emitted by the sun. Geomagnetic storms are commonly believed to be of two types (ref. 16): Type 1, the sudden commencement (or sc) storm, in which the initial increase of the horizontal intensity takes place in a matter of minutes, is intense, is associated with sunspots, follows flares by about 1 day, has worldwide sudden commencement, and shows no recurrence after 27 days, which is the period of rotation of the sun; type 2, the so-called M-region storm, is independent of sunspots, flares, and other visible disk features, begins gradually, and shows a strong tendency to recur within a period of 27 days. It is believed that the intense storms are due to short-lived solar disturbances which do not usually survive a solar rotation.

#### Irregular Disturbance $D_1$

The irregular disturbance  $D_1$  is of small intensity at low latitudes. With an increase of latitude, the intensity increases. The increase becomes very rapid as the auroral zone is reached. After a pronounced maximum under or nearly under the auroral zone, the intensity decreases as the inside of the zone is penetrated. This decrease in intensity has a seasonal variation. In summer it decreases to about one-half of the maximum and in winter, to about one-fifth. The minimum winter value of intensity at the auroral zone is, however, several times larger than the value at the equator, where there is little seasonal variation.

### Lunar Daily Variation $L$

If the lunar daily variation  $L$  is derived from all days in a particular month for a number of years or for all days in a year, it is found to be very simple. The curve representing this monthly mean variation  $L$  is a double sine wave;  $L$  can also be derived from a large number of days all at a particular phase of the moon. When so determined, the curve is not so simple as the curve for all days of the month of the year. It is found that the portion of the curve which corresponds to daylight hours has greater range than has the remaining portion which corresponds to the hours of darkness. Figure 10 (from ref. 2) represents a series of such curves drawn for successive phases of the moon. The heavy part of the curves denotes the daylight hours, and the thin part of the curves denotes the nighttime hours. A second way of showing the variation of  $L$  with the phase of the moon and at the same time obtaining a comparison with  $S$  is shown in figure 11 (from ref. 2).

In general, the  $L$  variations are about one-tenth of the  $S$  variations, but at the magnetic equator the lunar diurnal variation in  $H$  is of large magnitude, not only in absolute units but even related to  $S$  which is also exceptionally large there. At Huancayo, Peru, at the magnetic equator, the  $L$  variation in magnetic declination increases about tenfold from quietest to most disturbed days, whereas at Greenwich the increase is only about twofold. The latitude variation of  $L$ , outside of the equatorial region, is shown in figure 12 (from ref. 17).

The amplitude of  $L$  also shows a seasonal variation for which the percentage variation is much greater than that of  $S_q$ . The summer-to-winter ratio is about 1:2.6.

### GEOMAGNETIC-FIELD FLUCTUATIONS

A fluctuation of the geomagnetic field is regarded as a departure of the field from a normal undisturbed value followed by a subsequent recovery. No distinctions are made respecting the sign of the fluctuations. The amplitude is the maximum departure from the normal value. The material in this section is taken primarily from references 1 and 4.

#### Range

The daily range in the magnetic elements varies in a marked degree with geographical position. Large values of the daily ranges in  $H$ ,  $D$ , and  $Z$  occur more frequently in the auroral zones, whereas small values of the daily ranges occur more frequently in lower latitudes. Figures 13(a) to 13(c) (from ref. 4) show the frequency distribution of

daily ranges in H, Z, and D, respectively, at various latitudes for the polar year August 1932 to August 1933. Table XII (from ref. 4) gives the probability that the daily ranges of H, D, and Z will exceed various magnitudes in different geomagnetic latitudes. Table XIII (from ref. 4) gives the expectation of the number of days elapsing before the daily ranges in H, D, and Z will exceed various magnitudes in different geomagnetic latitudes. Table XIV (from ref. 4) gives the percent of time that the 3-hour range of disturbance in H, D, or Z is less than the various ranges for the year 1940.

### Short-Period Fluctuations

This section deals with geomagnetic fluctuations of duration from 10 seconds to 10 hours. There is a marked maximum in the amplitude of small fluctuations near and just inside the auroral zones. In these regions, the magnitude of the fluctuations is greatest in the horizontal component and least in the vertical component. In the low and middle latitudes, the number of fluctuations of appreciable intensity is sharply reduced and these intense fluctuations seldom appear in Z. At times of magnetic storm ( $K \geq 5$ ), marked fluctuations, both local and worldwide, may appear in all components in the lower latitudes. Large fluctuations are known as bays and are most pronounced in polar regions with a duration of about 1 to 5 hours. The bays are worldwide, but their amplitudes in the middle and low latitudes are, in general, small. These bays tend to show morning and evening maxima in frequency.

Figure 14 (from ref. 4) gives frequencies of fluctuations of various amplitudes as a function of duration in seconds at Petsamo, Finland (now Pechenga, U.S.S.R.), which is within the auroral zone, for the period August 1 to October 31, 1932. A maximum in frequency is shown to occur at a duration of about 40 to 50 seconds. Figure 15 (from ref. 4) shows the variation with latitude of frequencies of fluctuations of various durations, 10 to 500 seconds, for the mean of 6 days. Figure 16 (from ref. 4) shows the variation with geomagnetic latitude of the daily frequency of fluctuations with durations 10 to 500 seconds for various values of magnetic character figure C. Tables XV and XVI (from ref. 4) give the total numbers of fluctuations with various rates of change and semiduration of H, D, and Z at Petsamo, Finland and at Copenhagen, Denmark, which are, respectively, within the auroral zone and just outside of the auroral zone for the period September 1, 1932 to August 31, 1933.

### Micropulsations

Magnetic records of all three elements sometimes show rapid fluctuations in the form of oscillations lasting for an hour or so. The period

varies between a fraction of a minute and about 2 minutes and the amplitude is several gammas. There are exceptional micropulsations in which the amplitude is as great as  $15\gamma$  to  $30\gamma$ ; these are called giant micropulsations.

The giant micropulsations occur within a relatively limited area and their periods generally range from 1 to 2 minutes. An interesting feature observed about these giant micropulsations is that the oscillations of the different elements are not in phase. Besides such giant micropulsations, others of much less intensity and very short periods (5 to 15 seconds) occur at different parts of the earth. These small micropulsations seem to occur simultaneously all over the world. The micropulsations usually occur around midnight and show a tendency to occur at an interval of 27 days.

A more complete discussion of micropulsations may be found in references 18 to 23.

#### CURRENT SYSTEMS

The current systems (refs. 1, 2, 4, 24, and 25) that produce the transient magnetic fields are the result of motions of ionized layers of gas in the atmosphere and of charged elementary particles encircling the earth in the outer atmosphere (the exosphere). The upper atmosphere is ionized primarily by ultraviolet light and X-radiation from the sun. In addition, corpuscular streams from the sun also ionize the atmosphere but primarily at the auroral regions and provide the particles that encircle the earth in the exosphere. The ionized layers obtain their motion from potential differences, heating effects, and gravitational tides. For an observer on the earth's surface, there is an apparent motion as a result of the earth's rotation.

It is impossible to evaluate the distribution of the external current systems and their corresponding magnetic fields from surface data alone because there are infinite possibilities. The external current systems are therefore represented by spherical current sheets of zero thickness concentric with the earth. These current systems are derived by first obtaining the magnetic potential of the transient fields at the earth's surface, similar to the method used for the main earth field, and then solving for the current distribution. (See ref. 1, chs. XVII and XX.)

A much simpler approximation (ref. 1, ch. VII) considers the current system above a point on the earth to be a plane uniform current sheet of infinite horizontal extent. The transient magnetic intensity

and direction at a point immediately below the current sheet will be nearly the same as the transient magnetic intensity and direction existing at the surface after the field of the induced internal currents has been removed.

The sheet current intensity  $\bar{j}$  (current per unit horizontal line width) is tangential to the current sheet and in a direction perpendicular to the variable horizontal intensity due to external sources at the earth's surface in accord with the right-hand rule of electromagnetism. The sheet current intensity  $\bar{j}$  is given by  $\bar{j} = \frac{\bar{H}_{e,s}}{2\pi}$  where  $\bar{H}_{e,s}$  is the surface value of the variable horizontal intensity due to external sources;  $\bar{H}_{e,s}$  does not, in general, have the direction of the total magnetic field.

### $S_q$ Current System

The principal part of the magnetic field of the quiet-day solar daily variation  $S_q$  has its origin in currents external to the earth's surface. The remainder of the  $S_q$  field, about one-third, is the result of internal currents which are induced by the external currents. The external currents are thought to be located in the E-region of the ionosphere.

The external current system calculated from the magnetic-field data in the manner mentioned previously is shown in figure 17 (from ref. 1) for an altitude of 100 kilometers. The current system appears stationary to an observer on the sun. As the earth revolves, a point on a given latitude is brought successively under different parts of the current sheet and experiences a corresponding diurnal variation of magnetic force. The current lines are those along and between which the currents flow in the direction indicated. A current of 10,000 amperes flows between each pair of adjacent lines.

In the daytime, the current is locally intensified along or near the magnetic equator (refer back to fig. 7), indicating a laterally limited current. This current has been named the equatorial electrojet by Sydney Chapman. It has not been included in figure 17.

### L Current System

The external current system that produces the lunar daily variation L is primarily a tidal effect and is thought to be located in the  $F_2$ -region of the ionosphere. This current system is calculated by the same method as was used to determine  $S_q$ . Figures 18(a) and 18(b) (from ref. 1) depict the overhead current system at new moon for the equinoxes

and for the summer solstice, respectively. The meridian refers to the local lunar time. Since the figures are for the new moon, the sun is on the 12-hour meridian. The current lines are drawn 1,000 amperes apart. Similarly as for  $S_q$ , there is also an electrojet near the magnetic equator which is not shown.

#### D Current System

A current system for the average of 40 moderate magnetic storms has been derived by Sydney Chapman. The current system is drawn appropriate to a spherical earth having its geographic and geomagnetic axes coincident. It is intended to correspond, apart from irregular disturbances, with the geomagnetic variations of the earth's field additional to those present on magnetically quiet days - that is, the disturbance D - and is the combination of the two current systems that produce  $S_D$  and  $D_{st}$ .

The complete system of atmospheric currents corresponding to the D-field is shown in figure 19(a) (from ref. 1). A total current of 10,000 amperes flows between successive current lines. The currents are most concentrated along the zones of maximum auroral frequency. This concentrated current in the auroral region is called the auroral electrojet. In the forenoon hemisphere,  $0^h$  to  $12^h$  local time, the current between the auroral zones is everywhere westward; whereas in the afternoon hemisphere, the current, though mainly westward, is reversed at a latitude slightly south of the northern auroral zone and is eastward from there up to the auroral zone. Along the auroral zone itself, the current is westward over the greater part and extends right across the forenoon hemisphere and partly into the opposite hemisphere. The maximum westward intensity, 350,000 amperes at  $6^h$ , considerably exceeds the maximum eastward intensity, 200,000 amperes at  $18^h$ . On the latter meridian the current direction is reversed just within the auroral zone. It is in this region of reversal that the strongest Z-disturbance will occur.

The current system of  $S_D = S_d - S_q$  (fig. 19(b) from ref. 1) consists of 450,000 amperes across the polar cap during a moderate magnetic storm and 50,000 amperes flowing in any one of the four interzonal circuits. The current system of  $S_D = S - S_q$  (that is, for an average day), is only about one-fifth as intense as that of  $S_q$  so that the part of  $S_D$  between the auroral zones is decidedly less important than the  $S_q$  current system on such days, and on quiet days it is still smaller. The part of the  $S_D$  current system over the polar caps is more intense than that of the  $S_q$  current system even on the average day and is far more intense during storms.

The current system at the time of maximum intensity of the storm for  $D_{st}$  (fig. 19(c) from ref. 1) is twice as great (400,000 amperes) between the auroral zones as the combined currents that produce  $S_D$  and occupy the same region. The estimated zonal current along either auroral zone is 75,000 amperes and that within each polar cap up to the pole is 100,000 amperes.

Because the  $D_{st}$  current system between the auroral zones does not decrease on the night side of the earth, the current is thought to be outside the earth's atmosphere in the form of a torus, that is, a ring current about the earth. (See, also, refs. 26-33.) These so-called ring currents are believed to be on the order of a few earth radii distant from the earth with cross sections of 1 to 2 earth radii.

Figures 20 and 21 (from ref. 4) show current systems for the actual disturbance fields. Figure 20 represents the initial phase for the storm of October 14, 1932 and figure 21 represents the main phase for the storm of May 1, 1933. It will be seen, by comparing these currents with the idealized currents, that the storm-time currents of  $D_{st}$  in low latitudes flow from west to east in the initial phase instead of from east to west as in the main phase. The  $S_D$  current system of figure 21(b) resembles that of figure 19(b) in general type, but the polar circuits are much weaker relative to the low-latitude circuits. In the current system for an actual storm (fig. 21) the polar currents, as seen from above, appear to have been given a clockwise rotation relative to the position of the sun as compared with the currents shown in figure 19(a). As seen from figure 21, the auroral-zone currents follow elliptical paths rather than the ideal circular paths of figure 19. The auroral zone tends to expand with increasing intensity of the storms.

### Fluctuation Currents

The largest fluctuations of the earth's field are due to the intense electric currents that flow in the auroral zones. The auroral currents flow west on the morning side of the earth and east on the evening side. These currents are completed by a current sheet flowing across the polar cap toward the sun. Magnetic bays appear to result from a marked intensification of the current system responsible for the disturbance daily variations  $S_D$  and show maximums in frequency corresponding to the morning and evening maximums of the absolute values of  $S_D$ . Fleeting and patchy areas of varying ionization near the auroral zone, due to incoming groups of charged solar particles, may be the cause of many of the rapid small pulsations in current. The main flow of current may thereby be modified by the resulting changes in electric conductivity or electromotive forces in the air in ionized regions. The observed

rapid decay of the fluctuating fields suggests that the electric currents responsible for this decay are near or below the E-region of the ionosphere where the collision frequency of ions and electrons is greater so that rapid decay is possible.

### CORRELATION WITH SOLAR ACTIVITY

Solar phenomena may be roughly classified (ref. 1, p. 394) according to their effect on the earth's magnetism as follows: (1) Individual flares of ultraviolet light produce brief geomagnetic effects simultaneous with radio fadeouts. (2) The general change of ionizing electromagnetic radiation in the course of the sunspot cycle produces a corresponding change in the general intensity of the quiet-day solar daily variation  $S_q$ . (3) Moderate corpuscular radiation produces ordinary aurora and minor magnetic disturbances and is the main factor governing the daily magnetic character figure C. (4) Intense corpuscular radiation produces magnetic storms, expands the aurora to lower latitudes, and is the main factor affecting the u-measure of magnetic activity.

The amplitude of  $S_q$  varies with the sunspot cycle and is notably greater in years of sunspot maximum than in years of sunspot minimum. Figure 22 (from ref. 2) shows the correlation between sunspot numbers and the range R of the annual mean of the horizontal intensity of  $S_q$  at Bombay, India. The horizontal intensity of  $S_q$  is from 50 to 100 per cent greater at sunspot maximum than at sunspot minimum.

The lunar daily variation L shows little variation with the sunspot activity. It is only 20 percent greater at sunspot maximum than at sunspot minimum.

The correlation between magnetic disturbances and solar activity can best be shown by figure 23 (from ref. 1), in which the monthly values of both u and  $u_1$  averaged for each year are compared with the annual sunspot numbers over a period of many years. The relationship between the monthly sunspot numbers and the values of the magnetic activity of the same month (fig. 24 from ref. 1) is not as close as that for the year.

Sunspot groups have been divided into three basic categories (ref. 34): unipolar denoted by  $\alpha$ , bipolar denoted by  $\beta$ , and complex denoted by  $\gamma$ . Unipolar groups are single spots or groups of spots having the same magnetic polarity. Bipolar groups in their simplest form consist of two spots of opposite polarity. Often, however, a bipolar group is a stream of spots in which those in the preceding and those in the following parts of the group have opposite polarities.

Complex or multipolar groups are those having polarities so irregularly distributed that they cannot be classified as bipolar; sharply bounded regions of opposite polarities sometimes exist within the same penumbra. Intermediate between the complex and the bipolar groups are the semi-complex or  $\beta\gamma$  groups in which bipolar characteristics appear but no clearly marked dividing line occurs between the regions of opposite polarities.

The great storms, the type 1 storms, appear to be produced in about equal numbers by  $\gamma$ ,  $\beta\gamma$ , and  $\beta$  spot groups. However,  $\beta\gamma$  and particularly  $\gamma$  spot groups are relatively uncommon spot types and are more likely to be accompanied by a geomagnetic storm. An apparent dependence of storms on area (ref. 34) is a result of the fact that a higher percentage of the  $\gamma$  and  $\beta\gamma$  groups have large sunspot areas. Flare-active spot groups (ref. 16) are more likely to be geomagnetically disturbing than spots deficient in flares or having only an average number of flares. The  $\gamma$  spot groups tend to be more flare active than do the other types. However, for a given relative flare activity, the  $\gamma$  spots appear to be more disturbing geomagnetically than do the other classes. Therefore, it does not appear likely that the greater storm-producing tendency of  $\gamma$  spots arises wholly from their tendency to greater flare activity. Although there is some degree of positive relation between flare activity and geomagnetic conditions, the relation between sunspot magnetic class and geomagnetic conditions is the more pronounced and probably the more basic. On the other hand, magnetic class alone is not sufficient basis for accurate prediction.

Recurrent magnetic storms, type 2 storms, are most common on the declining branch of the sunspot cycle (ref. 16) and scarcest on the rising branch and around sunspot maximum. The hypothetical sources on the sun of the corpuscular streams producing recurrent magnetic storms have been named M-regions by Julius Bartels. The M-regions are most numerous and conspicuous in their effects 1 or 2 years before sunspot minimum and are longer lived phenomena than sunspots. These regions often occur when the visible solar hemisphere is bare of spots and tend to be absent when spots are near the central meridian of the sun.

Other correlations of geomagnetic storms with solar activity have been obtained. (See ref. 16.) Measurements of radiation of 158 Mc/sec have allowed classification of the visible active centers into two groups: Type R, which produces an increase in 158 Mc/sec radiation; and type Q, which produces no change or a slight decrease in 158 Mc/sec radiation. Noisy R spots appear to be the source of relatively dense corpuscular streams and quiet Q spots tend to inhibit the normal evaporation of corpuscles from the corona. The magnetic activity associated with R spots is the sudden-commencement storms rather than the M-region storms. The apparent storm-producing effect of a noisy spot tends to be diminished if it is paired with a quiet spot in the other solar hemisphere.

Passage through the central meridian (CMP) of the sun of active centers that show emission of the  $\lambda 5694$  coronal line tends to be associated with disturbed geomagnetic conditions (large values of  $K_p$ ); whereas CMP of centers in which  $\lambda 5694$  emission is clearly absent tends to be associated with diminished values of  $K_p$ . There is also a tendency for enhanced radio noise of 158 Mc/sec and  $\lambda 5694$  emission to be present or absent together.

Solar M-regions appear to be distinguished by unusual weakness of the green-coronal-line emission  $\lambda 5303$ . The efficacy of the M-region in producing geomagnetic storms is greater when the earth is on the same side of the solar equator as the M-region. The emission of strong  $\lambda 5303$  coronal lines appears to inhibit the escape of corpuscles.

## ROCKET AND SATELLITE MEASUREMENTS

High-altitude sounding rockets, earth satellites, and space probes have recently been used to obtain direct measurements of the geometric field and of the interplanetary magnetic field. The objectives of these measurements are to improve the description of the geomagnetic field both for its intrinsic value and for a more precise determination of the mirror points and orbits of radiation particles; to determine the radial extent of the geomagnetic field; to determine the existence and intensity of extraterrestrial magnetic fields; to locate, identify, and measure the intensity of the various current systems, particularly the ring currents; to examine any instabilities in these fields; and to relate any disturbances in these fields with solar phenomena.

### Comparison With Dipole Field

Measurements of the magnetic field obtained by a number of rockets, satellites, and space probes are presented in figures 25 to 37, in which magnetic intensity is shown as a function of altitude. For all flights except that for Vanguard III (1959 Eta) the measured field has been compared with either the centered or eccentric dipole field. The reason for using the centered dipole field, sometimes called the inverse-cube law, is that the  $n = 1$  term in the spherical harmonic analysis assumes the predominant role with increase in altitude and is easy to calculate. Table XVII (ref. 35) compares the root-mean-square potential for particular values of the degree  $n$  of the spherical harmonic series for various altitudes. The means were taken relative to a distribution over the earth's surface which was calculated from the coefficients of reference 4.

Measured geomagnetic-field data obtained by Vanguard III (refs. 36 and 37) have been compared with calculations based on both the coefficients of reference 8, which go through order  $m = 6$  and degree  $n = 6$ , and the coefficients of the Air Force Special Weapons Center (AFSWC), which go up to order  $m = 17$  and degree  $n = 24$ . (See ref. 9.) (There are two sets of derived AFSWC coefficients: one is derived from the U.S. Naval Hydrographic Charts for 1955 and the other is derived from Russian charts.)

For the rocket shots, the dipole field is matched at the peak altitude to the measured value and extrapolated back toward the earth. For the satellites, the dipole field is evaluated at points along the trajectory. Since, in both cases, the measured value is, in general, the component perpendicular to the spin axis of the vehicle, a knowledge of the position in space and of the attitude of the vehicle is necessary for the comparison.

From figures 25 to 37, it is seen that there was good agreement between the dipole field and the measured field, especially at the higher altitudes, as was expected. The major discrepancies are caused by surface anomalies, absence of higher order terms in the harmonic series, horizontal movement of the sounding rockets, and penetration of current systems.

#### Comparison With Field Calculated by Use of Higher Order Terms

In order to determine how accurately fields in space can be computed with use of higher order terms based on coefficients determined from analysis of surface charts, the geomagnetic-field data obtained by Vanguard III have been compared with the field values calculated by use of the coefficients of references 8 and 9. Differences between the measured field and the computed fields are shown in figures 25 to 27, in which there is some overlap of the regions covered. These differences are in general not greater than about 1 percent of the main field. The differences shown in these figures are interpreted in reference 37 to mean that the surface charts used for deriving coefficients are in error by at least 1 percent in low latitudes. From figures 25 to 27, a comparison of the differences obtained by using the two sets of coefficients indicates that inclusion of terms in the harmonic series of order greater than six, such as the coefficients discussed in reference 9, gives a better description of the field. (This is a question of accuracy of surface charts, not of mathematics.) If these coefficients (ref. 9), which were derived from the U.S. Naval Hydrographic Office charts are used, the sign of the errors in most regions is the same as the sign of the errors obtained by using a dipole field; whereas, if the coefficients of reference 8 are used, the sign of the error is the same

(that is, all negative) at all but one location. An adjustment to the dipole terms in the former coefficients should yield a better fit to the satellite data at low altitudes.

In figures 25 and 26, apparent discontinuities of the intensity and of the slope are caused by the transition of the orbit due to a weekly computation of the new orbit. The numbers to the right of the plot designate the "orbit week." Within each week there is a definite pattern which implies that the magnetic field is exceptionally stable at these altitudes when magnetic storms are absent.

However, these artificial discontinuities may possibly mask real field discontinuities at the lower edge of the inner Van Allen radiation belt. In order to examine this possibility, differences between the measured and theoretical values based on monthly computations of the new orbit are shown in figure 27. In figure 27(d) the sharp discontinuity of intensity that occurred at 1,250 kilometers in figure 26(a) has disappeared. On the other hand, in some regions the discontinuity in slope is not greatly altered. (Compare fig. 27(c) with fig. 26(b).) It must therefore be assumed either that there are real field discontinuities or that the various effects due to reference field and orbital errors accumulate in such a manner as to give false discontinuities. The reason for the remaining discontinuities will not be resolved until techniques of calculating the satellite's location in space can be improved.

### Magnetic Anomalies

Over the southern tip of Africa, there is a negative magnetic anomaly on the earth's surface that is conspicuous on maps showing total magnetic intensity. This anomaly may have important implications for the distribution of radiation in the region above the earth because of its influence on the mirror points of charged particles trapped in the earth's magnetic field. Thus, Dessler (ref. 38) attributes the decrease in radiation intensity between the inner and outer Van Allen belts to a low mirror altitude for trapped particles that have mirror points in this region. The data obtained by Vanguard III (ref. 36) were used to check whether or not this negative anomaly was still significant at altitude. Results are shown in table XVIII (from ref. 36). These results show that the anomaly is a much sharper feature and has a more negative intensity at altitude than was indicated by the computed field. Thus, the mirror altitude for particles of a given energy will be slightly lower than that predicted from the computed field, an effect which lends added support to Dessler's hypothesis.

The magnitude of another magnetic anomaly, the east Siberian anomaly, has been shown by data collected by the second Soviet cosmic rocket

(Lunik II, 1959 XI) to decrease with altitude considerably slower than was presumed (ref. 39). It is now assumed that the source of this magnetic anomaly is located in the nucleus of the earth at a depth equal to one-half its radius and not in the crust, as was considered earlier.

### Ionospheric Currents

Sounding rockets (refs. 40 and 41) that reached an altitude greater than 100 kilometers (figs. 28 and 29) all show penetration of current systems except for the flight at White Sands Proving Ground (WSPG), New Mexico. Current penetration is indicated by a sudden change of slope from that of the dipole variation. (The dipole variation with altitude is also called the inverse-cube law.) Figure 30 (from ref. 40) shows in greater detail the departure of the measurements obtained from the State University of Iowa (S.U.I.) flights from a dipole variation.

S.U.I. flight number 59 was made a day after a magnetic storm commenced, and magnetic disturbances were still occurring. The current indicated by figure 28(a) and figure 30(a) has its lower boundary at about 90 kilometers and represents the polar-cap current as the rocket passed just north of the auroral electrojet.

All the S.U.I. equatorial flights (figs. 28(b) to 28(d) and 30(b) to 30(d)) show current systems beginning at about 100 kilometers. Flight 83 shows a current flowing from east to west directly opposite to the predicted direction of the equatorial electrojet. It is thought that this current might be the less intense current sheet associated with the  $S_q$  current system in low latitudes. Flights 86 and 87 show penetration into the electrojet. Two distinct layers are indicated. The second layer does not appear to have been completely penetrated. The first layer has a lower boundary at about 97 kilometers and an upper boundary at about 110 kilometers. The height and thickness of the upper layer are uncertain and may vary with the degree of magnetic disturbance, the season, the time of day, and so forth. The greater intensity of the departure from the dipole field for flight 87 was caused by increased magnetic disturbance. It appears from a crude estimate based on data from rocket shots that the width of the equatorial electrojet is greater than 300 kilometers with its center located approximately at the magnetic equator.

The rocket flight at WSPG (fig. 29) did not indicate current penetration. However, this launching was at night and a discontinuity of only 10% to 20% could be expected as compared with a field decrease of 2,800% over the entire flight. Furthermore, a local anomaly has a surface value of about 0.046 gauss, which causes a discrepancy between the dipole field and the measured field.

### Ring Currents

The geomagnetic-field measurements obtained by Explorer VI, 1959 Delta (ref. 42) and by Soviet cosmic rockets I and II (ref. 43) are shown in figures 31 to 33 and indicate current systems probably in the form of toroidal rings - that is, ring currents. Explorer VI data indicate that these currents are located at distances beyond 5 earth radii, whereas the Soviet data indicate a current as close as 3 earth radii. Figure 32 shows data for successive days and suggests a variation of several thousand kilometers in the location of the current system in an interval of 24 hours or less, and figure 31 indicates that the currents can change direction in a relatively short time. (The notation  $B_{\perp}$  of the references has been modified to agree with notation  $F_{\perp}$  used elsewhere herein.)

To determine whether these currents were, in fact, ring currents, a model of the current system was hypothesized (ref. 44) from the data obtained by Explorer VI and the resultant field consisting of the main earth magnetic field and the magnetic field due to the ring current was computed. The model consisted of a current volume cylindrical in shape with a circular cross section of radius  $a$ ; the center of the ring current is located at a distance  $r_0$  from the center of the earth and lies in the geomagnetic equator. The total current has a magnitude  $i$  which is uniformly distributed throughout the volume and is directed westward. A close fit (fig. 34 from ref. 44) to the experimental data was obtained for  $r_0 = 60 \times 10^3$  kilometers ( $\approx 9R_E$ ),  $i = 5 \times 10^6$  amperes, and  $a = 3R_E$  or less.

The data obtained by Explorer VI and shown in figure 34 were taken on the evening side of the earth at about 2100 hours local time. To establish closure of the current system, a model was also made to approximate the data from Pioneer V (1960 Alpha), which passed through the geomagnetic field on the afternoon side of the earth. The results of the approximation are shown in figure 35; for this approximation the model parameters  $r_0 = 50 \times 10^3$  kilometers,  $i = 5 \times 10^6$  amperes, and  $a = 3R_E$  were used. The data of Pioneer V could not be adequately fitted for values of  $a$  less than  $3R_E$ . These models strongly suggest the existence of a ring current around the earth at altitudes of approximately  $8.5R_E$ .

### Magnetic Storm

During the life of Vanguard III a number of magnetic storms occurred (refs. 36 and 37) with intensities ranging from moderate to weak. Field measurements during three of these storms are presented in table XIX

(from ref. 36), in which the simultaneous disturbance values at the satellite are compared with those at a few ground stations. The letters ND indicate that the disturbance was less than the errors in the selection of quiet-hour values. These disturbances are also shown in figure 25.

The magnetic-field disturbances observed by the satellite during the magnetic storms are, with some exceptions, negative when they are negative on the earth's surface. This observation indicates that the main portion of an electric current producing a storm at low latitudes is located at some distance above the inner radiation belt. In the case of one magnetic storm, that of October 3 and 4, 1959, the readings indicate that a current shell existed in the inner part of the outer radiation belt during the main phase of the storm and moved closer to the earth as the storm progressed. It is postulated that a sudden change in the character of this storm at a point in the inner edge of the outer belt is a result of the current shell moving into the gap between the inner and outer radiation belts. This movement is substantiated by measurements of radiation (refs. 45 and 46), which show that the current-producing particles moved abruptly into the gap between the Van Allen radiation belts and were then absorbed by the atmosphere as a consequence of a lowering of their mirror altitudes. Furthermore, a measurement taken a number of hours after this sudden change in character at a point near the inner edge of the outer belt indicated that a current shell was then present slightly below the inner edge of the outer radiation belt. The general picture from the preliminary analysis is that electric current shells occur at different distances from the earth for different storms and that the distance may vary with time during a given storm.

#### Distant Geomagnetic Main Field and Its Instabilities

Measurements of the geomagnetic field on an unusually magnetically quiet day were made by Pioneer I, 1958 Eta (refs. 47 to 49) and are shown in figures 36 and 37 (from ref. 47). The distant-field measurements (fig. 37 from ref. 47) indicate that on such days the dipole field may extend out to 13.6 earth radii. At 78,000 kilometers to 85,000 kilometers, the data suggest a magnetic compression. The component of the field varies from about  $15\gamma$  to  $40\gamma$ , whereas the predicted value has a mean of about  $15\gamma$ . At approximately 93,000 kilometers, the measured value drops to approximately  $5\gamma$ , about one-half the predicted value. Thus, a steep decrease in the field takes place. This sudden drop is consistent either with the assumptions of a moving earth colliding with a stationary interplanetary plasma (ref. 50) or with a solar wind (ref. 51). Moreover, as can be seen from figure 38 (from ref. 49), rotations of the magnetic intensity vector through both large and small angles appear for the distant field. At least some of the rotations that are associated with large angular excursions have characteristic times of the order of 10 seconds.

In addition, almost periodic oscillations in amplitude occur (sometimes accompanied by rotational changes), having lifetimes of 2 to 5 cycles and periods of the order of 10 seconds. In general, the interface between the geomagnetic and the interplanetary magnetic fields may be considered to be between 5 and 10 earth radii from the earth with a magnetic-field total intensity between 0.1 $\gamma$  and 100 $\gamma$ , depending on the solar activity.

### Interplanetary Magnetic Field

In order to extend the investigation into the interplanetary magnetic field, Pioneer V (refs. 52 to 55) was placed in a solar orbit. (See fig. 39 from ref. 53.) The magnetometer data (fig. 40 from ref. 53) showed rapid fluctuations lasting throughout entire transmission periods, long intervals of constant field values, and isolated peaks sharply interrupting otherwise steady readings. From figure 41 (ref. 52), which represents values of  $F_1$  averaged over each period of data transmission, it is apparent that the field, except for a few excursions, lies between 2 $\gamma$  and 5 $\gamma$ . These observations suggest that, at this stage of the solar cycle, the interplanetary magnetic field, when undisturbed, is nearly constant in magnitude and nearly uniform in direction over the region explored so far.

These observations are inconsistent with many models of the interplanetary field (ref. 52) including the tacit assumption that the field is essentially zero. Thus, if the field were imbedded in clouds of turbulent gas emitted from the sun, the measurements would be much more irregular. Furthermore, not all clouds would be expected to have the same field strength and the orientations would be sufficiently varied to produce noticeable variations in  $F_1$ . On the other hand, a galactic interstellar field that is uniform over the solar system, although plausible in regard to intensity, would appear to preclude the arrival at the earth of solar cosmic rays of energy below  $10^{10}$  ev. The measured interplanetary field could be due to a solar dipole produced by currents in the sun, but in this case fields throughout the photosphere of the order of 200 $\gamma$  would be required. No evidence of any such fields exists. A final suggestion is that the interplanetary field might originate in a ring current with a radius of 5 to 20 solar radii in the equatorial plane of the sun. This hypothesis holds promise in many respects but faces serious difficulties when confronted by work on comet tails and is inconsistent with most current ideas on the nature of the solar wind. It is hoped that additional light can be cast on these models with future observations.

In reference 54, Pioneer V measurements are compared with magnetic indices at the earth's surface and are correlated with magnetic storms. For this comparison, individual data transmissions were averaged over intervals of  $\frac{1}{2}$  day. A smoothed graph was then produced by plotting the

mean of  $(F_{\perp,j-1})_{av}$ ,  $(F_{\perp,j})_{av}$ , and  $(F_{\perp,j+1})_{av}$  instead of each  $\frac{1}{2}$ -day magnetic field average  $(F_{\perp,j})_{av}$ . A smoothed magnetic-index curve at the earth's surface was prepared in exactly the same manner; the magnetic index used for this purpose was the average of the four 3-hour planetary equivalent amplitudes  $a_p$  occurring in each 12-hour period. These  $\frac{1}{2}$ -day intervals were used inasmuch as they were considered to be long enough to diminish the influence of short-term transients and short enough to display the correlation with short magnetic storms.

The comparison of Pioneer V data with the magnetic indices is shown in figure 42 (from ref. 54). Qualitative agreement of the two curves is strikingly evident. All but one of the magnetic-field excursions at the probe is matched by a similar excursion at the earth. In addition, of the 15 maxima in the probe data (including the rise on April 30, 1960) 14 are accompanied closely or followed within 1 day by the occurrence of magnetic storms at the earth. The one exception to the agreement between probe data and magnetic-index data or magnetic storms is the excursion of March 19 to 21. However, although no magnetic storms for this period appeared in reference lists of storms, disturbances were noted at College, Alaska. It is concluded from these data that enhancement of at least one magnetic-field component of the interplanetary magnetic field regularly accompanies terrestrial magnetic storms. Furthermore, this enhancement cannot be restricted exclusively to a magnetic-field component directed along radial lines from the sun since the probe was nearly normal to the sun-payload radius during an appreciable part of the observation period.

Further comparisons are made in figure 43 (from ref. 53) in which the occurrence of solar flares is also included. In this figure,  $F_{\perp,av}$  for the probe data is the difference between the average of one transmission interval and the next. The magnetic index is the 3-hour planetary equivalent amplitude  $a_p$ . Flares of importance smaller than 1+ have been disregarded. The arrowheads under the graph signify sudden-commencement storms and the designation M indicates the beginning of M-region storms. It will be noted that there are fewer magnetic storms shown on figure 43 than on figure 42. This discrepancy is the result of an incomplete analysis in reference 53, which is a preliminary report.

It is clear from figure 43 that the heaviest flare activity and the strongest perturbations are related. The generally intense solar activity during the final days of March and the early part of April 1960 was accompanied by corresponding storm activity both at the positions of the probe and on the earth, while several isolated flares are followed by isolated probe and terrestrial features. The occurrence of a class 2 flare on March 14 may have caused the sharp peak in the data of March 16 in the midst of what is supposed to have been an M-region storm, while the flares

at the latter part of April, coming after a long quiet period, are assumed to be the origin of the disturbances of April 23 and 28 at the earth and of the preceding fluctuations at the probe. Three of the four largest observed perturbations at the probe were preceded within 2 days by flares of importance  $\geq 2$ . Lesser storms recorded by Pioneer V were preceded in 12 out of 16 instances by major flares, and there was no major flare which was followed by entirely quiescent values at the probe. The three peaks in the probe data of March 20 and 26 and April 19, which are unaccounted for in the comparison with the planetary index, are also distinguished by the absence of any likely preceding flare event, in spite of almost complete flare patrol coverage. It is concluded, nevertheless, that most moderate to strong fluctuations in the interplanetary magnetic field seen in the Pioneer V data are related to the occurrences of major flares.

In reference 55 an attempt is made to obtain a better correlation of solar flares with Pioneer V data and the magnetic storms and thus explain the lack of concurrency of some of the events shown in figure 43. Reference 55 uses a solar flare index rather than flare importance which incorporates the number of flares occurring in a given time interval and the area on the sun covered by each flare. All optically observed  $H_{\alpha}$  flare events which occurred during the period March 10 to April 30, 1960, excluding only subflares, are used for this flare index.

In order to obtain the flare index, the corrected flare area, which is the true flare area as opposed to the flare area viewed from the earth, was partitioned into seven ranges of magnitude: 0 to 3, 3 to 4, 4 to 5, 5 to 7, 7 to 11, 11 to 16, and  $>16$  square degrees. The  $\frac{1}{2}$ -day sum, over all ranges, of the product of the number of flares contained in each range by the lower limit of that range was computed and its ratio to the number of observation hours during the same 12-hour period was taken as a  $\frac{1}{2}$ -day index of flare activity. For the lowest range (0 to 3 square degrees) the number 1, rather than 0, was used as the range value. For the ambient magnetic-field disturbances at the probe, the mean, taken over each  $\frac{1}{2}$  day, of the maximal values recorded during each transmission for that  $\frac{1}{2}$ -day period was computed. This procedure exaggerates intervals of high overall irregularity and accentuates relatively large individual disturbances. The data obtained are shown in figure 44 (from ref. 55). The flare-index curve has been shifted 2 days to the right with respect to the probe time scale as this shift showed the best uniform fit between the two curves when the time lag of the occurrence of the event at the sun and the probe was considered. Corresponding peaks in the two curves have been numbered. Omitted portions of the curves correspond to intervals

in which data transmission from the probe was too infrequent to provide continuity. Magnetic-storm occurrence is also indicated by horizontal bars.

As in figure 43, figure 44 shows that relatively high readings in the magnetometer record can be consistently identified with elevated portions of the flare index curve when the new flare criterion is used. Only a few peaks of the flare index curve are without corresponding effects in the probe magnetic-field curve. Correlation between the two curves is markedly better than that between either curve and geomagnetic-storm incidence. However, the important point is that the correlation between the flare index and probe data is much better in figure 44 than in figure 43. This higher degree of agreement indicates that, although the largest flares are the most probable source of magnetic disturbances at the probe, flares of lesser importance but of sufficient density of occurrence and area produce significant disturbances at the probe. In addition, figures 42, 43, and 44 indicate that flares of lesser importance are of greater significance for conditions outside the earth's magnetosphere than at the earth's surface. This greater significance can be seen most clearly in the three figures for the periods of March 19 to 20 and April 21 to 22, 1960. The use of smoothing as in figure 42 shows that events conspicuous at the earth's surface were associated with temporary changes in the background level itself as distinguished from the appearance of transients against the background level.

In addition to the new criterion for flare index, reference 55 also examined briefly the possibility of correlation of the probe data with measures of solar activity other than solar flares, such as coronal emission, sunspot numbers, and 2,800 Mc/sec radio noise. This study showed an apparent absence of correlation.

Delay times and velocities of the disturbances traveling outward from the sun to the probe were obtained from the corresponding numbered peaks in figure 44 which serve as guides to the pairing of specific flares and subsequent storms at the probe. The flare or flares identified in each pairing were those that contributed most to the corresponding peak in the flare-index curve; whereas, events at the probe were defined by noting the first appearance of high readings of the measured field responsible for the peaks in the payload curve. In only one pairing was the  $H_{\alpha}$  activity dominated by a single event. In all other situations the presence of two or more events created an ambiguity so that each flare had to be considered. Each set of events is summarized in table XX (from ref. 55) together with the velocities calculated for the corresponding time lags. The lowest velocity possible under the assumed correspondences is 580 and the highest is 1,670 km/sec. The average of the lower limit for all sets of events is 752 and of the upper limit is 1,140 km/sec. These results are consistent with velocities usually inferred for corpuscular streams.

In reference 55, it is thought that the reason that the events at the probe were poorly detected at the earth is associated with the dimensions of the corpuscular cloud and/or the total disturbance energy. It is thus proposed that the surface field at the earth is relatively insensitive to disturbances detected as brief transients by the probe but not to events of more persistent duration at the probe even though of lesser peak amplitude.

In reference 53, disturbance velocities computed for the travel distance from probe to earth averaged under 100 km/sec for four events: March 14 to 16, March 27 to 28, April 21 to 22, and April 25 to 26, 1960. This average velocity implies that the traveling disturbances spend as much time in passage from the vicinity of the probe to the earth, a distance of about  $7 \times 10^6$  kilometers, as in passage from the sun to the probe. Possible interpretations were that either the disturbances were subjected to a detour between the position of the probe and the earth or a considerable deceleration occurred which slowed them in transit to approximately one-tenth of their average velocity over the entire sun-probe distance. However, in the light of the statements of the preceding paragraph, these unaccountable delays may now be explained as the detection by Pioneer V of events unobserved at the earth's surface. In particular, the events of April 21 and 22 which contributed the most to the appearance of a phase lag in the averaging process (fig. 43) are seen to be without a companion magnetic-storm effect at the earth (fig. 44).

### Lunar Magnetic Field

Explorations of the moon's magnetic field have also been made. The second Soviet cosmic rocket (ref. 39) indicated that the magnetic field near the moon's surface does not exceed  $60\gamma$ , the order of sensitivity of the vehicle's magnetometer. Furthermore, there was no indication of an inverse cube variation near the moon.

Reference 56, however, points out that this single piece of data is inconclusive and suggests that, if a general lunar magnetic field exists, it will be confined by the solar corpuscular radiation to a thin layer above the sunlit surface. Yet, it could extend a considerable distance beyond the surface on the side away from the sun. It is maintained that the upper limit to the strength of the magnetic field which can be compressed so by the solar wind is on the order of  $1.4 \times 10^3\gamma$ . Since there is evidence that corpuscular radiation is incident without noticeable deflection on the lunar surface, the magnetic field can be no larger than this value. It is estimated that, if the moon has a surface field strength of  $700\gamma$  in the absence of the solar wind, the field strength in the presence of this wind would drop to  $1/e$  of this value at approximately 500 meters above the surface on the sunlit side. In this field the transverse displacement for protons that have velocities of 1,000 km/sec is

only about 8 meters which is hardly detectable. Thus, the question of a lunar magnetic field is still open.

#### APPROXIMATIONS USED IN CALCULATING FIELD CHANGES IN PASSING THROUGH A CURRENT SYSTEM

The material presented in this section is essentially quoted from reference 34.

In making first estimates of the change in  $F$  along the path of a rocket passing through a current system, it is convenient to idealize a current-carrying layer, whose thickness is small compared with its lateral extent, and to treat it as a mathematically thin current sheet. At each point the vector sheet current intensity  $\vec{j}$  is tangential there to the surface and is the integral of the volume current intensity  $\vec{J}$  through the actual layer. The change in  $F$  on passing through such a surface is discontinuous but will approximate to the total continuous change occurring in passing through the actual layer.

An analogous but less appropriate idealization is to treat an electrojet as a current  $\vec{i}$  along a mathematical line,  $\vec{i}$  being the integral of  $\vec{J}$  over the normal cross section of the electrojet. But the field of such a line current tends to infinity near the line and the line model is therefore useful only for points outside the electrojet, not for the more interesting regions inside it.

The field of a uniform sheet current intensity  $\vec{j}$  over an unbounded plane is opposite on the two sides, perpendicular to  $\vec{j}$ , and of magnitude  $2\pi j$  gauss if  $j$  is expressed in cgs electromagnetic units.

The field of a uniform current  $\vec{i}$  along an unbounded straight line, at a point  $P$  at a distance  $l$  from the nearest point  $P_0$  on the line, is perpendicular to  $\vec{i}$  and to  $P_0P$  and of magnitude  $2i/l$  gauss. This field is the same as the field outside a current  $i$  uniformly distributed over the circular cross section of a cylinder unbounded in both directions; inside the cylinder the field preserves the same direction along any radius from the axis, and its magnitude decreases uniformly from the surface to the axis of the cylinder. If the cross section is elliptic instead of circular, the field inside and outside is less simple, but still calculable.

The discontinuous change of  $F$  in passing perpendicularly at a point  $P$  through a current sheet, not necessarily uniform or plane, and forming part of a current system which may contain electrojets is due to the local part of the current sheet near  $P$ , and this part may be regarded as plane

and carrying a uniform surface current density  $\bar{j}$  equal to its local value at P. Thus the change is of magnitude  $4\pi j$  gauss, perpendicular to  $\bar{j}$ , and parallel to the tangential plane at P; the change of the part of  $\bar{F}$  due to the rest of the current system will be inappreciable in the infinitesimal change of position from one side of the sheet to the other.

In crossing the actual current layer, its thickness may be indicated by the part of the path along which the variation of  $\bar{F}$  differs from the theoretically expected variation of  $\bar{F}_0 + \bar{f}_1$  where  $\bar{F}_0$  is the main geomagnetic field and  $\bar{f}_1$  is the field due to internal transient currents induced by the external transient currents;  $\bar{F}_0 + \bar{f}_1$  can then be allowed for in inferring the change of  $\bar{f}_e$ , the field due to the external transient currents, in crossing the sheet. Allowance should also be made for the variation in the region of crossing of the field due to the nonlocal part of the external current system.

The current sheets comprising the  $S_q$  current system (apart from the equatorial electrojet) and the D current system (apart from the auroral electrojet and ring currents) are sensibly spherical, concentric with the earth, and therefore at each point horizontal. Hence, the field discontinuity  $4\pi j$  is also horizontal (and perpendicular to  $\bar{j}$ ). The whole field, however, at the point P of crossing of the sheet (where the local part vanishes), is made up of  $\bar{F}_0 + \bar{f}_1 + \bar{f}_e'$ , where  $\bar{f}_e'$  denotes the nonlocal part of  $\bar{f}_e$ . If the field at P is denoted by  $\bar{F}'$ , the field above and below P is  $\bar{F}' \pm 2\pi\bar{j}'$ , where  $\bar{j}'$  has the same magnitude as  $\bar{j}$  but is turned through  $90^\circ$  about the vertical according to the right-hand rule.

Although  $\bar{j}'$  is assumed to be everywhere horizontal, the vectors  $\bar{j}'$  and  $\bar{F}'$  are not in general parallel, and a rocket-borne magnetometer that measures only  $\bar{F}$  will not necessarily indicate the full field change of  $4\pi j'$ . This, of course, will be the condition away from the magnetic equator where  $\bar{F}'$  not only has a vertical component but its horizontal component is not necessarily parallel to  $\bar{j}'$ . However, if  $2\pi j'/F'$  is small, the discontinuity of  $\bar{F}$  in passing through the current sheet is approximately  $4\pi j' \cos \sigma$ , where  $\sigma$  is the angle between  $\bar{F}'$  and  $\bar{j}'$ . Therefore, under these conditions, it is possible to determine the field change and the current intensity if  $\sigma$  is known or can be reliably inferred.

At the magnetic equator,  $\bar{F}'$  and  $\bar{j}'$  are both horizontal and parallel to each other, as the current  $\bar{j}$  is directed either eastward or westward in accordance to the  $S_q$  and D current systems. Hence, the magnitude of  $\bar{F}'$  is  $F \pm 2\pi j$  on the two sides of the current sheet, and a rocket-borne magnetometer that measures only  $\bar{F}$  measures the full field change of  $4\pi j'$  and determines the current intensity  $\bar{j}$ .

Rocket-borne magnetometers that pass through the auroral zones with a north-south horizontal component can measure the field changes and current intensity by using the sheet-current approximation if, as seems likely, the thickness of the auroral arc is small compared with its nearly vertical extension along the lines of magnetic force. In this instance  $\bar{\mathbf{j}}$  is horizontal and lies along the east-west direction of the auroral arc, that is, nearly along the magnetic east-west direction. Hence  $\bar{\mathbf{j}}'$  will be along or opposite the local (almost vertical) direction of the main field  $\bar{\mathbf{F}}_0$ , so that (as  $\bar{\mathbf{F}}'$  is almost equal to  $\bar{\mathbf{F}}_0$ )  $\mathbf{F}$  is  $\mathbf{F}' \pm 2\pi\mathbf{j}$  on the two sides of the arc. Because of the large disturbances in the auroral zone, the measured field changes are hard to determine and depend on the path through the auroral zone.

#### ALTITUDE EXTRAPOLATION OF MAGNETIC INTENSITY

In the preceding section, it was shown that the current systems can be approximated by sheet and line currents. With these models, estimates of the magnetic intensity can be made for various altitudes.

When the sheet-current approximation is used, for altitudes below the current system  $\bar{\mathbf{F}}_e$  is constant with altitude and equal to  $\bar{\mathbf{H}}_{e,s}$  where  $\bar{\mathbf{H}}_{e,s}$  is the horizontal intensity due to the external current at the earth's surface. The sheet current intensity  $\bar{\mathbf{j}}$  is estimated and the magnetic intensity immediately above the current sheet is, as in the preceding section, taken as  $\bar{\mathbf{F}}' - 2\pi\bar{\mathbf{j}}'$ . The magnetic intensity due to the electrojets, assumed to be line currents, can be extrapolated from a number of points on the surface of the earth in the vicinity of the electrojets by means of Taylor series (ref. 57). Then, for points  $P$  adjacent to the electrojets, the magnetic intensity is given by

$$\bar{\mathbf{F}}' + \frac{2(\bar{\mathbf{l}} \times \bar{\mathbf{l}})}{l^2}.$$

The heights of the upper surfaces of the current sheets and the electrojets are estimated from rocket shots. A spherical shell is assumed to be concentric with the earth at the height of the upper surface of the current sheet and the magnetic-field-intensity distribution at this height is determined as in the previous paragraph. The method of spherical harmonic analysis is applied, and the magnetic intensity can be extrapolated above the ionosphere. When the current systems have been mapped in greater detail, the procedure of reference 6 may be used.

## MAGNETOMETERS

Heppner (ref. 58) has presented a table in which some of the basic differences between the various magnetometers in use are illustrated. This table is reproduced here with some modification in the interest of clarity as table XXI. Reference 59 is a bibliography on magnetometers, the references of which contain detailed information of specific magnetometers.

## CONCLUDING REMARKS

Throughout the years, extensive investigations of the geomagnetic field have been made from which considerable knowledge has been obtained. These investigations have for the most part been restricted to the surface of the earth and are well documented. Recently, however, rockets and satellite measurements have opened the new frontier of magnetic-field investigation in space. Since the results obtained from these rockets and satellites are new and still somewhat controversial, the following conclusions are restricted to these recent rocket and satellite measurements:

The dipole field is a good first approximation of the variation of the geomagnetic field with altitude. However, an improved description of the geomagnetic field with altitude can be obtained by including higher order terms in the harmonic series. This permits the magnetic field in space to be computed to within 1 percent from analysis of surface charts.

The negative magnetic anomaly over south Africa is found to be a sharper feature and to have more negative intensity than was shown by the computed field. This discovery supports the idea that the mirror altitude for reflection of trapped particles is especially low in this region and may be the cause of the slot between the Van Allen radiation belts. In addition, the east Siberian anomaly has been found to decrease considerably slower with altitude than was presumed.

Ionospheric currents occur at heights of the order of 100 kilometers and may consist of more than one layer. The lowest layer is about 10 kilometers thick. The equatorial electrojet appears to have a width greater than 300 kilometers with its center located approximately at the magnetic equator.

Ring currents have been indicated at altitudes beyond 3 earth radii. These currents show variations of thousands of kilometers in position in intervals of 24 hours or less. Changes in direction of the currents occur within relatively short times. During magnetic storms, the main

portion of the ring current appears to be located in the inner part of the outer radiation belt during the main phase and to move closer to the earth as the storm progresses. The current-producing particles move into the gap between the Van Allen radiation belts and are absorbed by the atmosphere in consequence of a lowering of their mirror altitudes.

The interface between the geomagnetic field and the interplanetary magnetic field is between 5 and 10 earth radii from the earth. The magnetic field at this interface has a total intensity between 0.1 $\gamma$  and 100 $\gamma$ . Both position and field strength depend on the solar activity. At these distances, almost periodic oscillations in amplitude occur, sometimes accompanied by rotational changes of the field direction.

The interplanetary magnetic field is nearly constant in magnitude between 2 $\gamma$  and 5 $\gamma$  and nearly uniform in direction. In addition, there is strong agreement in the daily trends and in the occurrences of magnetic disturbances between the interplanetary field and the field at the earth's surface. Most moderate to strong fluctuations in the interplanetary magnetic field, according to Pioneer V (1960 Alpha) data, follow closely after the occurrence of major flares. Flares of lesser importance are of greater significance for conditions outside the earth's magnetosphere than at the earth's surface. Events conspicuous at the earth's surface are associated with temporary changes in the background level of the magnetic field at the probe; whereas, the appearance of transients against the background level at the probe are indistinguishable at the earth's surface. The cause of the change of background level of the magnetic field as opposed to the transients is thought to be the difference in sizes and duration of the corpuscular clouds in transit.

At this time no evidence of a lunar magnetic field has been discovered. Any such field appreciably above the surface of the moon is indicated by a Soviet cosmic rocket to be less than 60 $\gamma$ , the lower limit of the rocket's magnetometer.

Langley Research Center,  
National Aeronautics and Space Administration,  
Langley Air Force Base, Va., November 21, 1961.

## REFERENCES

1. Chapman, Sydney, and Bartels, Julius: Geomagnetism. The Clarendon Press (Oxford), 1940.  
Vol. I - Geomagnetic and Related Phenomena.  
Vol. II - Analysis of the Data, and Physical Theories.
2. Mitra, S. K.: The Upper Atmosphere. Second ed., The Asiatic Society (Calcutta, India), 1952. (Available from Hafner Pub. Co., New York.)
3. Elsasser, Walter M.: The Earth as a Dynamo. Scientific American, vol. 198, no. 5, May 1958, pp. 44-48.
4. Vestine, E. H., Laporte, Lucile, Lange, Isabelle, and Scott, W. E.: The Geomagnetic Field, Its Description and Analysis. Pub. 580, Dept. Terrestrial Magnetism, Carnegie Inst. of Washington, 1959.
5. Anon.: Geomagnetic and Solar Data. Jour. Geophys. Res., vol. 59, no. 3, Sept. 1954, pp. 423-431.
6. Zmuda, Alfred J.: A Method of Analyzing Values of the Scalar Magnetic Intensity. Jour. Geophys. Res., vol. 63, no. 3, Sept. 1958, pp. 477-490.
7. Schmidt, Adolf: Tafeln der Normierten Kugelfunktionen. Engelhard-Reyher Verlag (Gotha), 1935.
8. Finch, H. F., and Leaton, B. R.: The Earth's Main Magnetic Field - Epoch 1955.0. Geophys. Supp. No. 7, Monthly Notices, Roy. Astronomical Soc., 1957, pp. 314-317.
9. Jensen, Duane C., and Whitaker, W. A.: Spheric Harmonic Analysis of the Geomagnetic Field. Paper presented at 41st Annual Meeting, American Geophys. Union (Washington, D.C.), Apr. 1960.
10. Williams, V. L.: The Simultaneity of Sudden Commencements of Magnetic Storms. Jour. Geophys. Res., vol. 65, no. 1, Jan. 1960, pp. 85-92.
11. Kozik, S. M.: Magnetic Disturbances of the "Sudden Onset" Type at Tashkent. Selected Articles From Trudy Nauch - Issl. Inst. Lemmogo Magnetizma (No. 5(15)). ATIC-293930, F-TS-10008/V, U.S. Air Force, 1950, pp. 80-98. (Available from ASTIA as AD No. 137562.)

12. Forbush, S. E., and Vestine, E. H.: Daytime Enhancement of Size of Sudden Commencements and Initial Phase of Magnetic Storms at Huancayo. Jour. Geophys. Res., vol. 60, no. 3, Sept. 1955, pp. 299-316.
13. Fukushima, Naoshi III.: Some Characteristics of Magnetic Storms (I) - (Magnetic Storm on August 3, 1949). Rep. of Ionosphere Res. in Japan, vol. 5, 1951, pp. 85-97.
14. Nagata, Takesi II.: Distribution of  $SC^*$  of Magnetic Storms. Rep. of Ionosphere Res. in Japan, vol. 6, 1952, pp. 13-30.
15. Matsushita, S.: On Sudden Commencements of Magnetic Storms at Higher Latitudes. Jour. Geophys. Res. (Letters to Editor), vol. 62, no. 1, Mar. 1957, pp. 162-166.
16. Bell, Barbara, and Glazer, Harold: Geomagnetism and the Emission-Line Corona, 1950-1953. Smithsonian Contributions to Astrophysics, vol. 2, no. 5, 1957, pp. 51-107.
17. Fleming, J. A., ed.: Terrestrial Magnetism and Electricity. McGraw-Hill Book Co., Inc., 1939.
18. Campbell, W. H.: Studies of Magnetic Field Micropulsations With Periods of 5 to 30 Seconds. Jour. Geophys. Res., vol. 64, no. 11, Nov. 1959, pp. 1819-1826.
19. Jacobs, J. A., and Sinno, K.: Occurrence Frequency of Geomagnetic Micropulsations, Pc. Jour. Geophys. Res., vol. 65, no. 1, Jan. 1960, pp. 107-113.
20. Kato, Yoshio, and Watanabe, Tomiya: A Survey of Observational Knowledge of the Geomagnetic Pulsation. Sci. Reps., ser. 5, vol. 8, Tôhoku Univ. (Japan), 1957, pp. 157-185.
21. Obayashi, T., and Jacobs, J. A.: Geomagnetic Pulsations and the Earth's Outer Atmosphere. Geophys. Jour. of Roy. Astronomical Soc., vol. 1, no. 1, Mar. 1958, pp. 53-63.
22. Scholte, J. G. J.: On the Theory of Giant Pulsations. Jour. Atmospheric and Terrestrial Phys., vol. 17, no. 4, Feb. 1960, pp. 325-336.
23. Storey, L. R. O.: An Investigation of Whistling Atmospherics. Phil. Trans. Roy. Soc. London, ser. A, vol. 246, no. 908, July 9, 1953, pp. 113-141.

24. Chapman, Sydney: Rockets and the Magnetic Exploration of the Ionosphere. Rocket Exploration of the Upper Atmosphere, R. L. F. Boyd and M. J. Seaton, eds., Pergamon Press Ltd. (London), 1954, pp. 292-305.
25. Martyn, D. F.: The Morphology of the Ionospheric Variations Associated With Magnetic Disturbance - I. Variations at Moderately Low Latitudes. Proc. Roy. Soc. (London), ser. A, vol. 218, no. 1132, June 9, 1953, pp. 1-18.
26. Dessler, A. J.: Large Amplitude Hydromagnetic Waves Above the Ionosphere. Jour. Geophys. Res., vol. 63, no. 3, Sept. 1958, pp. 507-511.
27. Dessler, A. J., and Parker, E. N.: Hydromagnetic Theory of Geomagnetic Storms. Jour. Geophys. Res., vol. 64, no. 12, Dec. 1959, pp. 2239-2252.
28. Parker, E. N.: Electrical Conductivity in the Geomagnetic Storm Effect. Jour. Geophys. Res. (Letters to Editor), vol. 63, no. 2, June 1958, pp. 437-438.
29. Parker, E. N.: Inadequacy of Ring-Current Theory for the Main Phase of a Geomagnetic Storm. Jour. Geophys. Res., vol. 63, no. 4, Dec. 1958, pp. 683-689.
30. Hines, C. O., and Storey, L. R. O.: Time Constants in the Geomagnetic Storm Effect. Jour. Geophys. Res., vol. 63, no. 4, Dec. 1958, pp. 671-682.
31. Hines, C. O., and Parker, E. N.: Statement of Differences Regarding the Ring-Current Effect. Jour. Geophys. Res., vol. 63, no. 4, Dec. 1958, pp. 691-692.
32. Hines, C. O., and Parker, E. N.: Statement of Agreement Regarding the Ring-Current Effect. Jour. Geophys. Res. (Letters to the Editor), vol. 65, no. 4, Apr. 1960, pp. 1299-1301.
33. Piddington, J. H.: Geomagnetic Storm Theory. Jour. Geophys. Res., vol. 65, no. 1, Jan. 1960, pp. 93-106.
34. Bell, Barbara, and Glazer, Harold: Sunspots and Geomagnetism. Smithsonian Contributions to Astrophysics, vol. 2, no. 8, 1958, pp. 161-179.

35. Ben'kova, N. P.: The Magnetic Field of the Earth at High Altitudes. ATIC 262983, F-TS-8991/V, U.S. Air Force, 1954. (Available from ASTIA as AD No. 128665.)
36. Heppner, J. P., Stolarik, J. D., Shapiro, I. R., and Cain, J. C.: Project Vanguard Magnetic-Field Instrumentation and Measurements. NASA TN D-486, 1960.
37. Heppner, James P., Cain, Joseph C., Shapiro, Ivan R., and Stolarik, John D.: Satellite Magnetic Field Mapping. NASA TN D-696, 1961.
38. Dessler, A. J.: Effect of Magnetic Anomaly on Particle Radiation Trapped in Geomagnetic Field. Jour. Geophys. Res., vol. 64, no. 7, July 1959, pp. 713-715.
39. Zygielbaum, Joseph L., trans.: Preliminary Results of Data Processing From the Second Soviet Cosmic Rocket - September 18-23, 1959. Astronautics Information Trans. No. 12 (Contract No. NASw-6), Jet Propulsion Lab., C.I.T., Oct. 23, 1959.
40. Cahill, Laurence J., Jr.: Magnetic Exploration of the Upper Atmosphere. IGY Rocket Rep. Ser. No. 4, Nat. Acad. Sci., Oct. 31, 1959. (Also available as Rep. No. 59-5, State Univ. of Iowa.)
41. Heppner, J. P., Stolarik, J. D., and Meredith, L. H.: The Earth's Magnetic Field Above WSPG, New Mexico, From Rocket Measurements. Jour. Geophys. Res., vol. 63, no. 2, June 1958, pp. 277-288.
42. Sonett, C. P., Smith, E. J., Judge, D. L., and Coleman, P. L., Jr.: Current Systems in the Vestigial Geomagnetic Field: Explorer VI. Phys. Rev. Letters, vol. 4, no. 4, Feb. 15, 1960, pp. 161-163.
43. Krassovsky, V. I.: Results of Scientific Investigations Made by Soviet Sputniks and Cosmic Rockets. Astronautica Acta, Vol. VI, Fasc. I., 1960, pp. 32-47.
44. Smith, E. J., Coleman, P. J., Judge, D. L., and Sonett, C. P.: Characteristics of the Extraterrestrial Current System: Explorer VI and Pioneer V. Jour. Geophys. Res. (Letters to the Editor), vol. 65, no. 6, June 1960, pp. 1858-1861.
45. Arnoldy, R. L., Hoffman, R. A., and Winckler, J. R.: Observations of the Van Allen Radiation Regions During August and September 1959, Part 1. Jour. Geophys. Res., vol. 65, no. 5, May 1960, pp. 1361-1376.

46. Rothwell, Pamela, and McIlwain, Carl E.: Magnetic Storms and the Van Allen Radiation Belts - Observations From Satellite 1958e (Explorer IV). Jour. Geophys. Res., vol. 65, no. 3, Mar. 1960, pp. 799-806.
47. Sonett, C. P., Judge, D. L., Sims, A. R., and Kelso, J. M.: A Radial Rocket Survey of the Distant Geomagnetic Field. Jour. Geophys. Res., vol. 65, no. 1, Jan. 1960, pp. 55-68.
48. Sonett, C. P.: Magnetic Compression in the Geomagnetic Field as Measured by Pioneer I. Presented at the San Francisco Meeting of the Astronomical Society of the Pacific, June 17-18, 1959. (Abstract in Pub. Astronomical Soc. Pacific, vol. 71, no. 422, Oct. 1959, pp. 390-392.)
49. Sonett, C. P., Judge, D. L., and Kelso, J. M.: Evidence Concerning Instabilities of the Distant Geomagnetic Field: Pioneer I. Jour. Geophys. Res., vol. 64, no. 8, Aug. 1959, pp. 941-943.
50. Hoyle, F.: Suggestion Concerning the Nature of the Cosmic-Ray Cutoff at Sunspot Minimum. Phys. Rev. (Letters to the Editor), vol. 104, no. 1, second ser., Oct. 1, 1956, pp. 269-270.
51. Parker, E. N.: Plasma Instability in the Interplanetary Magnetic Field. The Plasma in a Magnetic Field, Rolf K. M. Landshoff, ed., Stanford Univ. Press, 1958, pp. 77-84.
52. Coleman, P. J., Jr., Davis, Leverett, and Sonett, C. P.: Steady Component of the Interplanetary Magnetic Field: Pioneer V. Phys. Rev. Letters, vol. 5, no. 2, July 15, 1960, pp. 43-46.
53. Greenstadt, E. W., and Moreton, G. E.: Fluctuations in the Interplanetary Magnetic Field and Solar Activity: Pioneer V. Space Tech. Labs., Inc., and Lockheed Solar Observatory, 1960.
54. Greenstadt, Eugene W.: Magnetic Storms in Interplanetary Space as Observed by Pioneer V. Nature, vol. 191, no. 4786, July 22, 1961, pp. 329-331.
55. Greenstadt, E. W., and Moreton, G. E.: A Comparison of Solar Flare Incidence With Magnetic Transients Observed in the Nearby Interplanetary Region by Pioneer V. Space Tech. Labs., Inc., and Lockheed Solar Observatory, 1962.
56. Neugebauer, Marcia: Question of the Existence of a Lunar Magnetic Field. Phys. Rev. Letters, vol. 4, no. 1, Jan. 1, 1960, pp. 6-8.

57. Zmuda, Alfred J.: Limiting Form of Taylor Series Used in Extrapolating Components of the Geomagnetic Intensity. Trans., American Geophys. Union, vol. 37, no. 1, Feb. 1956, pp. 9-12.
58. Heppner, J. P.: Instrumentation for Space Magnetic Field Studies. [Preprint] 1018-59, American Rocket Soc., Nov. 1959.
59. Barber, Edda: Methods of Measuring Magnetic Fields. Astronautics Information Literature Search No. 195 (Contract No. NASw-6), Jet Propulsion Lab., C.I.T., Mar. 3, 1960.

TABLE I.- THE RELATION OF THE  $u_1$ -MEASURE TO THE  $u$ -MEASURE\*

$u$	0.3	0.5	0.7	0.9	1.2	1.5	1.8	2.1	2.7	$\geq 3.6$
$u_1$	0	20	40	57	79	96	108	118	132	140

\*From reference 1.

TABLE II. - Contributing observatories and lower limits of ranges (R) in D, H, or Z  
for three-hour-range indices (K)\*

Observatory (a) and abbreviation (b)		Geographical co-ordinates		For value of K									
(a)	(b)	$\phi$	$\lambda$ E	0	1	2	3	4	5	6	7	8	9
		°	°	$\gamma$	$\gamma$	$\gamma$	$\gamma$	$\gamma$	$\gamma$	$\gamma$	$\gamma$	$\gamma$	$\gamma$
Godhavn	Go	69.2	306.5	0	18	36	72	144	250	430	720	1200	1800
Sodankylä	So	67.4	26.6	0	10	20	40	80	140	240	400	660	1000
College	Co	64.9	212.2	0	25	50	100	200	350	600	1000	1650	2500
Dombaas	Do	62.1	9.1	0	8	15	30	60	105	180	300	500	750
Lerwick	Le	60.1	358.8	0	10	20	40	80	140	240	400	660	1000
Sloutzk	Sl	59.7	30.5	0	6	12	24	48	85	145	240	400	600
Sitka	Si	57.0	224.7	0	10	20	40	80	140	240	400	660	1000
Rude Skov	RS	55.8	12.5	0	6	12	24	48	85	145	240	400	600
Eskdalemuir	Es	55.3	356.8	0	8	15	30	60	105	180	300	500	750
Meanook	Me	54.6	246.7	0	15	30	60	120	210	360	600	1000	1500
Witteveen	Wi	52.8	6.7	0	5	10	20	40	70	120	200	330	500
Niemegk	Ni	52.1	12.7	0	5	10	20	40	70	120	200	330	500
Abinger	Ab	51.2	359.6	0	5	10	20	40	70	120	200	330	500
Chambon-la-Forêt	CF	48.0	2.3	0	5	10	20	40	70	120	200	330	500
Agincourt	Ag	43.8	280.7	0	6	12	24	48	85	145	240	400	600
Cheltenham	Ch	38.7	283.2	0	5	10	20	40	70	120	200	330	500
San Fernando	SF	36.5	353.8	0	4	8	16	30	50	85	140	230	350
Tucson	Tu	32.2	249.2	0	4	8	16	30	50	85	140	230	350
Zô-Sè	ZS	31.1	121.2	0	3	6	12	24	40	70	120	200	300
Honolulu	Ho	21.3	201.9	0	3	6	12	24	40	70	120	200	300
San Juan	SJ	18.4	293.9	0	3	6	12	24	40	70	120	200	300
Kuyper	Ku	- 6.0	106.7	0	3	6	12	24	40	70	120	200	300
Huancayo	Hu	-12.0	284.7	0	6	12	24	48	85	145	240	400	600
Apia	Ap	-13.8	188.2	0	3	6	12	24	40	70	120	200	300
Watheroo	Wa	-30.3	115.9	0	4	8	16	30	50	85	140	230	350
Pilar	Pi	-31.7	296.1	0	3	6	12	24	40	70	120	200	300
Cape Town	CT	-33.9	18.5	0	3	6	12	24	40	70	120	200	300
Amberley	Am	-43.2	172.7	0	5	10	20	40	70	120	200	330	500

\*From reference 4.

TABLE III.- RELATION BETWEEN  $K$  AND  $a_k^*$ 

$K$	0	1	2	3	4	5	6	7	8	9
$a_k$	0	3	7	15	27	48	80	140	240	400

\*From reference 5.

TABLE IV.- RELATION BETWEEN  $K_p$  AND  $a_p^*$ 

$K_p$	0o	0+	1-	1o	1+	2-	2o	2+	3-	3o	3+	4-	4o	4+
$a_p$	0	2	3	4	5	6	7	9	12	15	18	22	27	32
$K_p$	5-	5o	5+	6-	6o	6+	7-	7o	7+	8-	8o	8+	9-	9o
$a_p$	39	48	56	67	80	94	111	132	154	179	207	236	300	400

\*From reference 5.

TABLE V.- APPROXIMATE RELATION BETWEEN  $C_1$  AND  $A_p^*$ 

$C_1$	0.0	0.1	0.2	0.3	0.4	0.5	0.6	0.7	0.8	0.9	1.0
$A_p$	2	4	5	6	8	9	11	12	14	16	19
$C_1$	1.1	1.2	1.3	1.4	1.5	1.6	1.7	1.8	1.9	2.0	
$A_p$	22	26	31	37	44	52	63	80	110	160	

\*From reference 5.

TABLE VI. - Scalings of values of north component (X) of magnetic field intensity for 1945  
expressed in units of  $10^{-4}$  CGS from U. S. Hydrographic Office charts \*

Geographic east longitude in degrees	Geographic colatitude in degrees								
	10	20	30	40	50	60	70	80	90
30	67.4	106.3	150.4	196.8	252.9	304.0	340.0	342.9	309.3
60	50.2	87.4	141.3	196.5	259.9	318.7	362.0	371.9	342.3
90	27.0	68.8	129.7	204.4	285.9	350.0	393.8	405.7	385.4
120	27.8	73.0	144.8	216.3	288.5	341.5	377.0	392.8	387.6
150	36.3	101.5	172.2	233.0	275.9	306.8	331.0	340.3	363.6
180	33.1	111.6	183.8	225.1	246.9	269.2	291.7	320.4	346.1
210	17.4	81.8	142.8	190.8	231.4	258.7	287.0	315.2	331.7
240	1.7	26.6	90.4	155.7	220.1	267.2	301.6	323.2	323.7
270	-	8.2	10.9	55.4	116.0	186.5	246.4	317.6	314.7
300	11.2	41.3	73.2	121.7	170.7	215.6	255.8	283.8	295.3
330	44.4	76.7	114.8	162.1	208.6	243.2	268.4	281.2	270.0
360	69.2	107.2	141.4	189.5	238.4	288.1	316.3	312.5	276.2

Geographic east longitude in degrees	Geographic colatitude in degrees								
	100	110	120	130	140	150	160	170	
30	244.2	178.9	133.0	123.5	131.6	130.7	136.1	104.5	
60	281.4	218.7	163.4	138.1	130.6	124.9	104.0	30.7	
90	333.3	266.1	200.7	148.0	113.9	85.0	38.9	- 48.0	
120	358.5	317.8	255.0	184.8	118.3	61.0	3.4	- 89.0	
150	359.2	329.4	275.5	213.0	142.0	67.0	- 8.7	- 94.0	
180	350.4	326.7	284.0	233.7	176.6	103.5	- 25.0	- 61.0	
210	330.5	312.3	283.9	247.6	204.9	144.5	69.0	- 14.0	
240	311.7	296.9	275.3	253.3	223.1	176.9	111.0	37.0	
270	306.3	277.6	257.4	240.3	233.9	211.5	160.0	103.8	
300	280.3	255.8	236.0	229.2	235.4	238.0	207.0	157.2	
330	243.6	210.0	186.3	185.0	198.9	210.5	215.5	185.0	
360	226.5	178.2	148.3	140.1	152.9	162.3	162.2	164.1	

\* From reference 4.

TABLE VII. - Scalings of values of east component (Y) of magnetic field intensity for 1945  
expressed in units of  $10^{-4}$  CGS from U. S. Hydrographic Office charts \*

Geographic east longitude in degrees	Geographic colatitude in degrees								
	10	20	30	40	50	60	70	80	90
30	9.2	12.3	13.9	9.6	7.9	3.2	- 3.0	- 9.0	- 20.5
60	29.1	37.1	36.8	31.5	24.1	12.8	3.2	- 7.8	- 22.1
90	26.7	27.2	24.3	16.1	5.5	- 3.7	- 11.7	- 15.6	- 22.2
120	11.3	- 12.0	- 25.5	- 34.3	- 29.3	- 18.5	- 2.6	11.7	- 17.6
150	7.0	- 17.4	- 31.0	- 30.3	- 25.1	- 10.7	5.8	21.4	31.8
180	16.5	- 17.7	- 20.6	- 29.2	- 39.5	- 45.5	50.4	54.2	58.5
210	20.7	48.4	67.5	69.4	74.3	65.9	58.9	49.4	53.7
240	9.9	33.8	59.1	70.6	73.2	69.1	62.5	55.8	53.0
270	- 16.0	- 14.4	- 13.3	6.6	13.0	28.5	37.7	46.9	52.1
300	- 43.6	- 65.0	- 65.2	- 69.2	- 65.9	- 60.6	- 52.0	- 42.4	- 31.6
330	- 43.2	- 62.6	- 67.1	- 73.5	- 75.9	- 86.1	- 98.8	- 107.4	- 105.8
360	- 16.1	- 24.7	- 27.5	- 30.7	- 35.6	- 41.0	- 48.4	- 59.0	- 70.4

Geographic east longitude in degrees	Geographic colatitude in degrees								
	100	110	120	130	140	150	160	170	
30	- 29.6	- 38.4	- 43.7	- 54.9	- 67.7	- 92.2	- 136.1	- 164.0	
60	- 38.1	- 57.0	- 75.5	- 93.9	- 111.9	- 137.7	- 165.2	- 174.1	
90	- 33.3	- 56.6	- 77.0	- 100.6	- 115.1	- 123.2	- 136.6	- 134.8	
120	18.2	11.7	0	20.7	40.3	46.3	44.2	77.1	
150	36.5	41.6	44.1	41.4	34.1	26.9	5.0	3.0	
180	63.0	69.4	71.9	76.8	77.9	78.3	70.6	72.7	
210	60.7	69.8	80.3	88.7	97.7	100.1	101.1	114.0	
240	57.8	65.3	77.4	90.7	105.9	123.9	138.1	150.6	
270	59.5	64.6	74.8	91.3	106.6	119.2	134.7	137.7	
300	- 20.1	- 8.9	4.1	19.2	34.8	52.8	77.8	74.6	
330	- 96.4	- 83.6	- 70.0	- 58.3	- 45.2	- 25.1	- 10.5	- 3.2	
360	- 70.3	- 81.6	- 78.9	- 75.1	- 74.3	- 69.6	- 82.5	- 96.7	

\* From reference 4.

TABLE VIII. - Scalings of values of vertical component (Z) of magnetic field intensity for 1945  
expressed in units of  $10^{-4}$  CGS from U. S. Hydrographic Office charts \*

Geographic east longitude in degrees	Geographic colatitude in degrees								
	10	20	30	40	50	60	70	80	90
30	5360	5110	4810	4370	3710	2790	1470	-20	-1390
60	5530	5460	5400	4940	4250	3260	1820	370	-1120
90	5730	5840	5840	5440	4650	3420	1840	160	-1530
120	5780	6110	5930	5420	4520	3280	1870	340	-1180
150	5780	5720	5330	4580	3580	2620	1540	460	-870
180	5730	5510	5080	4180	3370	2550	1750	840	-320
210	5760	5640	5320	4720	3940	3180	2270	1320	140
240	5790	5930	5920	5560	4870	3960	2850	1630	430
270	5690	5810	6080	5980	5480	4680	3610	2350	1120
300	5510	5590	5530	5380	5020	4410	3550	2580	1490
330	5260	5130	4930	4620	4070	3220	2330	1330	300
360	5190	5010	4690	4270	3610	2710	1470	80	-1130

Geographic east longitude in degrees	Geographic colatitude in degrees								
	100	110	120	130	140	150	160	170	
30	-2380	-2050	-2980	-3080	-3300	-3800	-4730	-5450	
60	-2330	-3050	-3260	-3530	-3760	-4480	-5320	-5800	
90	-3000	-4040	-4670	-5020	-5150	-5530	-5980	-6170	
120	-2710	-4060	-5130	-5850	-6420	-6510	-6630	-6530	
150	-2280	-3670	-4860	-5760	-6420	-6850	-6970	-6630	
180	-1680	-3030	-4170	-5070	-5830	-6540	-6670	-6560	
210	-1120	-2270	-3360	-4280	-5140	-5970	-6290	-6370	
240	-670	-1710	-2670	-3580	-4430	-5350	-5630	-5910	
270	-40	-1070	-1870	-2580	-3330	-4120	-4770	-5470	
300	440	-430	-1070	-1660	-2360	-3310	-4240	-5180	
330	570	-1180	-1560	-1880	-2400	-3110	-4120	-5110	
360	-1890	-2290	-2470	-2630	-2950	-3370	-4270	-5200	

\*From reference 4.

TABLE IX. - Values of spherical harmonic coefficients, main field, 1945  
expressed in units of  $10^{-4}$  CGS \*

m	n	$A_n^m$		$\alpha_n^m$	$B_n^m$		$\beta_n^m$
		X	Y	Z	X	Y	Z
1	1	-3057		6114			
2	2	-253		357			
3	3	344		-427			
4	4	368		-499			
5	5	-121		192			
6	6	34		-48			
1	1	-190	-230	455	577	584	-1158
1	2	594	590	-882	-329	-334	514
1	3	-510	-527	703	-154	-157	187
1	4	309	313	-375	70	43	-58
1	5	163	116	-219	-12	42	5
1	6	38	87	-29	1	-85	32
2	2	331	322	-495	124	90	-142
2	3	364	362	-481	61	50	-82
2	4	244	217	-296	-103	-119	146
2	5	82	115	-82	47	24	-52
2	6	10	41	-35	73	103	-88
3	3	243	282	-369	17	-	1
3	4	-153	-151	203	-41	-25	52
3	5	-35	-25	27	-8	-14	1
3	6	-159	-150	170	-18	0	13
4	4	123	120	-146	-51	-51	61
4	5	-71	-74	78	-63	-72	77
4	6	-13	-19	19	2	0	4
5	5	-30	-38	59	26	-51	-55
5	6	14	22	-27	0	9	4
6	6	-60	-69	66	-35	-17	

\*From reference 4.

TABLE X. - The first eight Gauss coefficients of the Earth's magnetic potential (V)  
expressed in units of  $10^{-4}$  CGS\*

Source	Epoch	$g_1^0$	$g_1^1$	$h_1^1$	$g_2^0$	$g_2^1$	$h_2^1$	$g_2^2$	$h_2^2$
Gauss	1835	-3235	-311	+625	+51	+292	+12	-2	+157
Erman-Petersen	1829	-3201	-284	+601	-8	+257	-4	-14	+146
Adams	1845	-3219	-278	+578	+9	+284	-10	+4	+135
Adams	1880	-3168	-243	+603	-49	+297	-75	+61	+149
Fritsche	1885	-3164	-241	+591	-35	+286	-75	+68	+142
Schmidt	1885	-3168	-222	+595	-50	+278	-71	+65	+149
Dyson and Furner	1922	-3095	-226	+592	-89	+299	-124	+144	+84
Afanasieva (8)	1945	-3032	-229	+590	-125	+288	-146	+150	+48
Vestine and Lange	1945	-3057	-211	+581	-127	+296	-166	+164	+54

\*From reference 4.

TABLE XI.- GAUSSIAN COEFFICIENTS EPOCH 1955.0\*

[The reversal of sense between the two systems arises from the change of sign in the definition of the potential]

Gaussian coefficients							
	Solution 1		Solution 2		Solution 1		Solution 2
	1	2			1	2	
	Gauss		Schmidt		Gauss		Schmidt
$g_1^0$	0.3054	0.3055	-0.3055	$g_3^3$	-0.0072	-0.0072	0.0091
$g_2^0$	.0228	.0228	-.0152	$g_4^3$	.0079	.0080	-.0038
$g_3^0$	-.0295	-.0295	.0118	$g_5^3$	.0021	.0017	-.0004
$g_4^0$	-.0419	-.0415	.0095	$g_6^3$	.0229	.0241	-.0024
$g_5^0$	.0198	.0209	-.0027	$h_3^3$	.0008	.0008	-.0009
$g_6^0$	-.0149	-.0150	.0010	$h_4^3$	.0008	.0008	-.0004
$g_1^1$	.0226	.0227	-.0227	$h_5^3$	.0019	.0023	-.0005
$g_2^1$	-.0524	-.0525	.0303	$h_6^3$	.0004	-.0004	.0000
$g_3^1$	.0585	.0586	-.0191	$g_4^4$	-.0023	-.0023	.0031
$g_4^1$	-.0440	-.0440	.0080	$g_5^4$	.0034	.0034	-.0015
$g_5^1$	-.0325	-.0322	.0032	$g_6^4$	.0017	.0016	-.0003
$g_6^1$	-.0108	-.0093	.0005	$h_4^4$	.0012	.0012	-.0017
$h_1^1$	-.0592	-.0590	.0590	$h_5^4$	.0032	.0031	-.0014
$h_2^1$	.0330	.0329	-.0190	$h_6^4$	.0005	.0006	-.0001
$h_3^1$	.0140	.0138	-.0045	$g_5^5$	.0005	.0005	-.0007
$h_4^1$	-.0080	-.0082	.0015	$g_6^5$	-.0001	-.0001	.0000
$h_5^1$	-.0022	-.0017	.0002	$h_5^5$	-.0006	-.0006	.0009
$h_6^1$	.0055	.0044	-.0002	$h_6^5$	.0006	.0006	-.0003
$g_2^2$	-.0137	-.0137	.0158	$g_6^6$	.0007	.0007	-.0011
$g_3^2$	-.0245	-.0244	.0126	$h_6^6$	.0001	.0001	-.0001
$g_4^2$	-.0225	-.0227	.0058				
$g_5^2$	-.0155	-.0155	.0020				
$g_6^2$	-.0013	-.0025	.0002				
$h_2^2$	-.0022	-.0021	.0024				
$h_3^2$	-.0056	-.0057	.0029				
$h_4^2$	.0116	.0121	-.0031				
$h_5^2$	-.0068	-.0075	.0010				
$h_6^2$	-.0177	-.0166	.0011				

\*From reference 8.

TABLE XII. - Probability that daily ranges of horizontal intensity (H), magnetic declination (D), and vertical intensity (Z) will exceed various magnitudes in different geomagnetic latitudes ( $\Phi$ ), 12 months, 1932-33†

Element	Observatory	$\Phi^*$	Probability that daily ranges will exceed magnitude in $\gamma$ of																
			0	50	100	150	200	300	400	500	600	700	800	900	1000	1100	1200	1300	
H	Thule	+88.0	1.000	.943	.730	.490	.298	.098	.035	.012	.003								
	Godhavn	+79.8	1.000	.990	.935	.775	.578	.239	.174	.100	.056	.036	.024	.013	.006	.001			
	Bear Island	+71.1	1.000	.990	.962	.909	.840	.671	.498	.341	.221	.137	.086	.056	.035	.020	.009	.002	
	Juliannehaab	+70.8	1.000	.990	.971	.926	.862	.699	.529	.373	.256	.174	.120	.085	.058	.038	.021		
	Fort Rae	+69.0	1.000	.990	.971	.926	.870	.719	.565	.426	.310	.226	.168	.126	.095	.074	.058		
	Tromsø	+67.1	1.000	.943	.855	.746	.641	.478	.365	.278	.211	.159	.118	.087	.062	.043	.029		
	Petsamo	+64.9	1.000	.909	.735	.633	.549	.427	.331	.252	.189	.139	.098	.067	.044	.027	.015		
	Sodankylä	+63.8	1.000	.862	.592	.478	.402	.299	.231	.181	.144	.115	.090	.070	.053	.037	.025		
	Sitka	+60.0	1.000	.654	.309	.205	.152	.098	.063	.037	.016	.003							
	Rude Skov	+55.8	1.000	.602	.123	.026	.006												
	Cheltenham	+50.1	1.000	.463	.060	.012	.003												
	Tucson	+40.4	1.000	.372	.030	.005													
	Honolulu	+21.1	1.000	.186	.022	.005													
	Huancayo	- 0.6	1.000	.980	.685	.212	.045												
	Pilar	-20.2	1.000	.375	.047	.008	.000												
	Watheroo	-41.8	1.000	.272	.013														
	South Orkneys	-50.0	1.000	.348	.028	.005													
D	Thule	+88.0	1.000	.901	.654	.389	.208	.043	.007	.002									
	Godhavn	+79.8	1.000	.980	.870	.667	.412	.204	.113	.069	.044	.027	.015	.007	.002				
	Bear Island	+71.1	1.000	.971	.885	.741	.585	.353	.198	.096	.037	.012	.003						
	Juliannehaab	+70.8	1.000	.962	.826	.690	.568	.385	.251	.158	.096	.057	.030	.012	.003				
	Fort Rae	+69.0	1.000	.971	.847	.714	.599	.413	.275	.174	.103	.055	.027	.012	.003				
	Tromsø	+67.1	1.000	.885	.602	.467	.362	.217	.132	.086	.055	.031	.014	.003					
	Petsamo	+64.9	1.000	.826	.538	.407	.310	.178	.099	.052	.023	.006							
	Sodankylä	+63.8	1.000	.794	.408	.232	.153	.087	.051	.027	.009	.001							
	Sitka	+60.0	1.000	.855	.418	.222	.128	.056	.031	.015	.004								
	Rude Skov	+55.8	1.000	.725	.176	.061	.022												
	Cheltenham	+50.1	1.000	.746	.173	.043	.012												
	Tucson	+40.4	1.000	.680	.041	.005													
	Honolulu	+21.1	1.000	.403	.008														
	Huancayo	- 0.6	1.000	.176	.008														
	Pilar	-20.2	1.000	.380	.010														
	Watheroo	-41.8	1.000	.595	.056	.016	.007												
	South Orkneys	-50.0	1.000	.488	.064	.013	.005												
Z	Thule	+88.0	1.000	.709	.373	.179	.075	.013	.001										
	Godhavn	+79.8	1.000	.990	.962	.877	.756	.505	.299	.156	.080	.041	.020	.009	.003				
	Bear Island	+71.1	1.000	.990	.935	.855	.756	.599	.375	.244	.164	.113	.078	.049	.028	.012	.003		
	Juliannehaab	+70.8	1.000	.990	.971	.917	.840	.629	.424	.287	.203	.150	.114	.088	.068	.052	.039		
	Fort Rae	+69.0	1.000	.990	.943	.862	.775	.588	.429	.304	.209	.139	.089	.055	.033	.016	.005		
	Tromsø	+67.1	1.000	.917	.741	.565	.446	.306	.205	.139	.091	.058	.035	.020	.009	.004	.001		
	Petsamo	+64.9	1.000	.917	.769	.617	.490	.324	.224	.155	.108	.075	.050	.034	.022	.014	.008		
	Sodankylä	+63.8	1.000	.847	.645	.508	.405	.255	.148	.081	.044	.026	.016	.009	.005	.003	.001		
	Sitka	+60.0	1.000	.637	.424	.284	.193	.104	.063	.044	.028	.016	.008	.002					
	Rude Skov	+55.8	1.000	.364	.126	.059	.039	.025	.011	.003									
	Cheltenham	+50.1	1.000	.137	.024	.007													
	Tucson	+40.4	1.000	.053	.009	.004													
	Honolulu	+21.1	1.000	.483															
	Huancayo	- 0.6	1.000	.011															
	Pilar	-20.2	1.000	.015															
	Watheroo	-41.8	1.000	.408	.125														
	South Orkneys	-50.0																	

† From reference 4.

\* Geomagnetic latitude.

TABLE XIII.- Expectation of number of days elapsing before daily ranges in horizontal intensity (H), magnetic declination (D), and vertical intensity (Z) will exceed various magnitudes in different geomagnetic latitudes ( $\phi$ ), 12 months 1932-33†

Ele- ment	Observatory	$\phi^*$	Expected number of days elapsing before daily ranges exceed magnitude in $\gamma$ of															
			0	50	100	150	200	300	400	500	600	700	800	900	1000	1100	1200	1300
H	Thule	+88.0	1	1	1	2	3	10	28	85	380							
	Godhavn	+79.8	1	1	1	1	2	4	6	10	18	28	41	74	185	740		
	Bear Island	+71.1	1	1	1	1	1	1	2	3	5	7	12	18	29	50	110	445
	Juliannehaab	+70.8	1	1	1	1	1	1	2	3	4	6	8	12	17	27	48	
	Fort Rae	+69.0	1	1	1	1	1	1	2	2	3	4	6	8	10	14	17	
	Tromsø	+67.1	1	1	1	1	2	2	3	4	5	6	8	12	16	23	35	
	Petsamo	+64.9	1	1	1	2	2	2	3	4	5	7	10	15	23	36	65	
	Sodankylä	+63.8	1	1	2	2	2	3	4	6	7	9	11	14	19	27	40	
	Sitka	+60.0	1	2	3	5	7	10	16	27	61	325						
	Rude Skov	+55.8	1	2	8	39	155											
	Cheltenham	+50.1	1	2	17	80	400											
	Tucson	+40.4	1	3	33	200												
	Honolulu	+21.1	1	5	46	215												
	Huancayo	- 0.6	1	1	1	5	22											
	Pilar	-20.2	1	3	21	125	2400											
	Watheroo	-41.8	1	4	75													
	South Orkneys	-50.0	1	3	36	220												
D	Thule	+88.0	1	1	2	3	5	23	150	630								
	Godhavn	+79.8	1	1	1	2	2	5	9	14	23	38	65	140	490			
	Bear Island	+71.1	1	1	1	1	2	3	5	10	27	86	380					
	Juliannehaab	+70.8	1	1	1	1	2	3	4	6	10	17	33	81	300			
	Fort Rae	+69.0	1	1	1	1	2	2	4	6	10	18	37	80	320			
	Tromsø	+67.1	1	1	2	2	3	5	8	12	18	32	72	315				
	Petsamo	+64.9	1	1	2	2	3	6	10	19	43	160						
	Sodankylä	+63.8	1	1	2	4	7	12	20	37	110	1900						
	Sitka	+60.0	1	1	2	4	8	18	32	68	240							
	Rude Skov	+55.8	1	1	6	16	46											
	Cheltenham	+50.1	1	1	6	24	82											
	Tucson	+40.4	1	1	24	180												
	Honolulu	+21.1	1	3	125													
	Huancayo	- 0.6	1	6	125													
	Pilar	-20.2	1	3	104													
	Watheroo	-41.8	1	2	18	64	140											
	South Orkneys	-50.0	1	2	16	75	190											
Z	Thule	+88.0	1	1	3	6	13	80	720									
	Godhavn	+79.8	1	1	1	1	1	2	3	6	12	25	51	110	380			
	Bear Island	+71.1	1	1	1	1	1	2	3	4	6	9	13	20	36	83	330	
	Juliannehaab	+70.8	1	1	1	1	1	2	2	3	5	7	9	11	15	19	25	
	Fort Rae	+69.0	1	1	1	1	1	2	2	3	5	7	11	18	30	61	180	
	Tromsø	+67.1	1	1	1	2	2	3	5	7	11	17	29	51	106	275	1400	
	Petsamo	+64.9	1	1	1	2	2	3	4	6	9	13	20	30	44	71	130	
	Sodankylä	+63.8	1	1	2	2	2	4	7	12	23	38	64	110	190	380	1500	
	Sitka	+60.0	1	2	2	4	5	10	16	23	35	61	130	460				
	Rude Skov	+55.8	1	3	8	17	26	40	90	360								
	Cheltenham	+50.1	1	7	42	150												
	Tucson	+40.4	1	19	110	230												
	Honolulu	+21.1	1	21														
	Huancayo	- 0.6	1	94														
	Pilar	-20.2	1	69														
	Watheroo	-41.8	1	2	8													
	South Orkneys	-50.0																

†From reference 4.

\*Geomagnetic latitude.

TABLE XIV.- Percent of time that three-hour range of disturbance in D, H, or Z is less than the various ranges (R) derived from three-hour-range indices (K) for 1940 from 28 observatories\*

Observatory	Geo-magnetic latitude	Ranges (R) in gammas								
		5	10	20	30	50	75	100	200	500
	°	%	%	%	%	%	%	%	%	%
Godhavn	79.8	0	0	1.3	6.6	19.0	38.9	55.9	83.8	98.3
College	64.5	0	6.6	19.3	29.2	48.8	61.1	69.4	82.1	93.6
Sodankylä	63.8	3.0	19.4	40.8	51.9	63.2	71.6	77.6	90.0	97.8
Lerwick	62.5	0	9.6	34.6	52.6	71.1	82.7	89.3	95.7	98.2
Dombaaas	62.3	11.0	26.1	46.6	61.9	76.7	86.8	90.7	96.1	98.5
Meanook	61.8	0	7.0	32.7	43.1	57.3	68.1	74.9	87.2	96.7
Sitka	60.0	0	16.6	41.5	53.6	70.4	80.1	85.8	94.1	98.0
Eskdalemuir	58.5	0	11.0	40.6	61.3	80.4	91.3	94.8	98.2	99.5
Sloutzk	56.0	2.0	18.9	41.1	59.2	79.7	89.8	94.6	98.1	99.3
Rude Skov	55.8	13.8	34.0	55.5	69.1	84.5	92.0	95.3	98.3	99.5
Agincourt	55.0	7.0	28.0	51.0	65.9	83.1	90.1	93.7	98.1	99.7
Witteveen	54.2	12.4	31.5	58.2	72.1	87.3	94.3	96.7	99.1	99.9
Abinger	54.0	1.7	23.9	53.3	69.3	87.9	94.6	97.1	99.0	99.9
Niemegk	52.2	13.3	38.0	64.9	76.0	88.8	95.0	97.0	99.2	99.9
Chambon-la-Forêt	50.4	17.3	43.7	72.0	83.3	94.3	97.6	98.7	99.8	100.0
Cheltenham	50.1	13.9	35.0	60.7	73.1	88.7	94.8	97.4	99.0	99.9
San Fernando	41.0	13.8	32.3	60.2	75.8	91.1	96.7	98.2	99.6	100.0
Tucson	40.4	21.1	45.0	70.9	85.1	94.6	97.7	98.9	99.6	100.0
San Juan	29.9	37.5	65.6	86.7	93.7	98.0	98.7	99.0	99.9	100.0
Honolulu	21.1	43.2	66.9	87.0	94.6	97.9	99.0	99.2	99.9	100.0
Z6-Sè	19.8	10.7	34.3	70.6	86.6	96.1	98.3	98.9	99.9	100.0
Huancayo	- 0.6	9.0	30.0	54.6	70.6	86.8	93.0	95.5	98.8	99.9
Apia	-16.0	25.7	57.5	84.7	94.5	97.9	99.0	99.2	100.0	100.0
Kuyper	-17.5	33.0	59.2	82.3	92.5	97.0	98.6	99.0	100.0	100.0
Pilar	-20.2	24.3	48.9	77.6	88.9	97.1	98.5	99.0	99.9	100.0
Cape Town	-32.7	40.0	64.3	86.1	94.5	97.9	99.0	99.3	99.9	100.0
Watheroo	-41.8	23.0	48.0	78.6	89.8	96.5	98.3	98.7	99.6	100.0
Amberley	-47.7	9.8	33.8	67.2	80.3	92.7	96.7	98.1	99.5	99.9

\* From reference 4.

TABLE XV.- Total number of fluctuations of various rates of change and semidurations for H, D, and Z, Petsamo  
September 1, 1932, to August 31, 1933\*

Semi- dura- tion, sec	Number of fluctuations for rate of change in $\gamma$ /sec																	
	Horizontal intensity						Declination						Vertical intensity					
	1	2	4	6	8	Total	1	2	4	6	8	Total	1	2	4	6	8	Total
10	421	141	33	13	13	621	985	135	28	9	11	1,168	67	35	11	7	3	123
20	848	296	49	6	3	1,202	970	105	8	2	3	1,088	294	120	27	8	3	452
30	812	231	47	1	0	1,091	597	75	7	0	0	679	309	112	27	2	0	450
40	493	139	20	8	0	660	342	52	2	1	0	397	196	85	16	1	0	298
50	353	109	22	1	2	487	243	33	4	2	0	282	151	59	23	3	2	238
60	196	54	12	1	0	263	136	20	3	0	0	159	102	33	4	2	1	142
70	177	38	3	3	0	221	116	13	2	0	0	131	50	36	6	0	0	92
80	102	32	8	1	1	144	80	12	1	0	0	93	41	16	6	3	0	66
90	88	16	3	0	0	107	52	2	1	0	0	55	29	17	4	0	0	50
100	79	36	11	0	0	126	49	8	0	0	0	57	57	16	2	0	0	75
110	46	14	2	2	0	64	34	2	2	0	0	38	26	6	5	1	0	38
120	33	11	4	2	0	50	37	1	0	0	0	38	23	6	3	0	1	33
130	21	11	2	1	0	35	27	2	0	0	0	29	15	6	1	1	0	23
140	21	4	1	0	0	26	17	3	0	0	0	20	16	5	3	0	0	24
150	22	16	1	0	0	39	16	0	0	0	0	16	15	8	1	0	0	24
160	10	2	0	0	0	12	7	0	0	0	0	7	3	5	0	0	0	8
170	9	3	0	0	0	12	15	1	0	0	1	17	4	6	0	0	0	10
180	8	4	0	0	0	12	6	2	0	0	0	8	2	4	0	0	0	6
190	4	2	1	0	0	7	2	1	0	0	0	3	9	5	0	0	0	14
200	12	4	0	0	0	16	10	1	0	0	0	11	11	2	0	0	0	13
210	3	1	0	0	0	4	4	1	0	0	0	5	4	0	0	0	0	4
220	4	5	1	0	0	10	3	0	0	0	0	3	8	1	0	0	0	9
230	4	2	0	0	0	6	3	1	0	0	0	4	2	2	1	0	0	5
240	6	3	0	0	0	9	4	1	0	0	0	5	2	2	1	0	0	5
250	4	1	1	0	0	6	7	0	0	0	0	7	4	1	1	0	0	6
260	4	2	0	0	0	6	3	0	0	0	0	3	1	1	0	0	0	2
270	3	1	0	0	0	4	3	0	0	0	0	3	1	4	1	0	0	6
280	3	2	0	0	0	5	1	0	0	0	0	1	0	2	0	0	0	2
Total	3,786	1,180	221	39	19	5,245	3,769	471	58	14	15	4,327	1,442	595	143	28	10	2,218

\* From reference 4.

TABLE XVI.- Total number of fluctuations of various rates of change and semidurations for H, D, and Z,  
Copenhagen, September 1, 1932, to August 31, 1933\*

Semi- dura- tion sec	Number of fluctuations for rate of change in $\gamma$ /sec																			
	Horizontal intensity										Declination**									
	0.1	0.2	0.4	0.6	0.8	1	2	4	6	8	Total	0.1	0.2	0.4	0.6	0.8	1	2	4	Total
10	9,011	6,555	997	130	98	24	2	0	0	1	16,818	3,958	5,670	1,169	113	51	4	2	1	10,968
20	20,208	9,620	1,073	110	29	20	0	0	1	0	31,061	7,395	6,396	892	128	24	4	1	0	14,840
30	10,651	3,634	505	41	21	6	1	0	0	0	14,859	4,044	2,958	284	22	5	3	0	0	7,316
40	3,663	1,132	160	13	6	3	0	0	0	0	4,977	1,700	685	72	13	4	1	0	0	2,475
50	1,729	414	64	13	4	1	0	0	0	0	2,225	875	235	24	3	1	0	0	0	1,138
60	797	200	26	3	1	0	0	0	0	0	1,027	393	100	16	0	0	0	0	0	510
70	418	96	11	2	0	2	0	0	0	0	529	281	50	10	0	0	0	0	0	341
80	259	50	12	1	0	0	0	0	0	0	322	148	24	4	2	0	1	0	0	179
90	154	38	4	1	0	0	0	0	0	0	198	91	13	3	1	0	0	0	0	108
100	184	40	5	0	0	0	0	0	0	0	229	91	8	2	0	0	0	0	0	101
110	85	13	3	2	0	2	0	0	0	0	105	30	9	1	0	0	0	0	0	41
120	88	17	2	1	0	0	0	0	0	0	108	46	10	4	0	0	0	0	0	60
130	64	13	3	0	1	0	0	0	0	0	81	22	2	3	0	0	0	0	0	28
140	57	10	2	1	0	0	0	0	0	0	70	29	3	1	0	0	0	0	0	33
150	58	12	1	0	0	0	0	0	0	0	71	36	4	1	0	0	0	0	0	42
160	16	8	0	0	0	0	0	0	0	0	24	14	0	0	0	0	0	0	0	14
170	29	7	1	0	0	0	0	0	0	0	37	10	1	0	0	0	0	0	0	11
180	18	7	1	0	0	0	0	0	0	0	26	16	1	0	0	0	0	0	0	17
190	15	4	3	1	0	0	0	0	0	0	23	8	1	0	0	0	0	0	0	9
200	22	4	0	0	0	0	0	0	0	0	26	14	3	1	0	0	0	0	0	18
210	12	4	2	0	0	0	0	0	0	0	18	6	1	0	0	0	0	0	0	8
220	12	1	0	0	0	0	0	0	0	0	13	5	2	0	0	0	0	0	0	7
230	11	3	0	0	0	0	0	0	0	0	14	6	2	1	0	0	0	0	0	9
240	5	0	0	0	0	0	0	0	0	0	5	5	1	1	0	0	0	0	0	7
250	17	2	0	0	0	0	0	0	0	0	19	5	5	0	0	0	0	0	0	10
260	7	0	0	0	0	0	0	0	0	0	7	1	2	0	0	0	0	0	0	8
270	6	0	0	0	0	0	0	0	0	0	7	4	2	0	0	0	0	0	0	3
Total	47,596	21,884	2,875	319	162	58	3	0	1	1	72,899	19,233	16,188	2,490	282	89	13	3	1	38,299
																				58
																				7
																				307

\*From reference 4.

\*\*There were no fluctuations in D for 6 and 8  $\gamma$ /sec and in Z for 0.6, 0.8, 1, 2, 4, 6, and 8  $\gamma$ /sec.

TABLE XVII.- ROOT-MEAN-SQUARE POTENTIAL OF THE EARTH'S

MAGNETIC FIELD  $V_n$ , CGS UNITS\*

Height above earth's surface	$n = 1$	$n = 2$	$n = 3$	$n = 4$	Height above earth's surface	$n = 1$	$n = 2$	$n = 3$	$n = 4$
0 km	118.8	9.6	5.4	2.5	2,000 km	67.1	4.2	1.8	0.7
100 km	115.1	9.2	5.1	2.3	1 $R_E$	29.2	1.1	.4	.1
200 km	111.6	8.8	4.8	2.2	2 $R_E$	13.2	.4	.07	.01
300 km	108.4	8.4	4.5	2.0	3 $R_E$	7.4	.15	.02	-
400 km	105.1	8.0	4.3	1.9	4 $R_E$	4.7	.08	-	-
1,000 km	88.8	6.2	3.0	1.3	5 $R_E$	3.3	.04	-	-

\*From reference 35.

TABLE XVIII.- MEASUREMENTS OF CAPETOWN ANOMALY\*

Location			Measured value minus computed value	
Longitude, °E.	Latitude, °S.	Height, km	SWC, gammas	Finch and Leaton, gammas
26	10	2,990	40	138
29	13	1,790	-214	-41
28	27	3,740	-188	-80
28	29	2,750	-290	-119

\* From reference 36.

TABLE XIX. - SATELLITE READINGS OF MAGNETIC-FIELD DISTURBANCE\*

Figure	Point	Date	Time, GMT	Longitude, °W.	Latitude, °N.	Satellite height, km	Disturbance $\Delta F$ at satellite, gauss	Disturbance at observatories (all values $\pm 10\gamma$ )					
								38° N., 77° W., Fredericksburg, Va.		32° N., 111° W., Tucson		18° N., 66° W., San Juan	
								$\Delta H$	$\Delta Z$	$\Delta H$	$\Delta Z$	$\Delta H$	$\Delta Z$
25(c)	A	19 Sept.	00:42	79	29.3	1,435	-15 to -25	-55	30	-63	ND	-60	ND
Not shown	---	20 Sept.	22:02	77	17.2	2,517	-35 to -50	-55	60	-63	ND	-67	ND
25(d)	B	21 Sept.	00:25	77	30.8	1,530	-20 to -30	-90	60	-83		-73	
25(e)	C	21 Sept.	02:32	117	28.8	1,735	0 to -20	-25	20	-33		-50	
25(d)	D	21 Sept.	02:43	79	33.3	954	Approx. 0	-33	-17	-50		-43	
Not shown	---	21 Sept.	05:05	62	18.0	514	Approx. 0	-33	-23	-15		-33	
25(e)	E	21 Sept.	07:10	117	27.8	629	-20 to -50	-57	-65	-83		-30	
25(d)	F	03 Oct.	22:25	77	33.4	2,695	-100 to -120	-46	67	-95	ND	-95	ND
25(c)	G	04 Oct.	00:47	76	28.2	1,807	-130 to -155	-105	55	-90		-110	
25(c)	H	04 Oct.	19:50	79	27.6	3,562	200	-25	20	-60		-57	

\* From reference 36.

TABLE XX.- PROPOSED FLARE-SATELLITE EVENT IDENTIFICATION WITH SUN TO  
PIONEER V (1960 ALPHA) DELAY TIMES AND MEAN VELOCITIES\*

Flare							Pioneer V							
Case	Date	Time	Nom. Plage <sup>2</sup> Imp. <sup>1</sup>	Activity Region <sup>3</sup>	Disk Position		End of Last Trans- mission Preceding Event		Beginning of First Trans- mission Ex- hibiting Event	Elapsed Time, (Hrs)	Approx. Distance (Km x 10 <sup>-6</sup> )	Average Velocity (Km/sec) (x 10 <sup>-3</sup> )		
							Date	Time	Date	Time		Low	High	
1.	Mar 17	1616	1+	5597	----	N04W29	Mar 19	0735	Mar 19	1400	39 - 46	147	.89	1.05
		1908	1	5597	----	N05W32		0735		1400	36.5 - 43	147	.95	1.12
2.	24	0645	2	5604	60-SB	N20W33	26	0220	26	0640	43.5 - 48	147	.85	.94
		0934	1+	5604	60-SB	N16W33		0220		0640	41 - 45	147	.91	1.0
		1055	1+	5600	60-SD	S10W65		0220		0640	40 - 44	147	.93	1.02
3.	25	1504	1+	5610	(60-R)?	N12E04	28	0700	28	1310	64 - 70	147	.58	.64
		0558	1	5604	60-SB	N16W60		0700		1310	49 - 55	147	.74	.83
		0150	1+	5607	60-SA	N12W51		0700		1310	29.5 - 35.5	147	1.15	1.38
		0634	3	5607	60-SA	N20W50		0700		1310	24.5 - 30.5	147	1.34	1.67
4.	27	0150	1+	5607	60-SA	N12W51	29	0700	29	1330	53.5 - 60	147	.68	.76
		0634	3	5607	60-SA	N20W50		0700		1330	48.5 - 55	147	.74	.84
		0912	1+	5607	60-SA	N20W53		0700		1330	46 - 52	147	.78	.89
5.	Apr 9	0123	2+	5627	60-J	N15E68	Apr 11	0230	Apr 11	0535	49 - 52	145	.77	.82
		1045	2	5619	----	N11W61		0230		0535	40 - 43	145	.94	1.01
		1140	2	5627	60-J	N17E64		0230		0535	39 - 42	145	.96	1.03
6.	10	1353	2	5627	60-J	N10E45	11	1720	12	0545	27.5 - 40	145	1.01	1.46
		1649	1+	5619	----	N17W82		1720		0545	24.5 - 35	145	1.15	1.64
7.	12	0551	1+	5625	60-L	S10W16	13	2310	14	1130	41 - 54	144	.74	.98
		0925	2	5627	60-J	N15E20		2310		1130	37.5 - 50	144	.80	1.07
		1205	2	5627	60-J	N10E18		2310		1130	35 - 47.5	144	.84	1.04
8.	14	0305	1+	5627	60-J	N07W04	16	0530	16	1120	50.5 - 56	144	.71	.79
9.	17	0309	1+	5627	60-J	N10W44	18	2330	19	0510	44.5 - 53	144	.76	.90
		0333	1+	5633	60-R	N09E49		2330		0510	43 - 49.5	144	.81	.93
		0410	1+	5630	60-SD	S09W13		2330		0510	43.5 - 49	144	.82	.92
10.	Apr 19	0847	1+	5633	60-R	N11E07	Apr 20	1710	Apr 21	1045	32 - 50	143	.79	1.24
		1500	1+	5630	60-SD	S10W44		1710		1045	26 - 44	143	.90	1.53
11.	20	1021	1+	5634	60-SA	N25E08	22	1110	22	1640	49 - 54	143	.74	.81
		1256	1+	5634	60-SA	N25E04		1110		1640	46 - 52	143	.76	.86
		1314	2	5633	60-R	N12W17		1110		1640	46 - 51	143	.78	.86
		0020	2-	5634	60-SA	N26W08		1110		1640	35 - 40	143	.99	1.13
12.	26	0304	2	5645	60-K	S09E61	27	1640	28	1030	38 - 55.5	142	.71	1.04
		0605	1+	5636	----	N08W61		1640		1030	35 - 52.5	142	.75	1.13

\*From reference 55.

<sup>1</sup>Nominal importance.

<sup>2</sup>McMath plage number.

<sup>3</sup>High Altitude Observatory designation.

TABLE XXI.- GENERAL CHARACTERISTICS OF MAGNETOMETERS<sup>†</sup>

	Types of magnetometer		
	Component class*	Proton precessional	Optical pumping
Quantity measured**	Field along one axis	Total intensity	Total intensity
Detected signal	Voltage or current	Frequency	Frequency
Measurement obtained	Percentage of range scale; dependent on drifts, calibrations, etc.	Absolute	Absolute
Dependence on orientation	Dependent on	Not dependent on	Not dependent on
Range	Wide if special techniques are used	Not practical in very weak fields beyond one Earth radii	Exceptionally wide
Power requirements	Low	High	Low

<sup>†</sup>Reference 58.

\*Included in this type are saturable cores, electron beams, spinning coils, and Hall generators.

\*\*With additional instrumentations and special techniques, all magnetometers can measure the complete vector field.

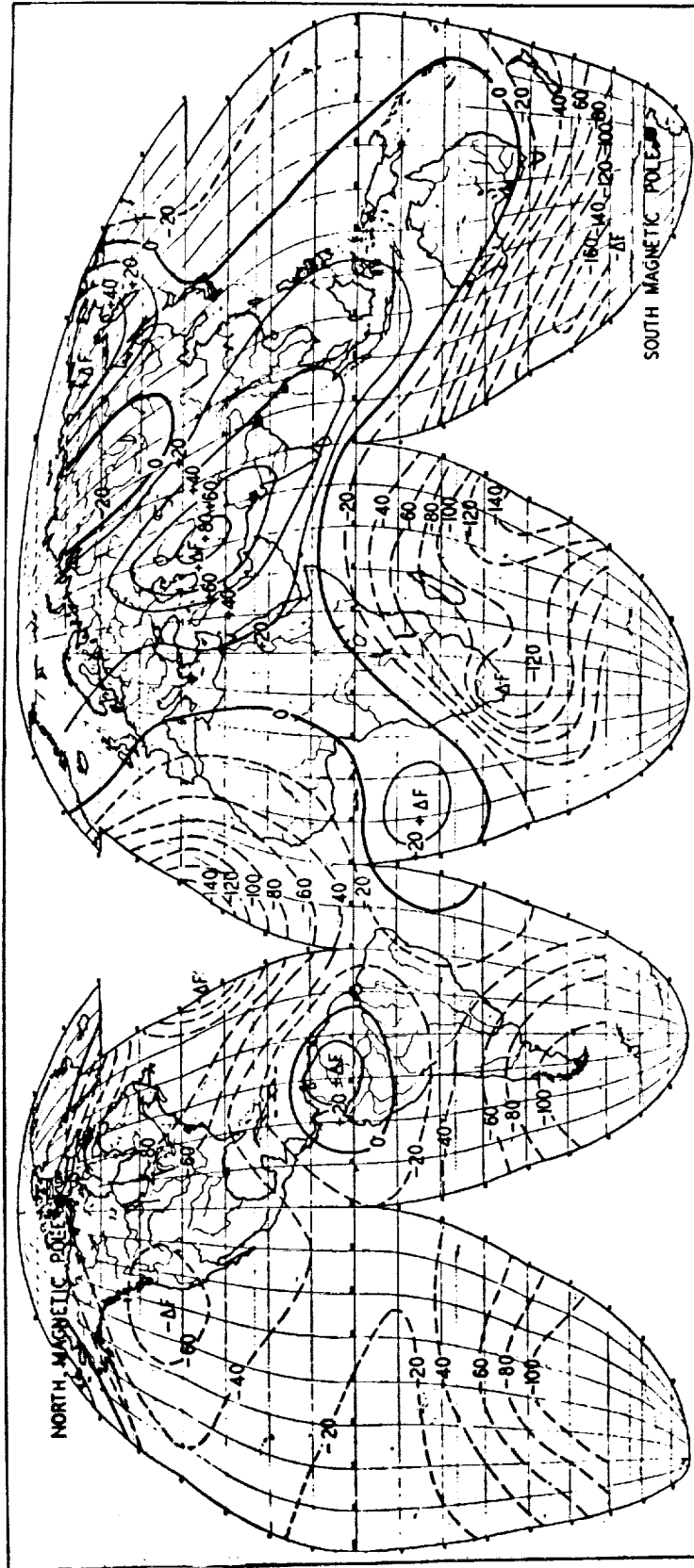


Figure 1.- Isoporic chart for the total magnetic intensity  $F$ , showing the lines of equal annual change in  $F$ , in gammas per year, for the approximate epoch 1922. (From ref. 1.)

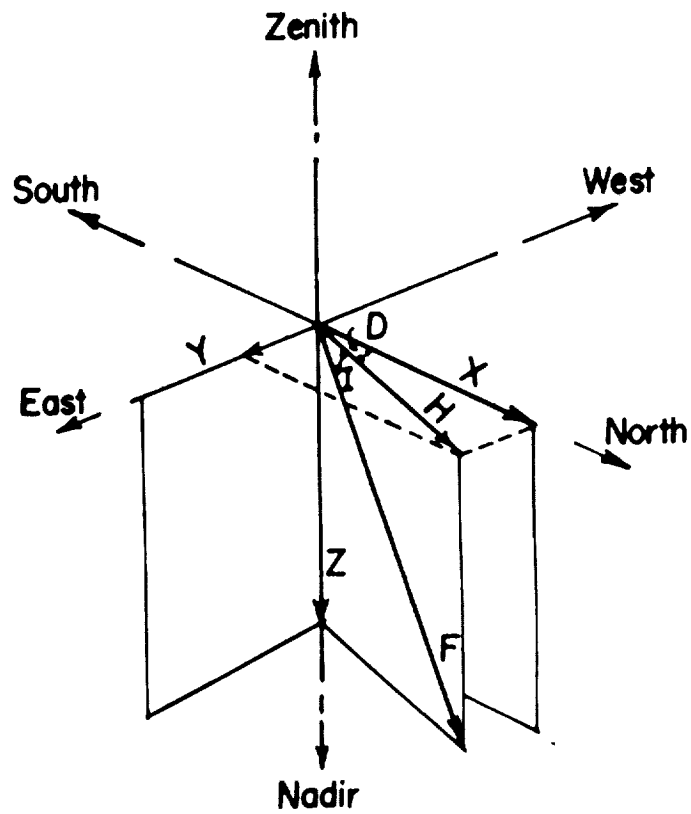


Figure 2.- The total magnetic-field intensity  $F$ , its rectangular components  $X$ ,  $Y$ ,  $Z$ , and the elements  $H$ ,  $D$ ,  $I$ . (From ref. 2.)

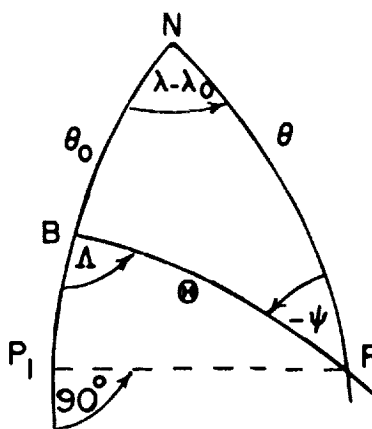


Figure 3.- Illustrating the calculation of geomagnetic coordinates.  
(From ref. 1.)

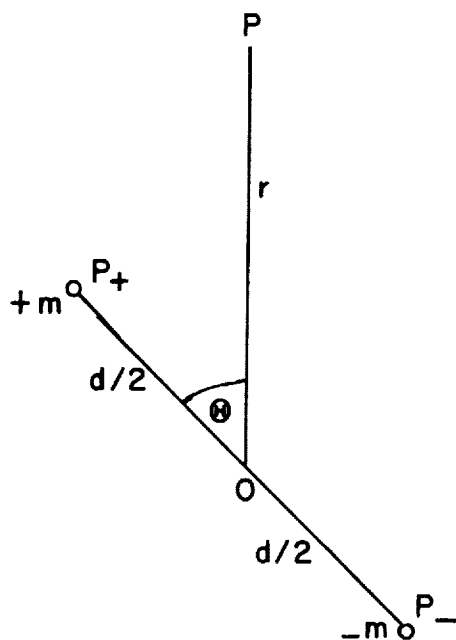


Figure 4.- Illustration of the magnetic dipole. (From ref. 1.)

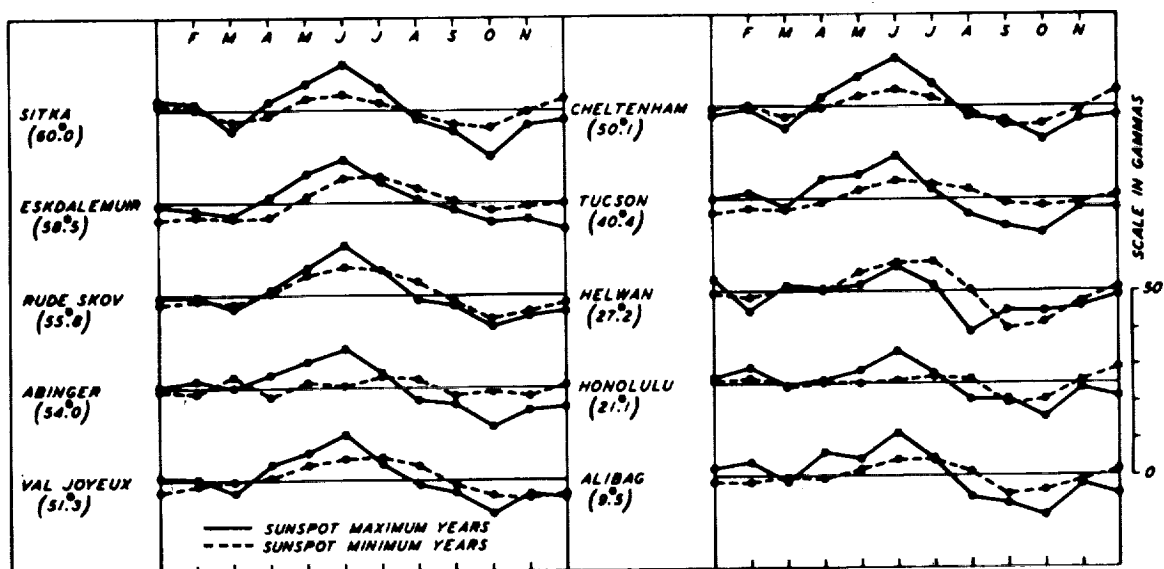


Figure 5.- Monthly mean departures from annual means of geomagnetic component  $\Delta X'$  averaged over sunspot minimum (1912-14, 1922-24) and maximum (1916-18, 1927-29) years. (Geomagnetic latitudes indicated in parentheses. From ref. 4.)

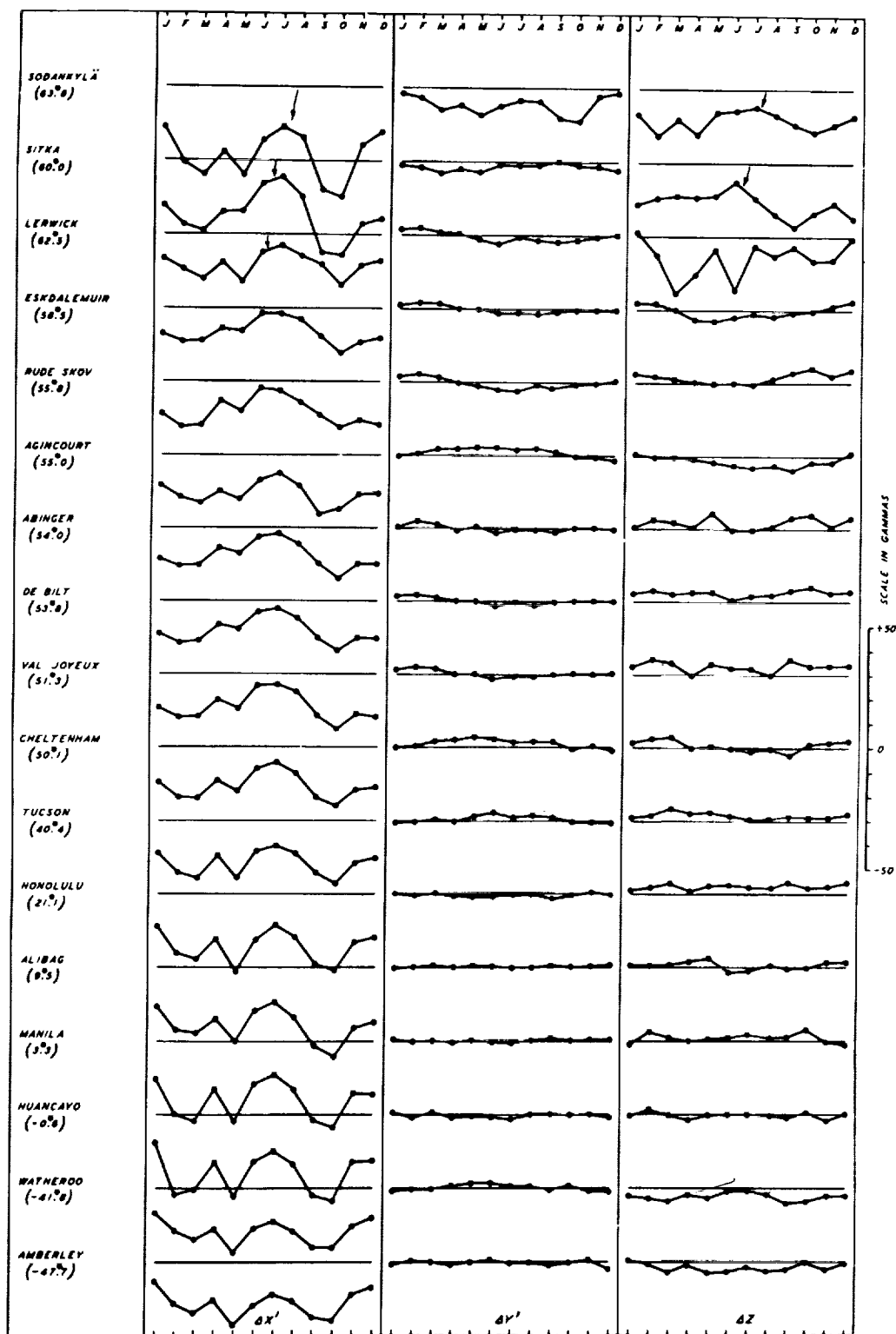
(a) Total  $D_{m1}$ .

Figure 6.- Annual variation of geomagnetic components of  $D_{m1}$  averaged for the same month over the years 1922 to 1933. Geomagnetic latitudes indicated in parentheses. (From ref. 4.)

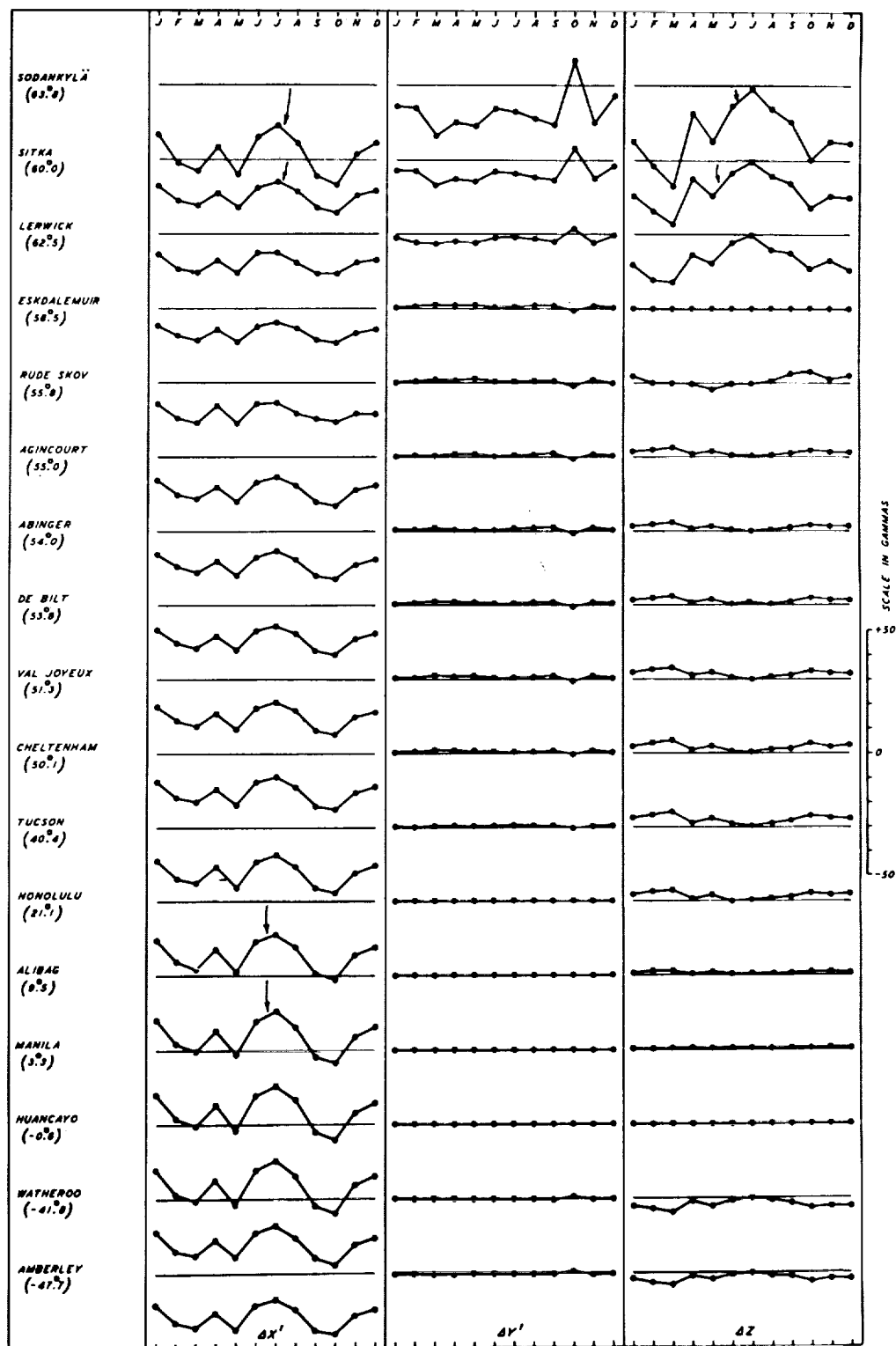
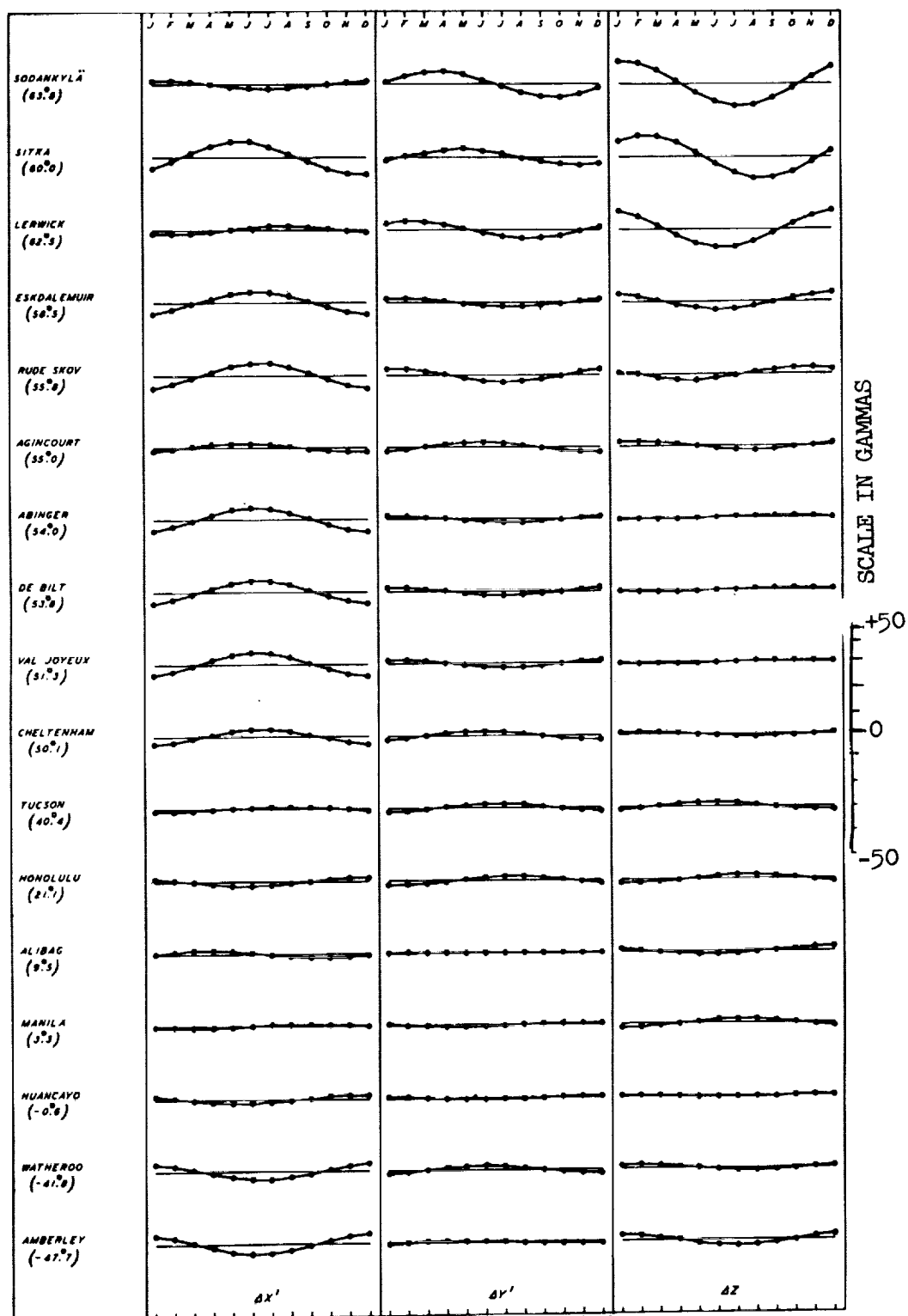
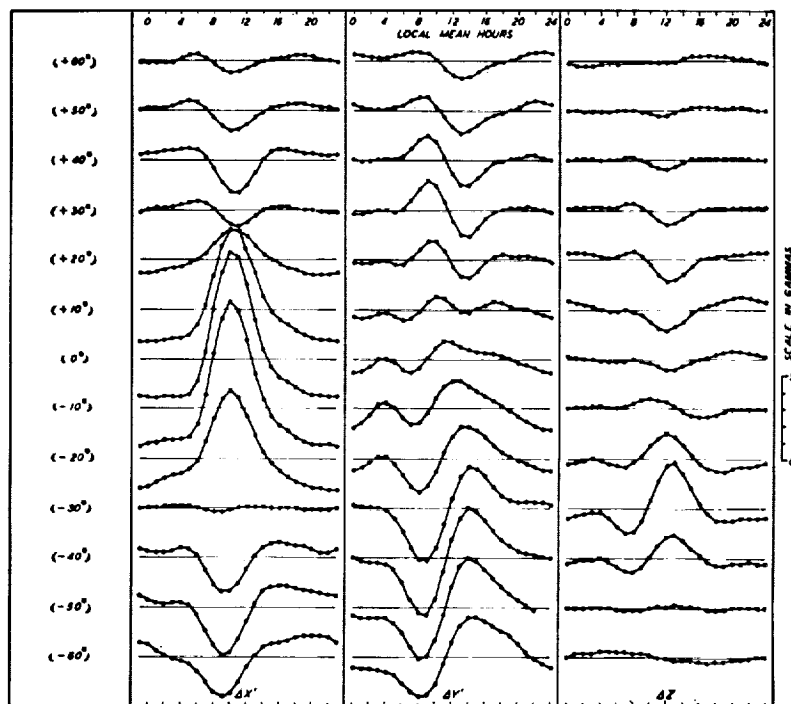
(b) Part of  $D_{mi}$  symmetrical about equator.

Figure 6.- Continued.

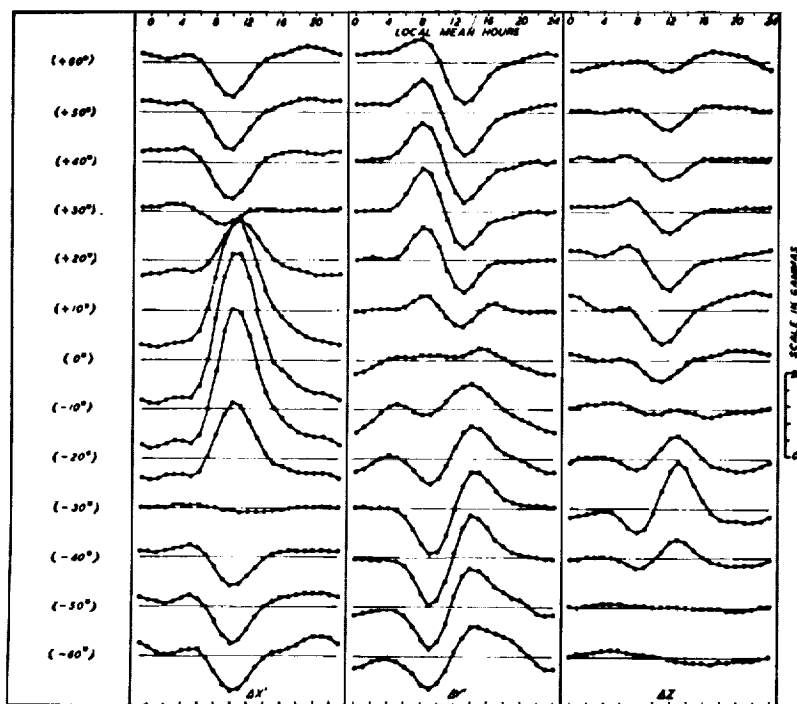


(c) Part of  $D_{m1}$  antisymmetrical about equator and sinusoidal with time.

Figure 6.- Concluded.

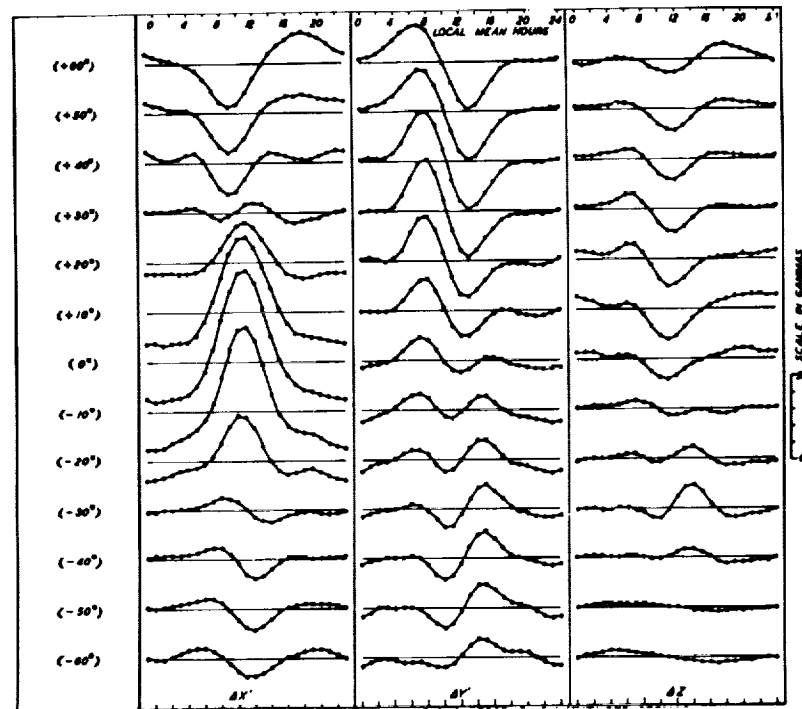


(a) Winter, northern hemisphere.

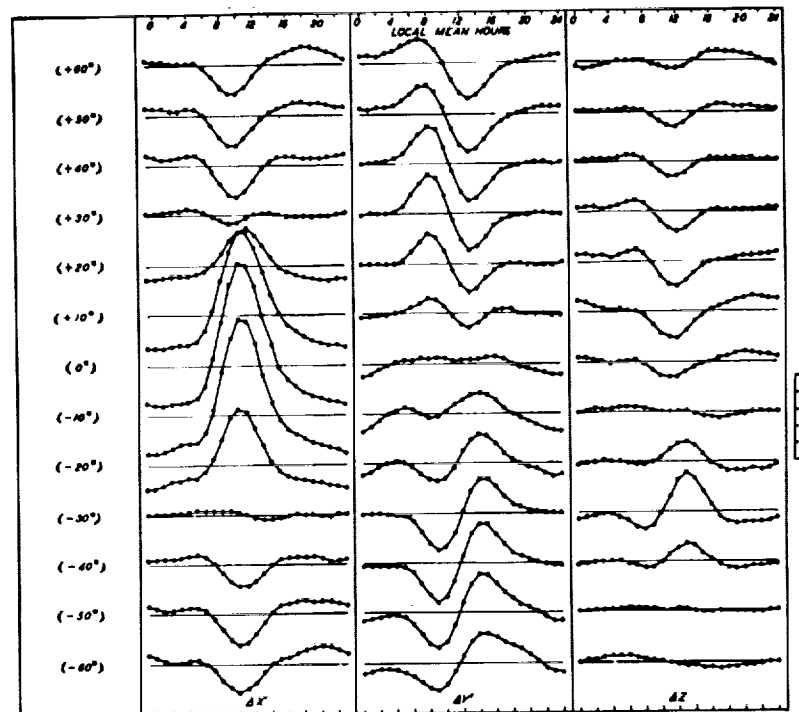


(b) Equinox.

Figure 7.- Geomagnetic components of quiet-day solar daily variation  $S_q$  averaged over the years 1922 to 1933 for various geographic latitudes. (From ref. 4.)

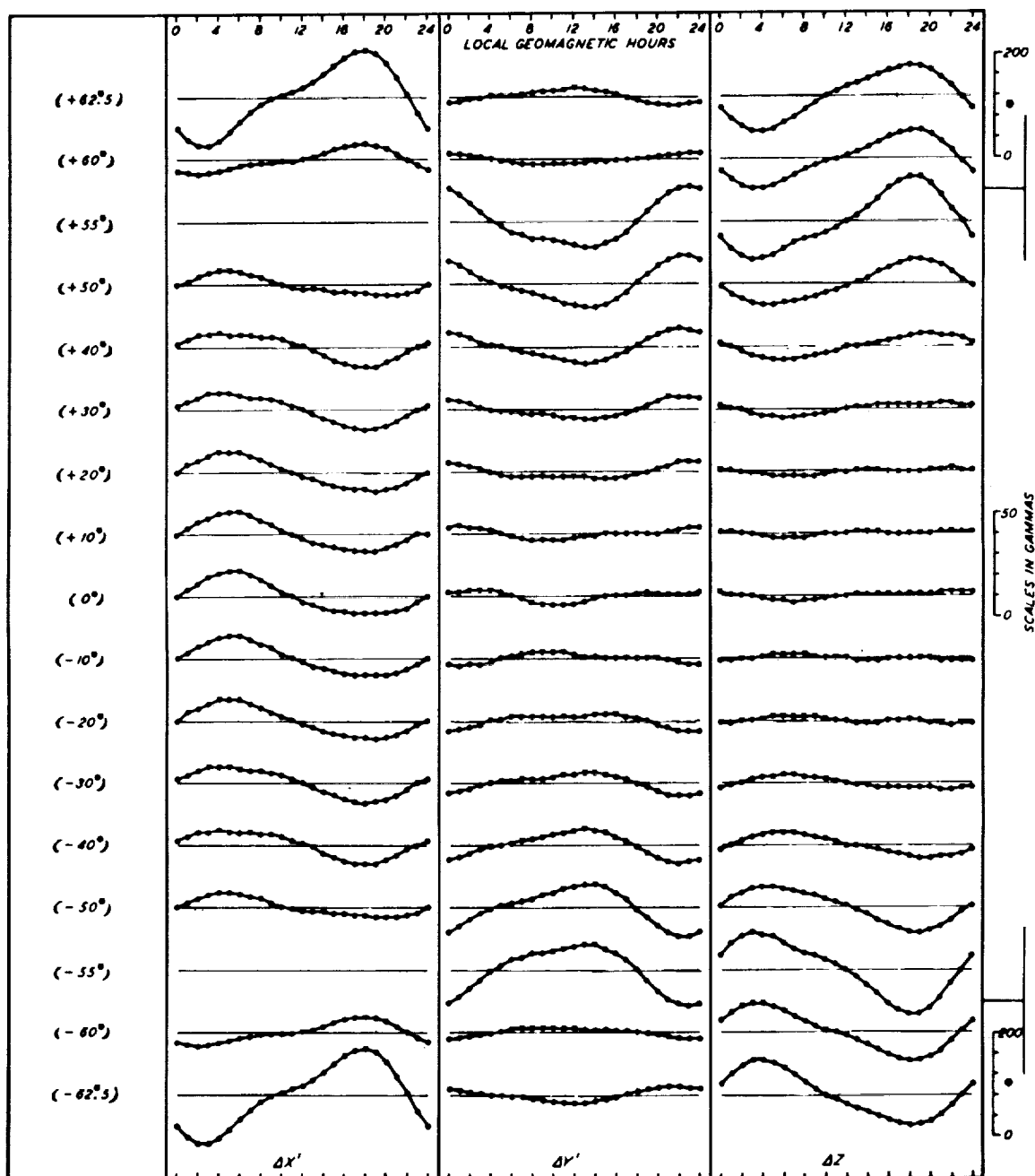


(c) Summer, northern hemisphere.



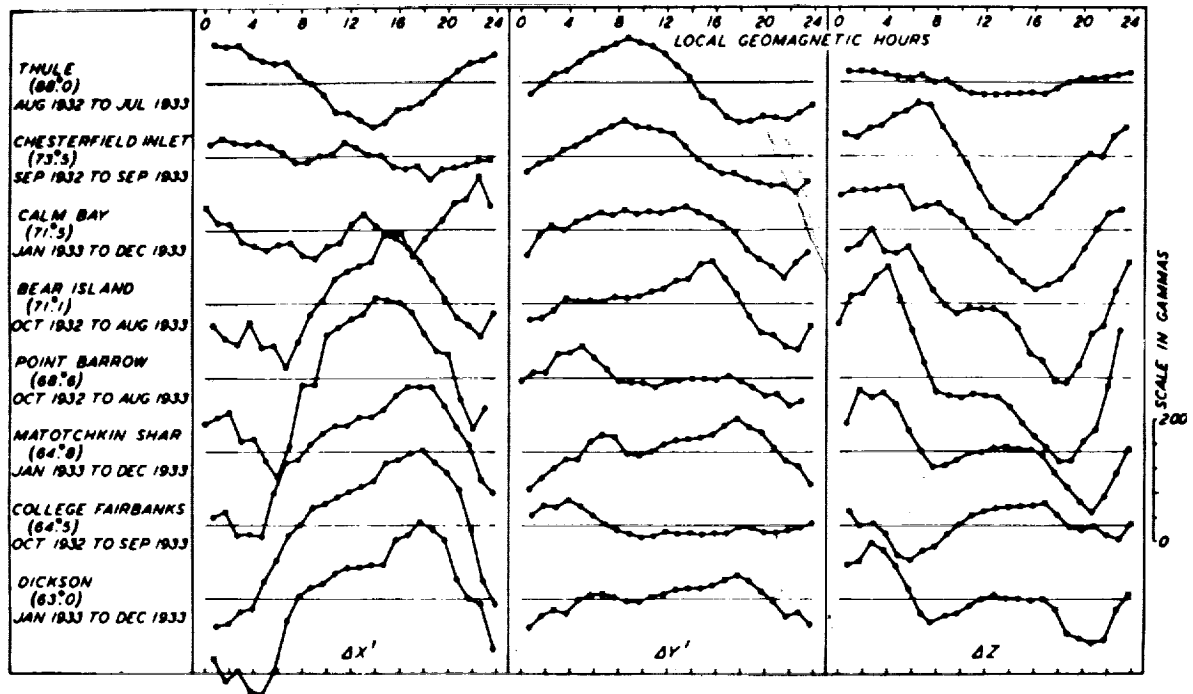
(d) Year.

Figure 7.- Concluded.



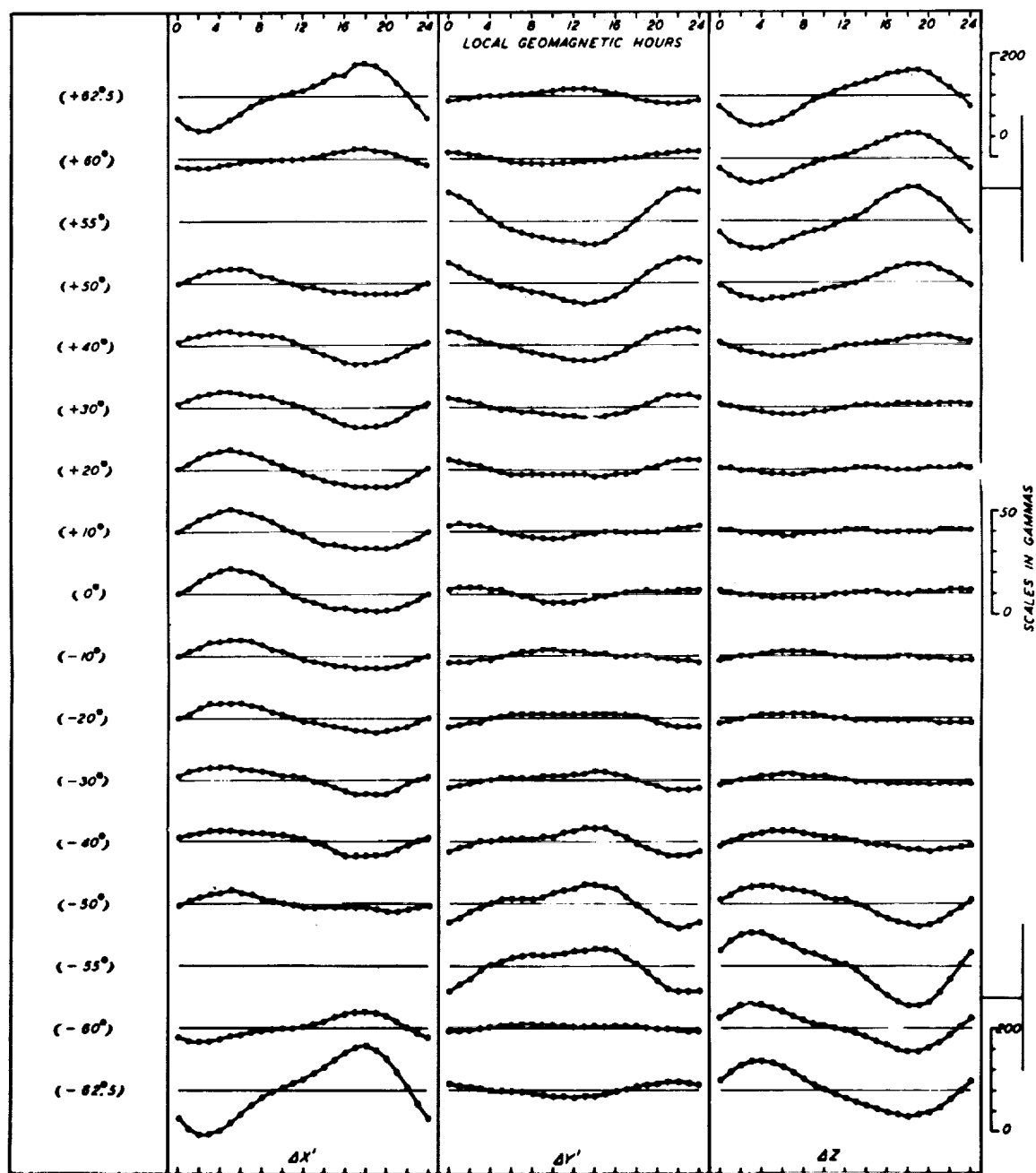
(a) Year. Mean over years 1922 to 1933.

Figure 8.- Geomagnetic components of disturbance daily variation  $S_D = S_d - S_q$  in various geomagnetic latitudes (ref. 4). (Note particularly that scales for graphs in auroral regions are different from others.)



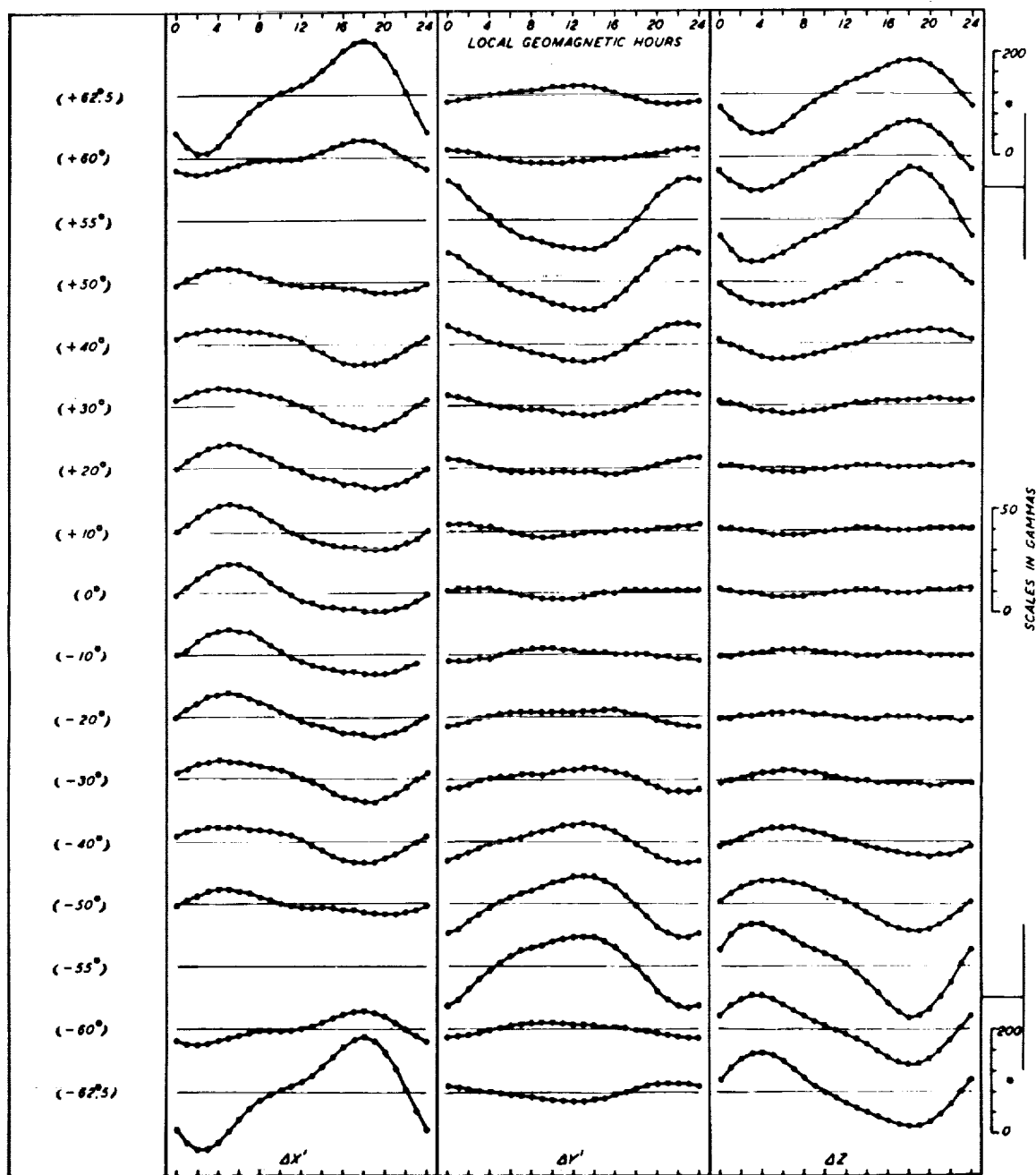
(b) Polar regions, inhomogeneous data, polar year 1932 to 1933.

Figure 8.- Continued.



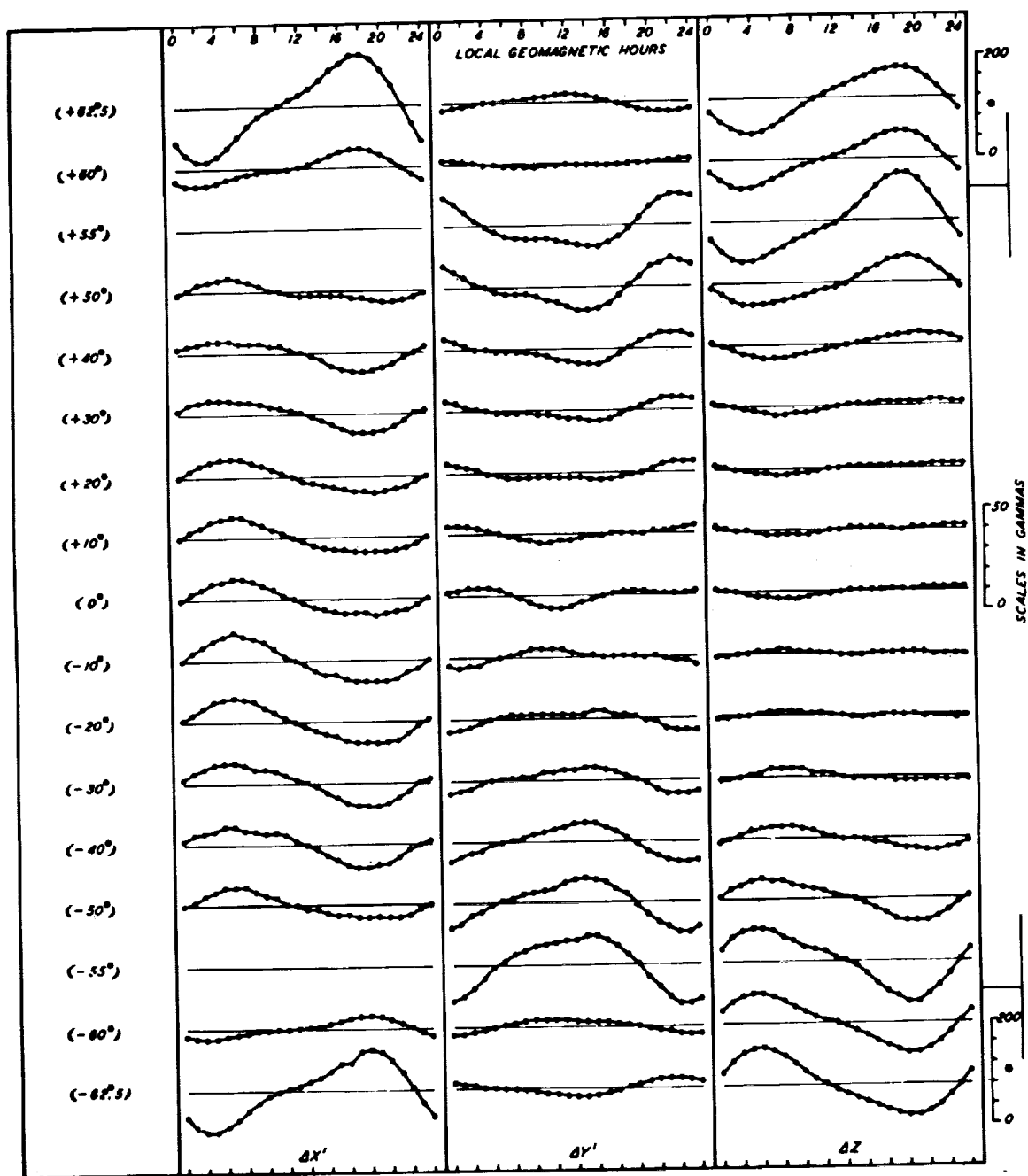
(c) Winter, northern hemisphere. Mean over years 1922 to 1933.

Figure 8.- Continued.



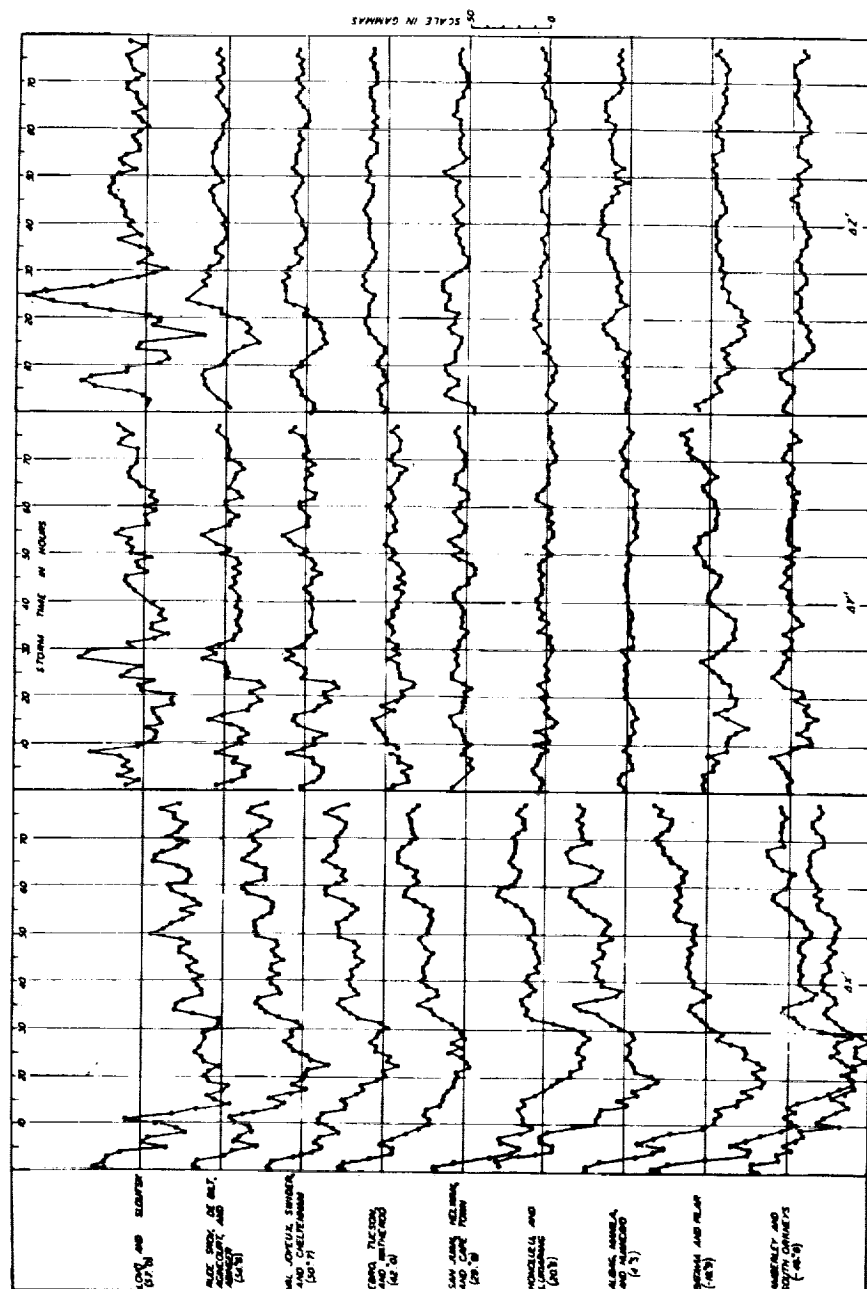
(d) Equinox. Mean for years 1922 to 1933.

Figure 8.- Continued.



(e) Summer, northern hemisphere. Mean over years 1922 to 1933.

Figure 8.- Concluded.



(a) Middle and low latitudes.

Figure 9.- Geomagnetic components of storm-time variation  $D_{st}$  at various geomagnetic latitudes. The components are a composite of the weighted average of 11 storms for the polar year 1932-1933 which are also averaged for the various observatories at a given latitude. The latitudes shown are the average values of the latitudes of the corresponding observations. (From ref. 4.)

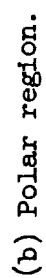


Figure 9.- Concluded.

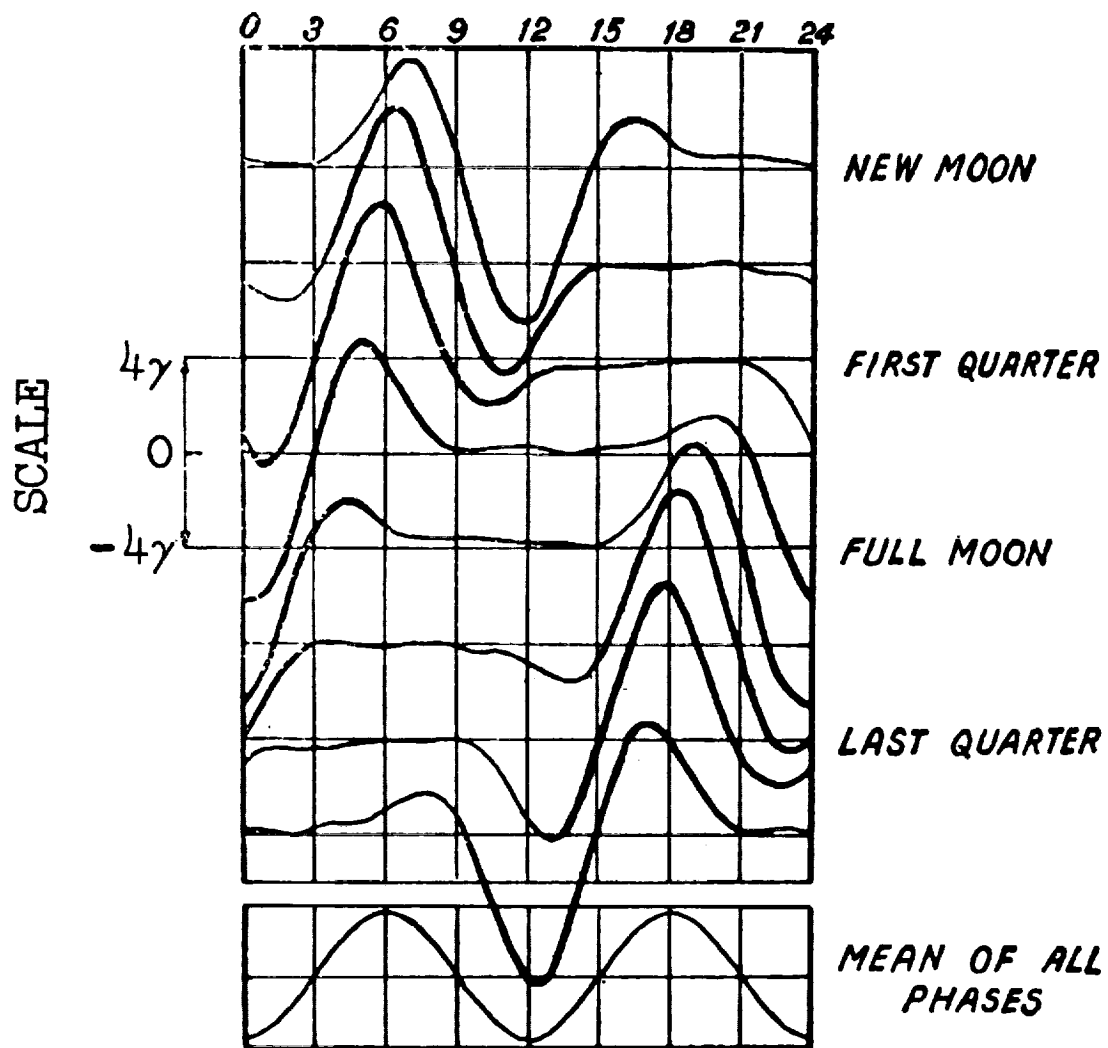


Figure 10.- Lunar diurnal variation of magnetic west component at Batavia, Java (now Djakarta, Indonesia) for different phases of the moon and the mean variation averaged over all the phases. (From ref. 2.)

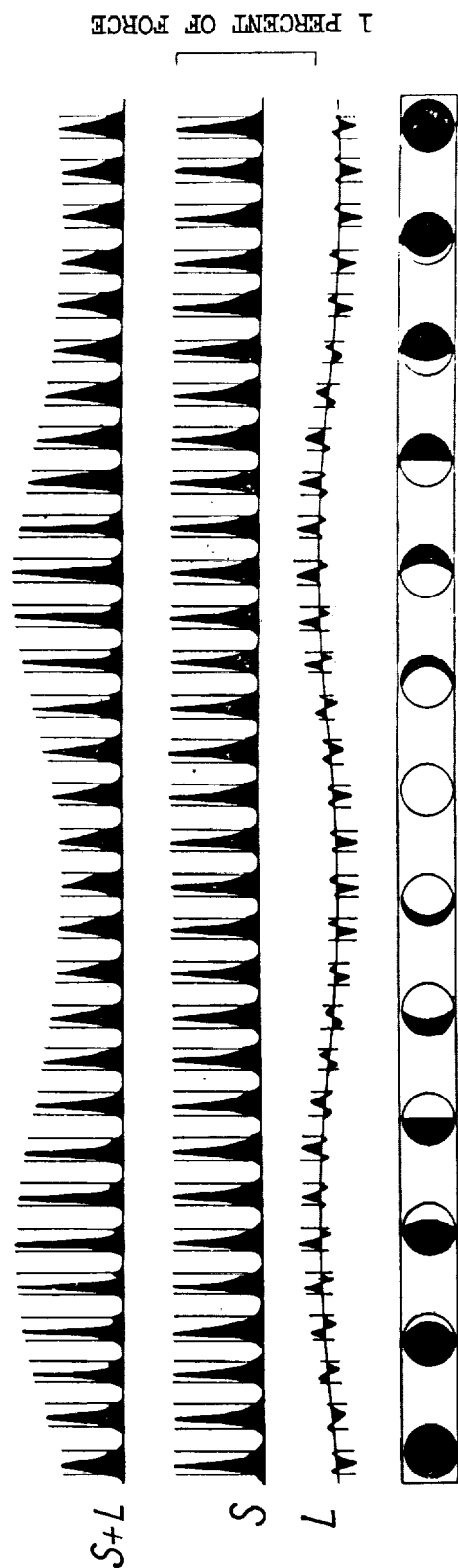


Figure 11.- Illustrating diurnal changes in one lunar month in the range of  $H$  caused by  $S$  and  $L$  at Huancayo, Peru (the solid curves). Advantage has been taken of the fact that the tidal effects at this station are exceptionally large. In the uppermost set of curves  $S$  and  $L$  are superposed. In the second set  $S$  only is depicted. In the third set  $L$  only is depicted superposed on a wave representing the variation of the  $L$  daily average value. The phases of the moon are shown at the bottom. The computations are for a period of sunspot maximum. Similar computations made for a period of sunspot minimum show that the amplitudes of the variations are much smaller. (From ref. 2.)

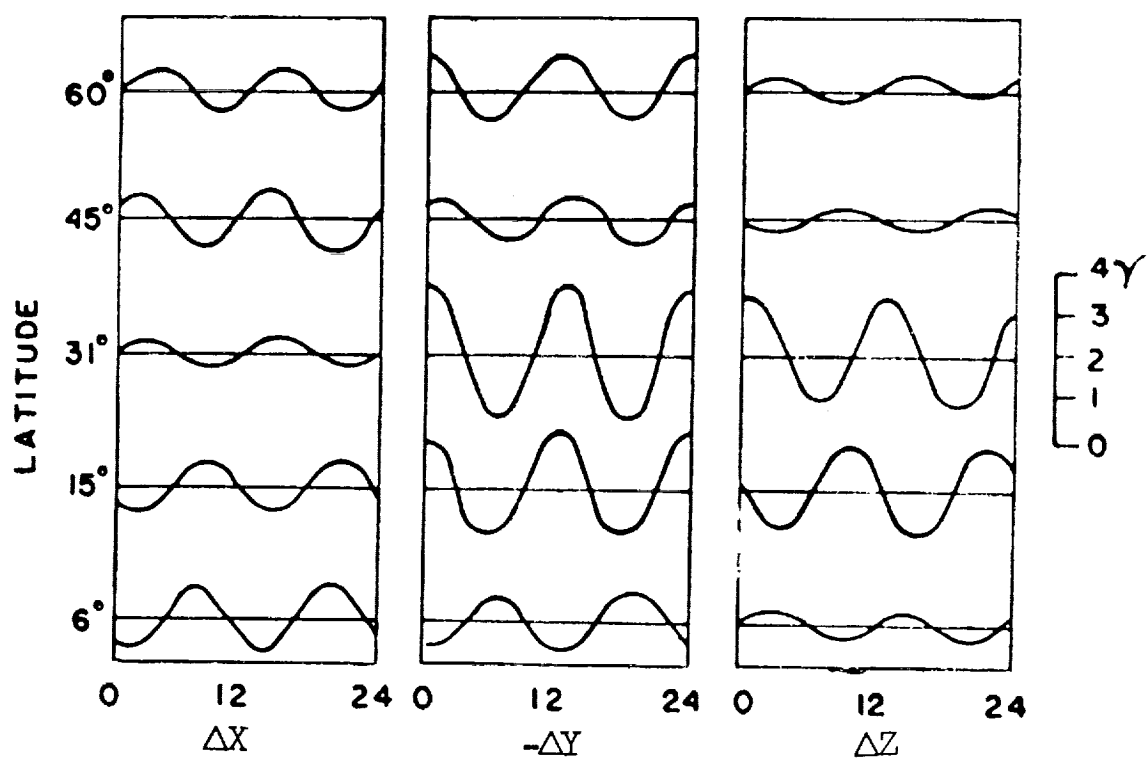
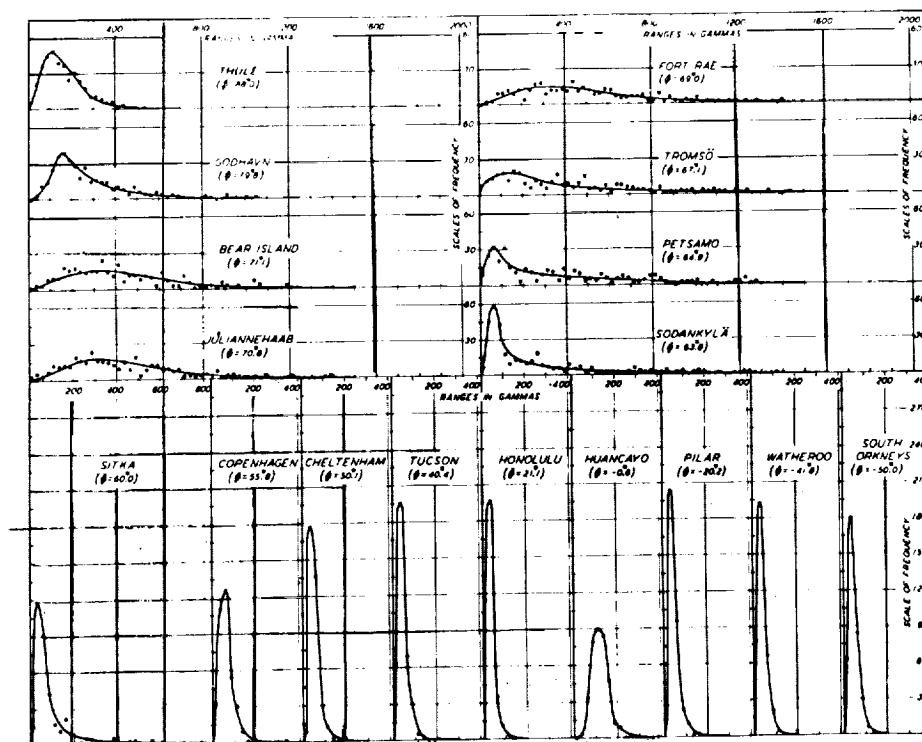
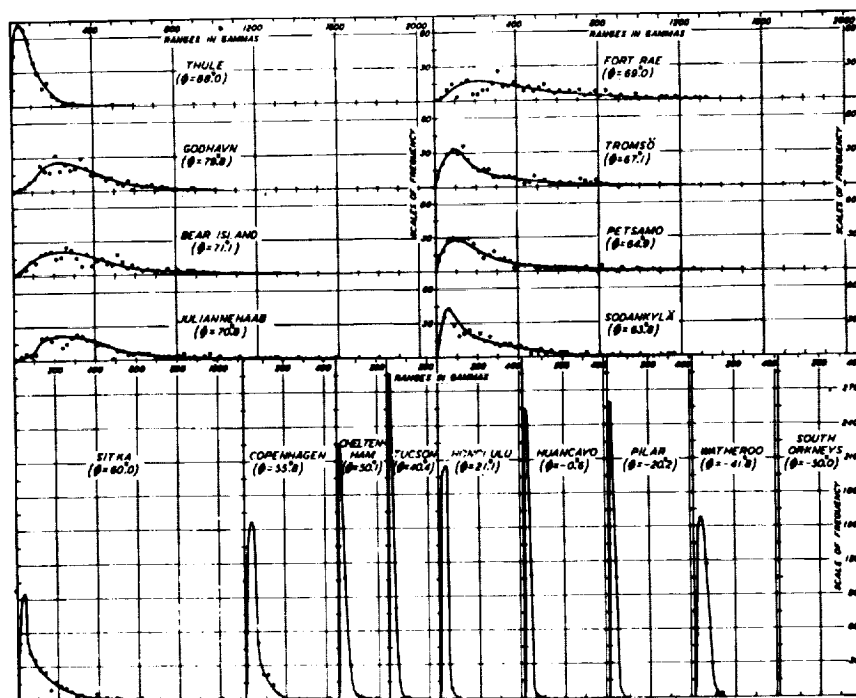


Figure 12.- Average lunar variation of terrestrial magnetic elements.  
(From ref. 17.)



(a) Horizontal intensity H.



(b) Vertical intensity Z.

Figure 13.- Frequency distributions of daily ranges at various magnetic observatories for the 12 months of polar year August 1932 to August 1933. (From ref. 4.)

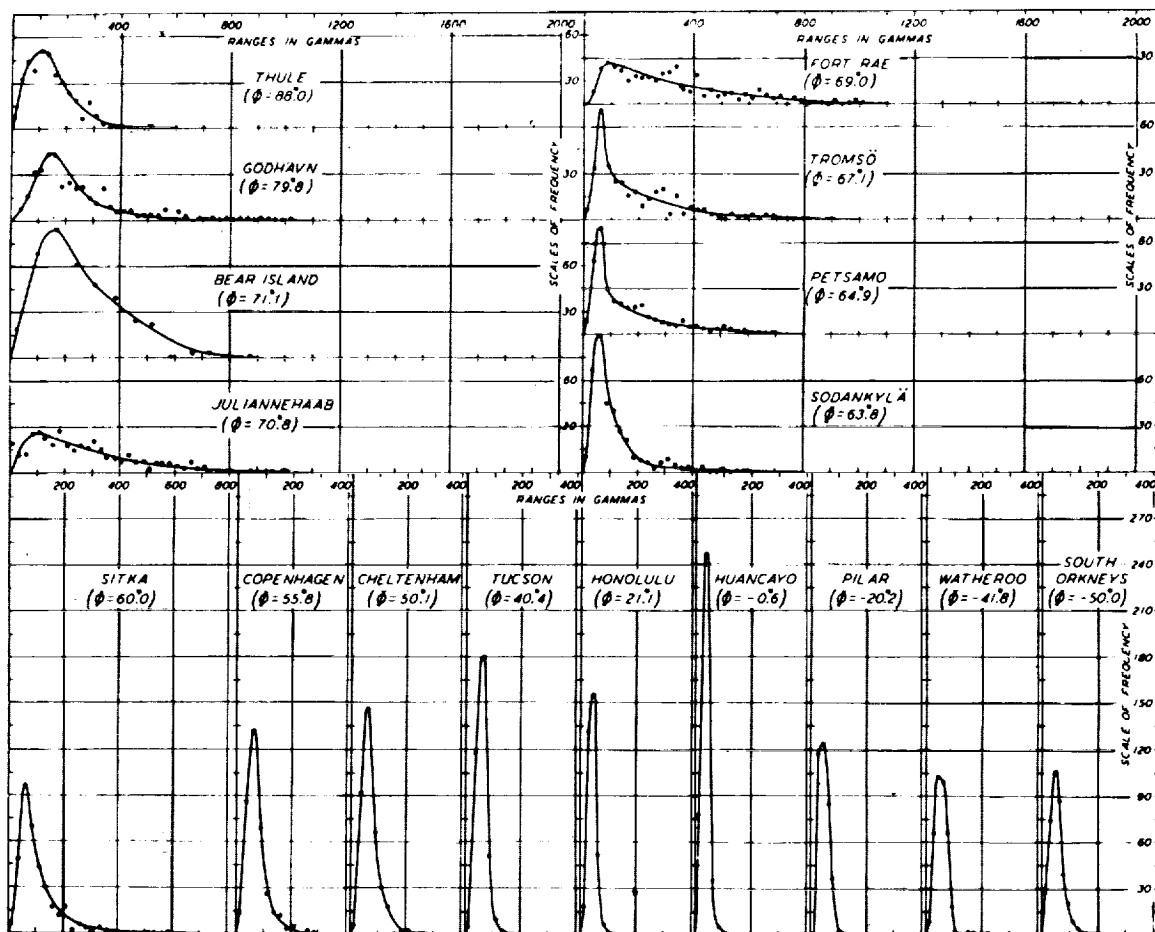
(c) Magnetic declination  $D$ .

Figure 13.- Concluded.

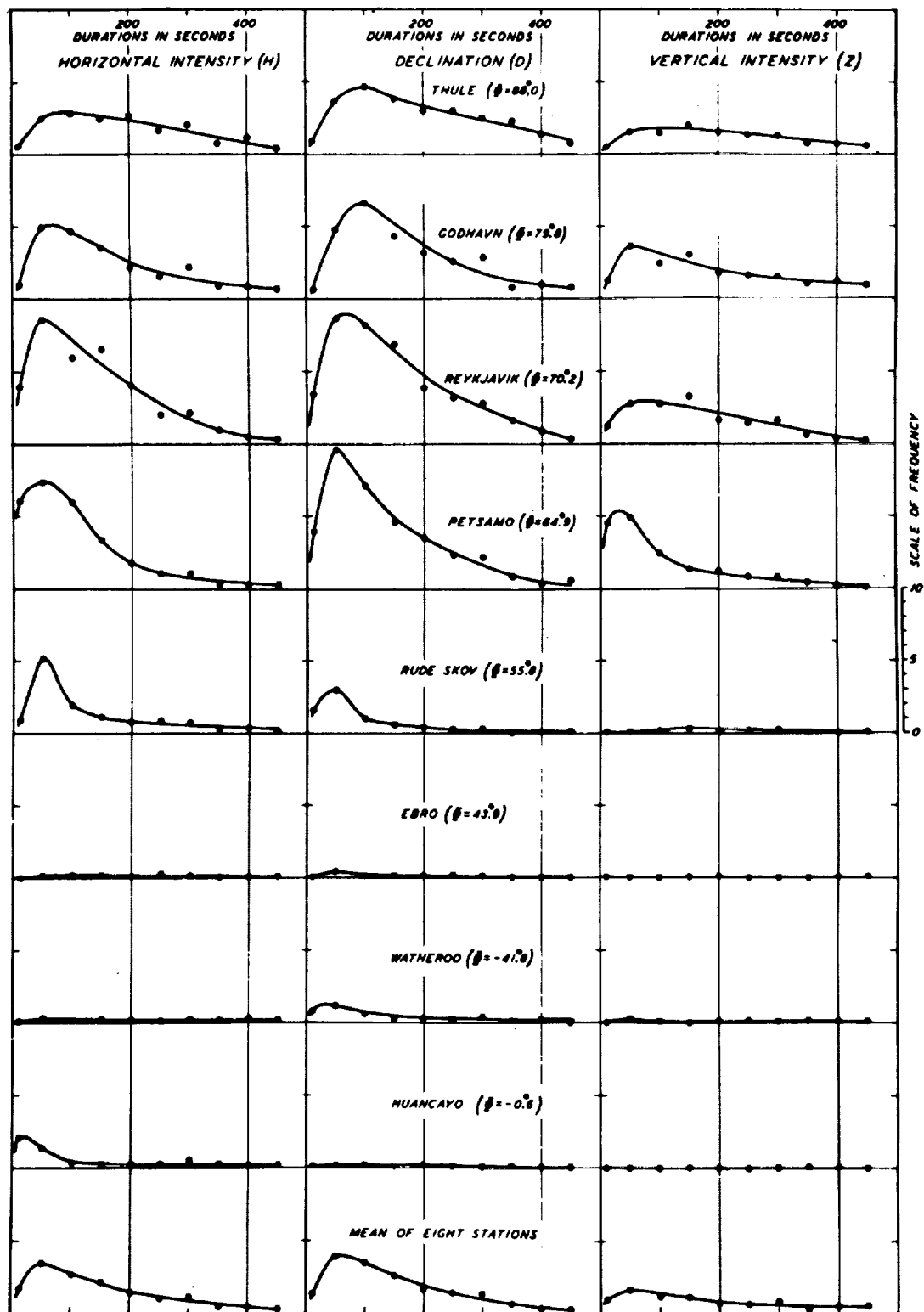


Figure 15.- Variation with latitude of frequencies of fluctuations of various durations (10 to 500 seconds) for H, D, and Z for mean of 6 days, May 9 ( $C=0.0$ ), July 4 ( $C=0.4$ ), May 5 ( $C=0.8$ ), May 31 ( $C=1.2$ ), March 24 ( $C=1.5$ ), and May 1 ( $C=1.9$ ), 1933. (From ref. 4.)

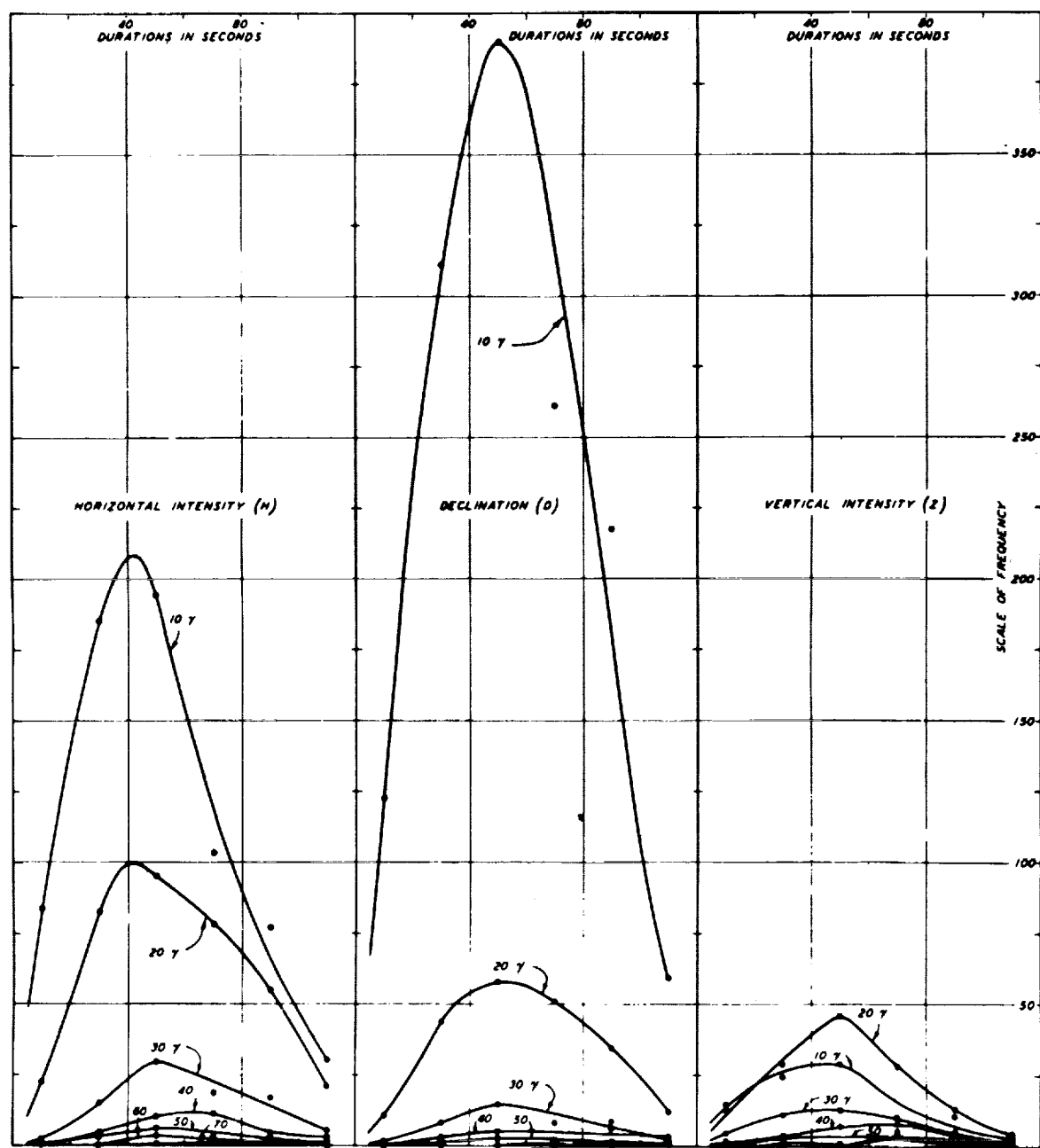


Figure 14.- Frequencies of fluctuations of various amplitudes as a function of duration in seconds for H, D, and Z at Petsamo, Finland, from August 1 to October 31, 1932. (From ref. 4.)

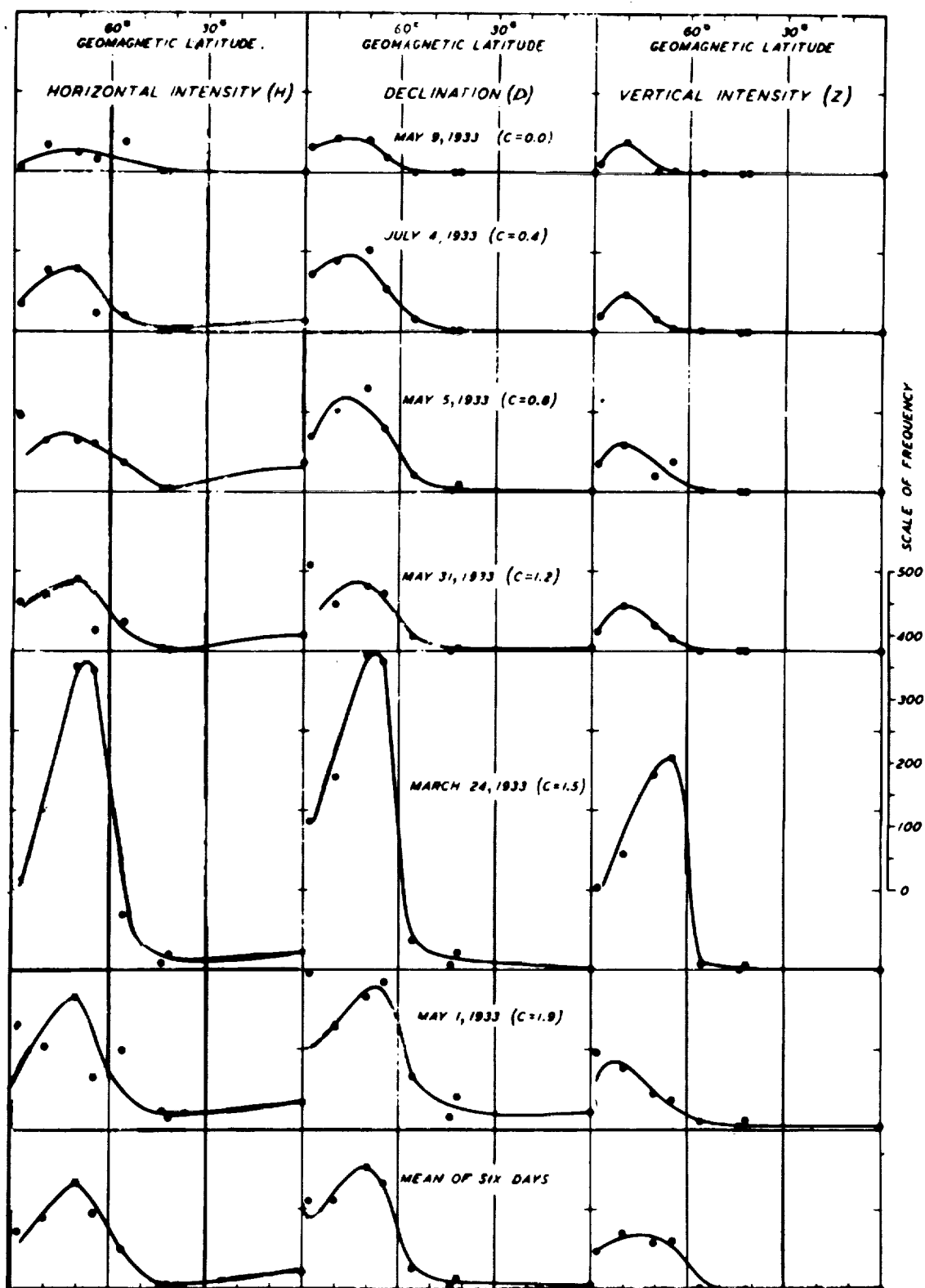
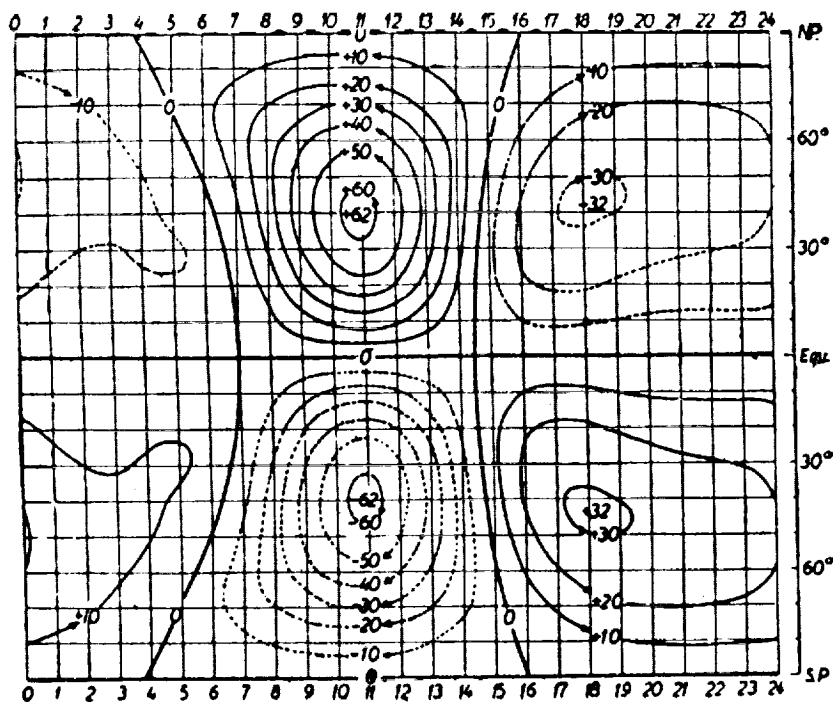
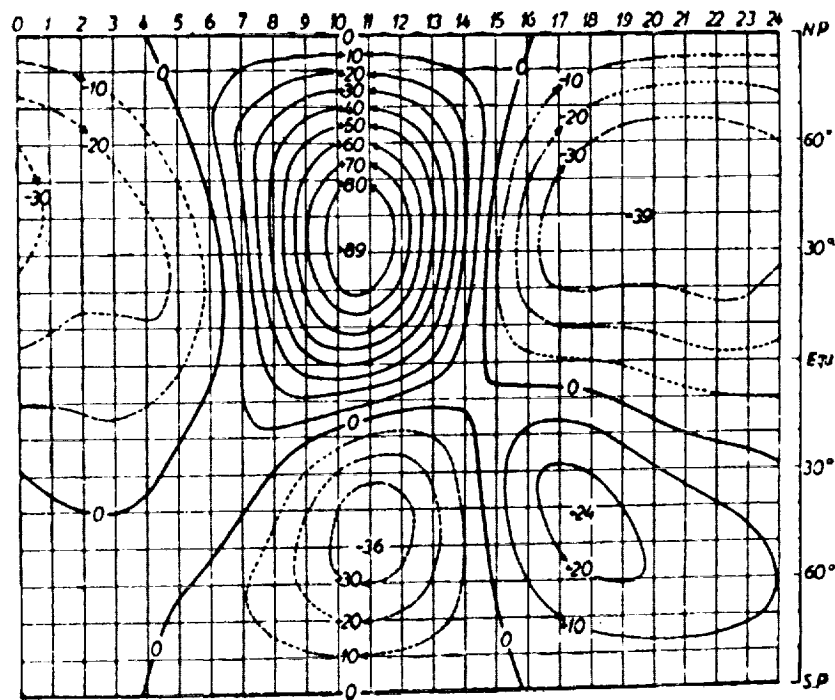


Figure 16.- Variation with geomagnetic latitude of daily frequency of fluctuations with durations from 10 to 500 seconds for H, D, and Z for various values of magnetic character figure C. (From ref. 4.)

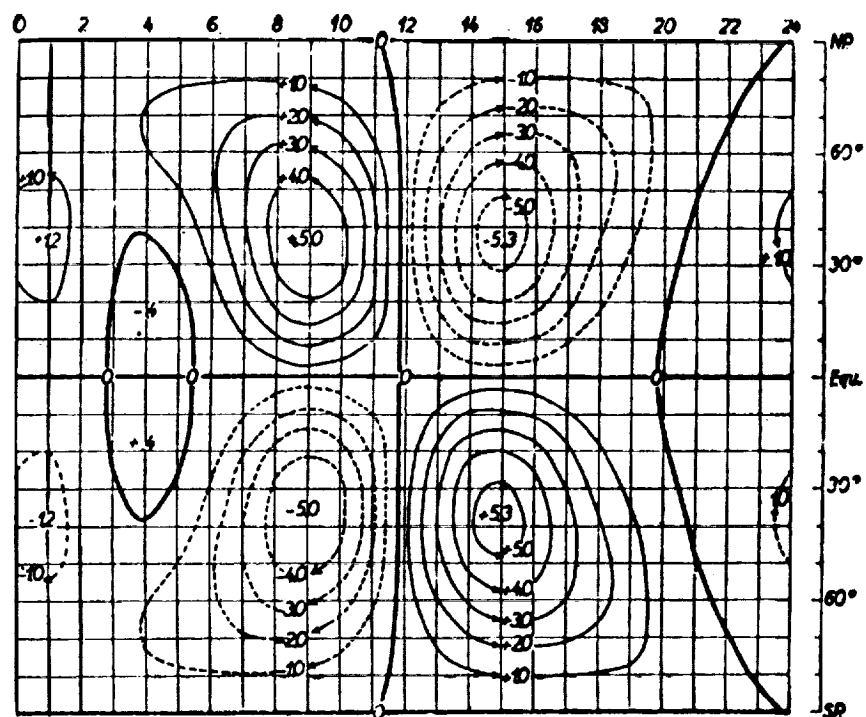


(a) Equinoxes.

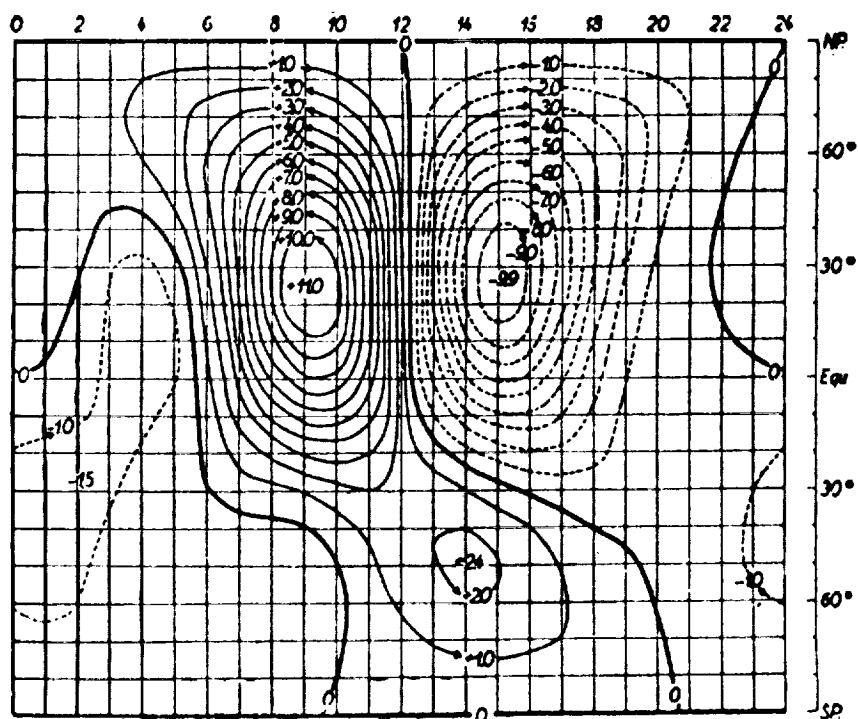


(b) June solstice.

Figure 17.- Ionospheric current system corresponding to  $S_q$  in the sunspot-minimum year 1902. 10,000 amperes flow between adjacent lines. (From ref. 1.)

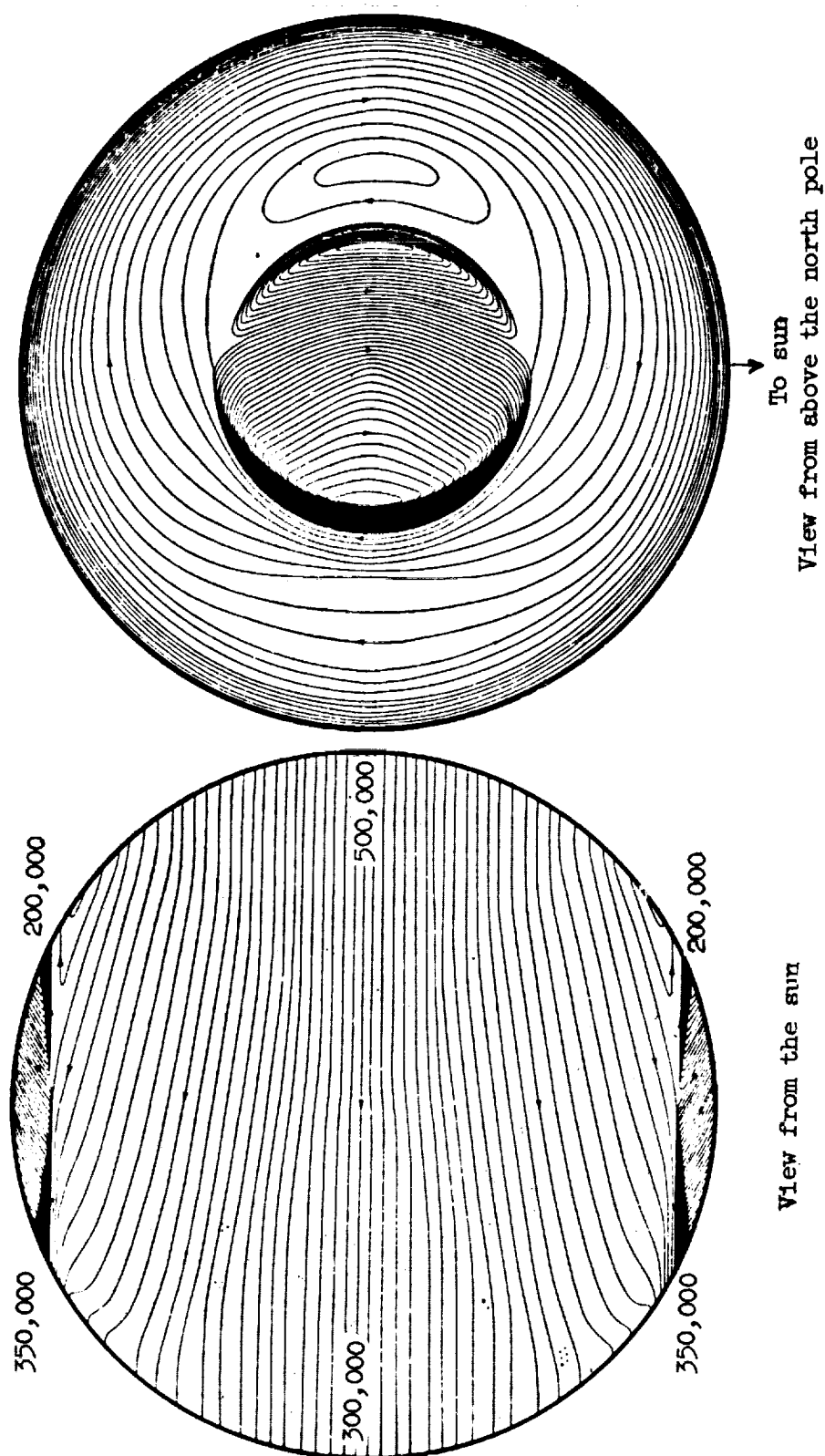


(a) Equinoxes.



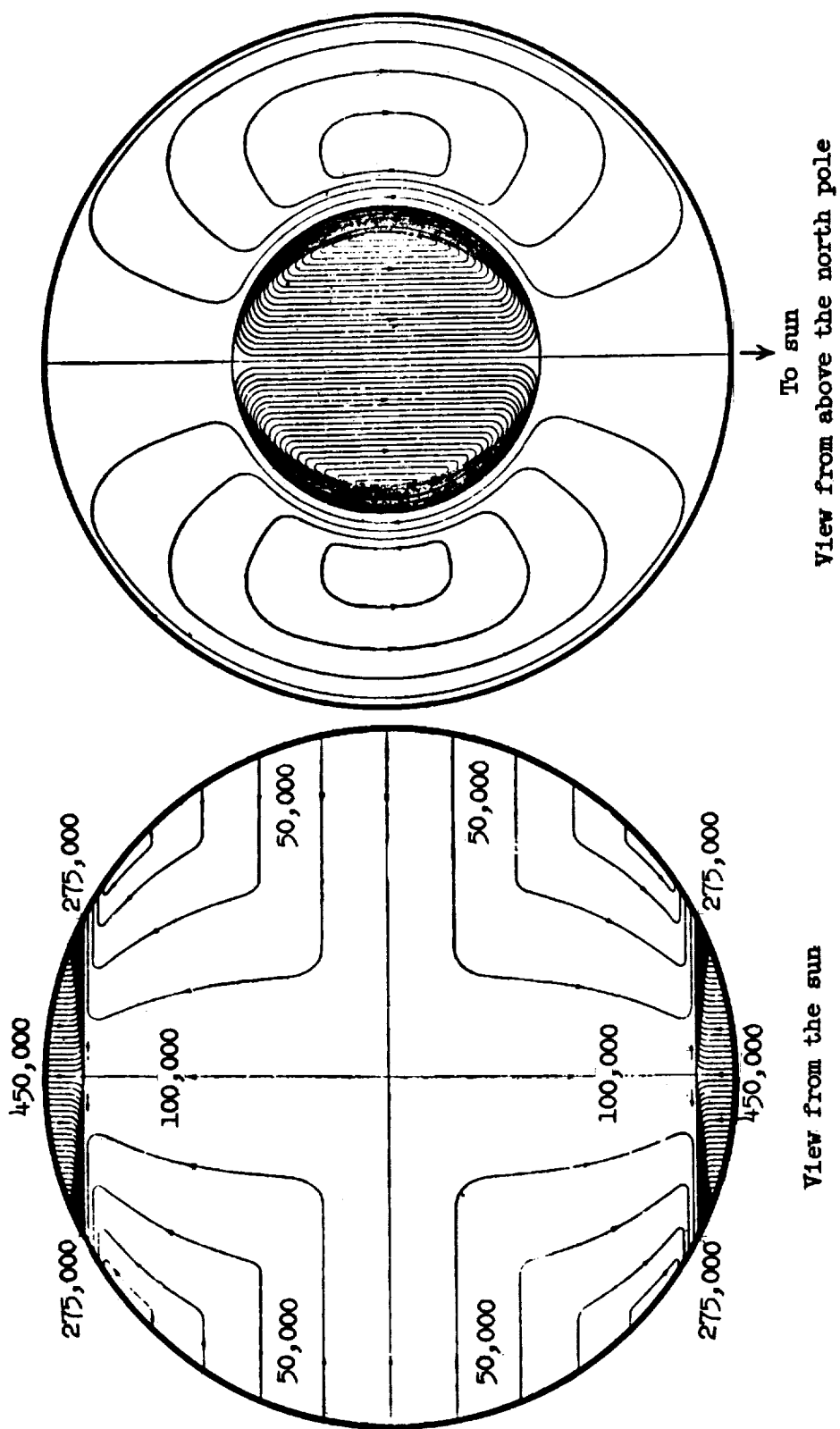
(b) June solstice.

Figure 18.- Ionospheric current system corresponding to L for the new moon. 1,000 amperes flow between adjacent lines. (From ref. 1.)



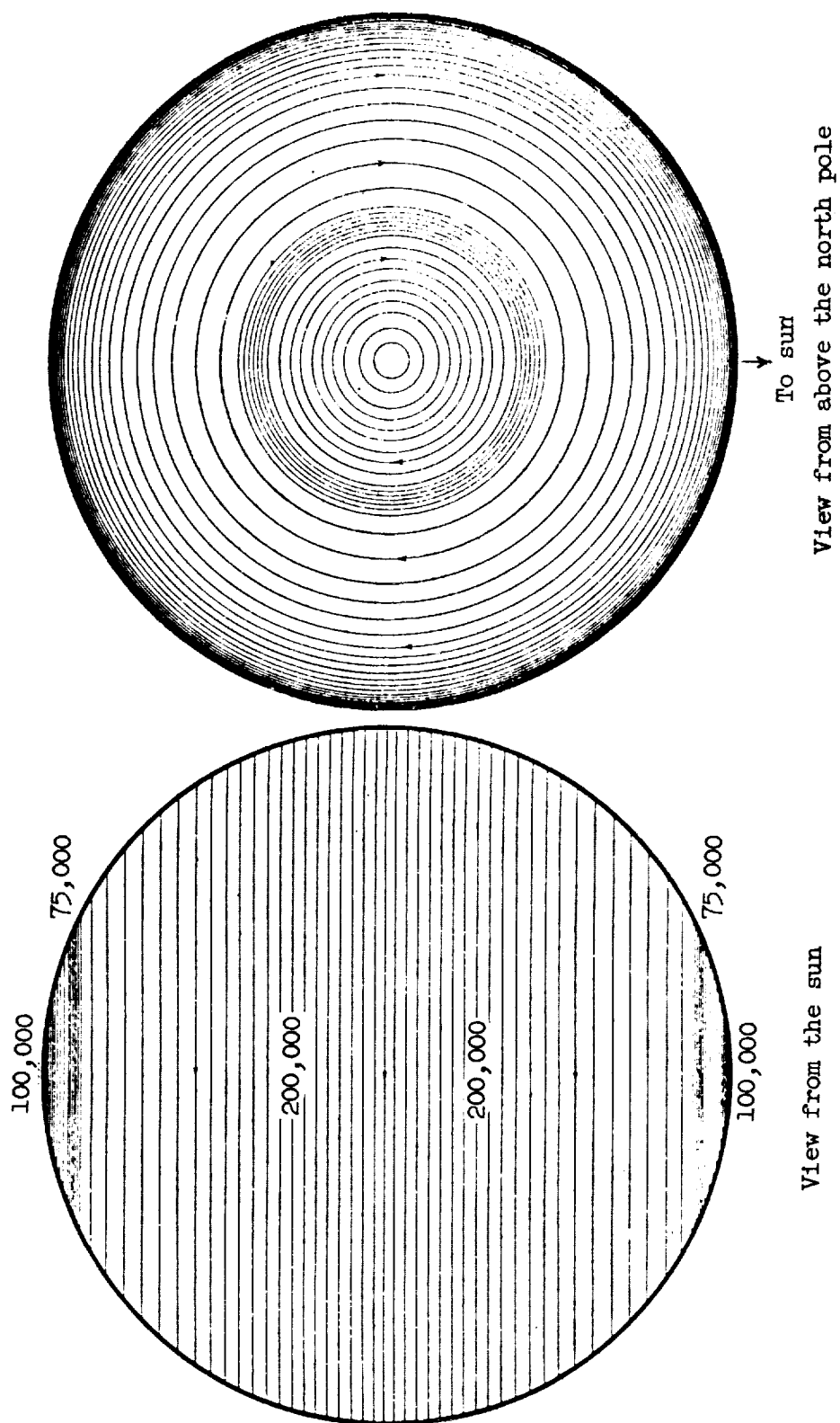
(a) Total current system.

Figure 19.- Views of the idealized overhead current systems that could produce the "regular" field of a geomagnetic storm. (From ref. 1.)



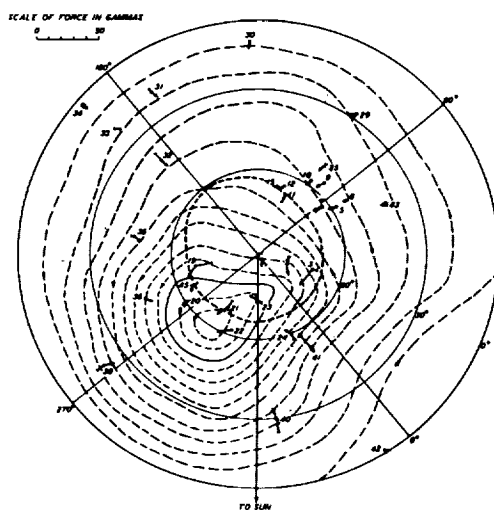
(b)  $S_D$  current system.

Figure 19.- Continued.

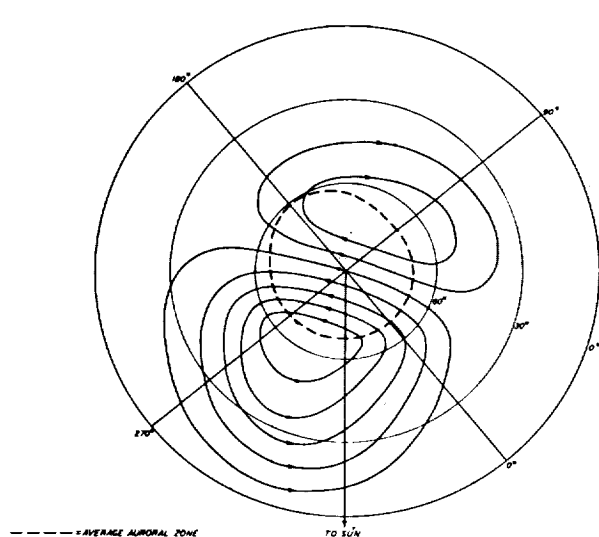


(c)  $D_{st}$  current system.

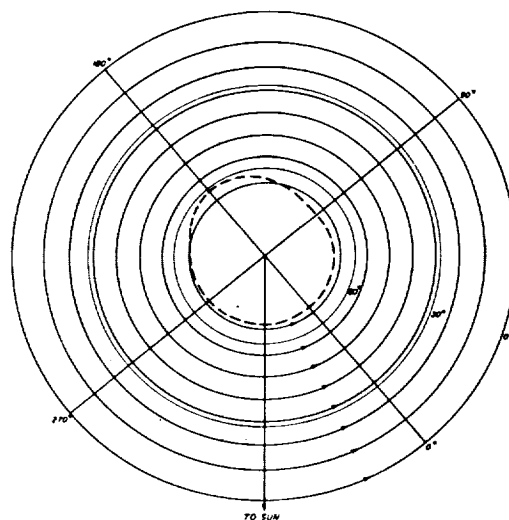
Figure 19.- Concluded.



(a) Total current system.

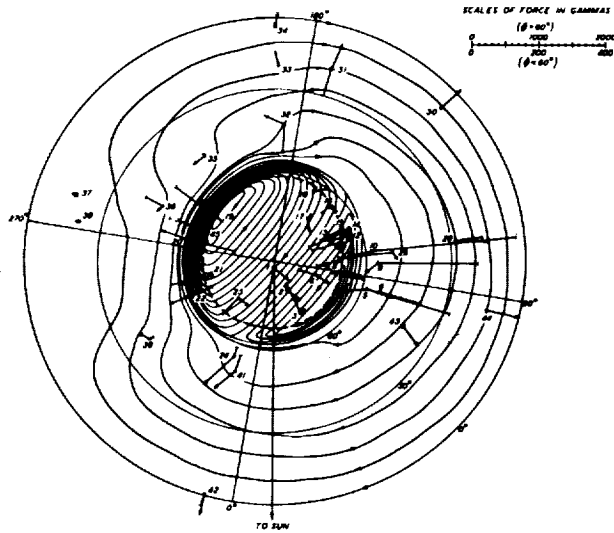


(b)  $S_D$  current system.



(c)  $D_{st}$  current system.

Figure 20.- Current systems for a height of 150 kilometers for maximum of initial phase of magnetic storms; view from above geomagnetic north pole; 100,000 amperes flow between successive full-drawn current lines. (From ref. 4.)



(a) Total current system.

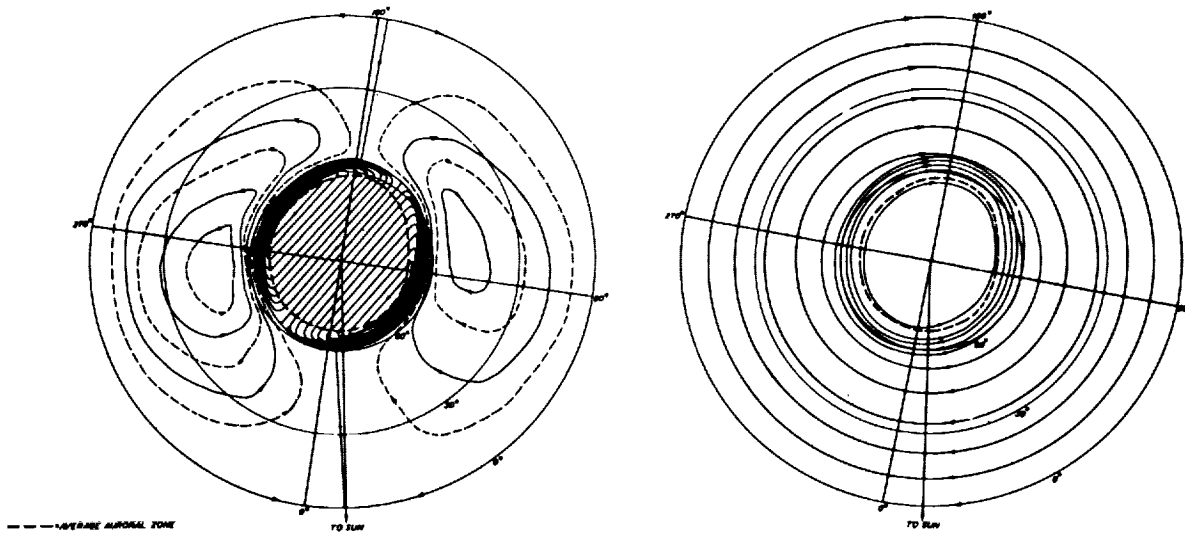
(b)  $S_D$  current system.(c)  $D_{st}$  current system.

Figure 21.- Current systems for a height of 150 kilometers for main phase of magnetic storms. View from above geomagnetic north pole; 100,000 amperes flow between successive full-drawn current lines. (From ref. 4.)

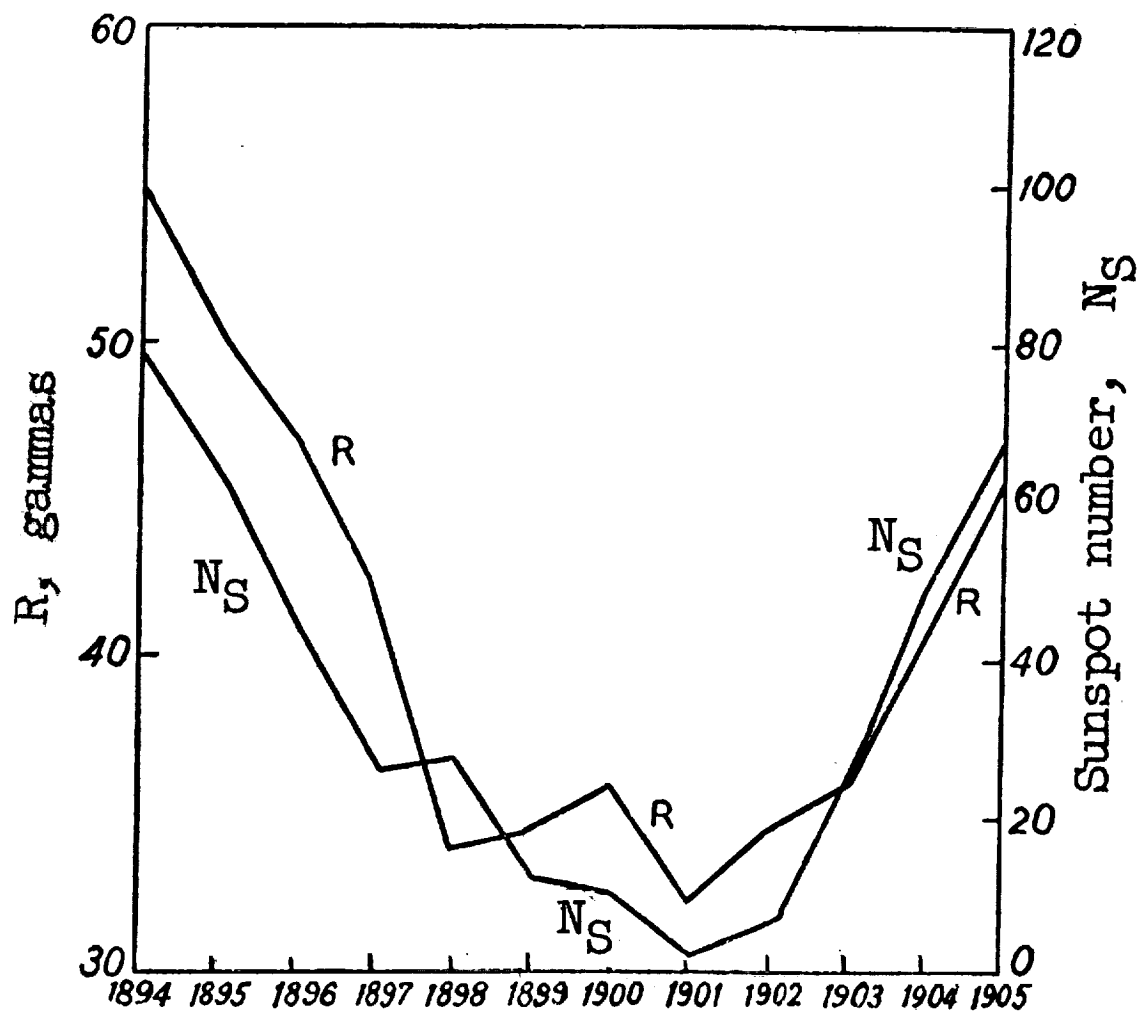


Figure 22.- Illustrating the parallelism between the range  $R$  of annual mean of  $S_q$  of the horizontal force  $H$  (at Bombay, India) and annual mean sunspot numbers  $N_s$ . (From ref. 2.)

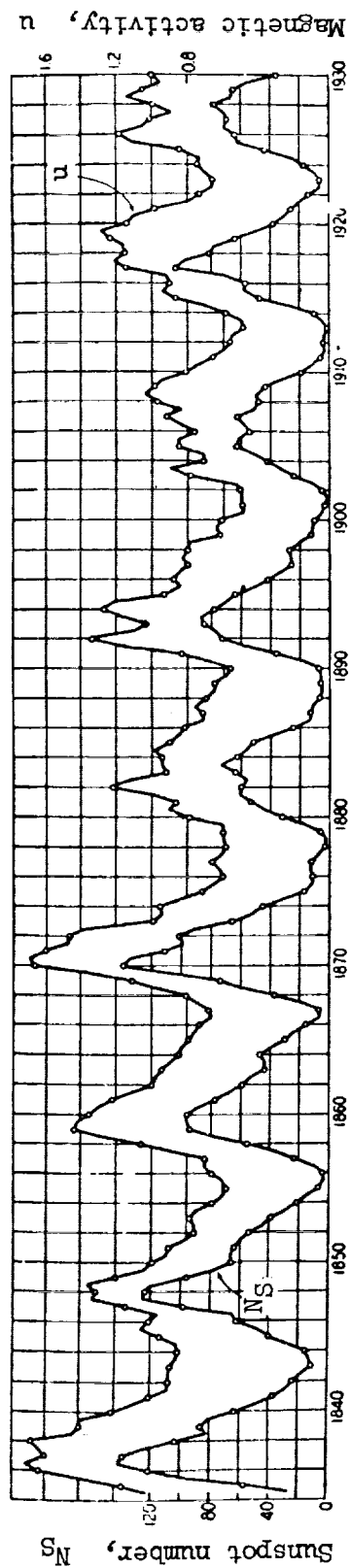
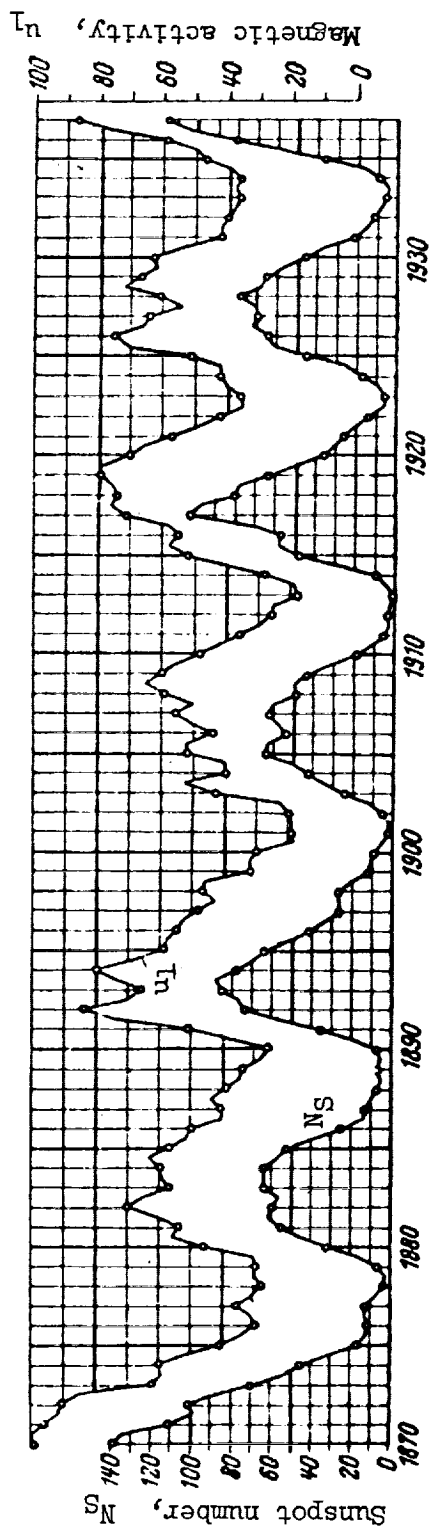
(a) Magnetic activity  $u$ .(b) Magnetic activity  $u_l$ .

Figure 23.- Comparison of magnetic activity and sunspot number (annual means). (From ref. 1.)

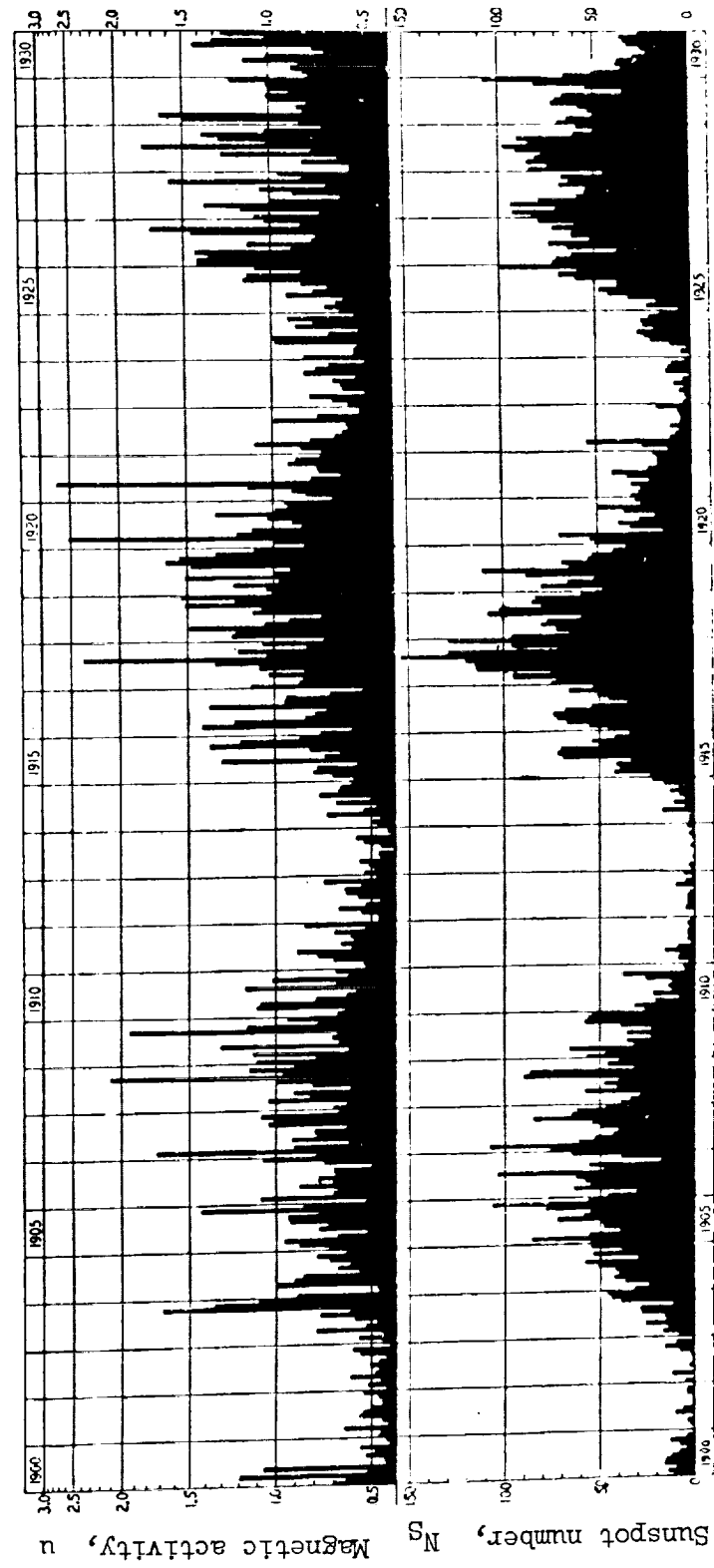
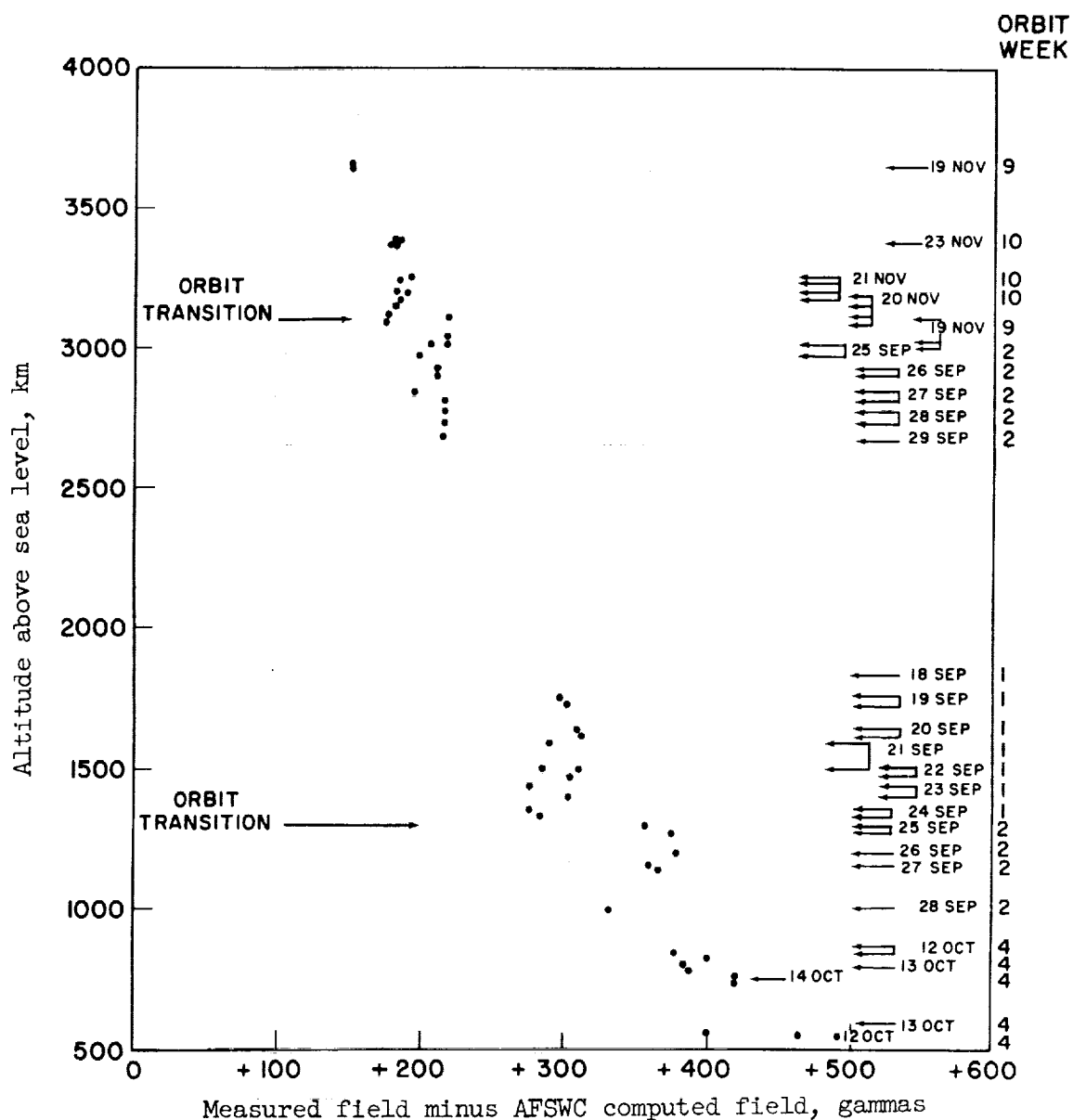
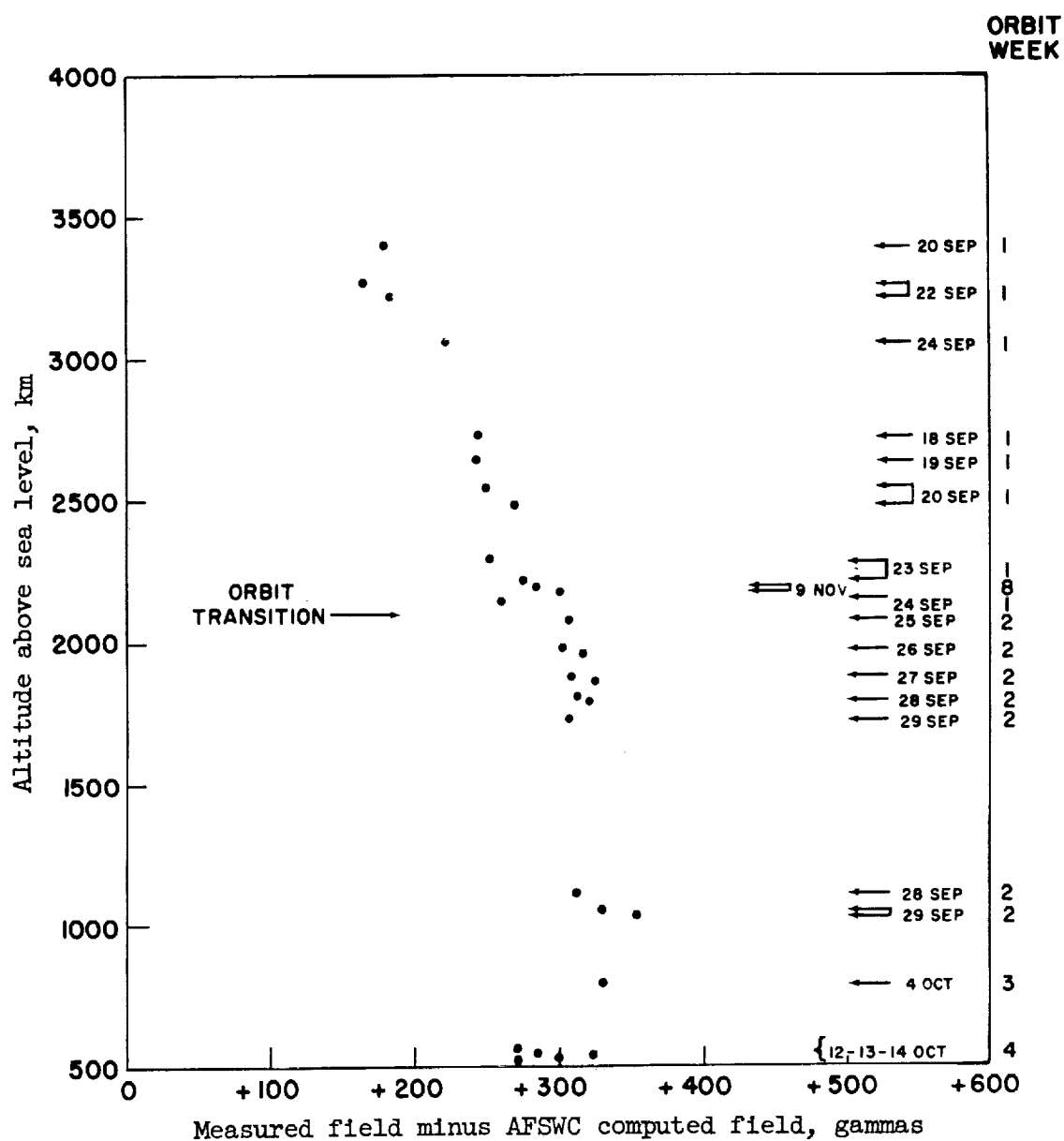


Figure 24.- The magnetic activity  $u$  and the sunspot number  $N_s$  (monthly means). (From ref. 1.)



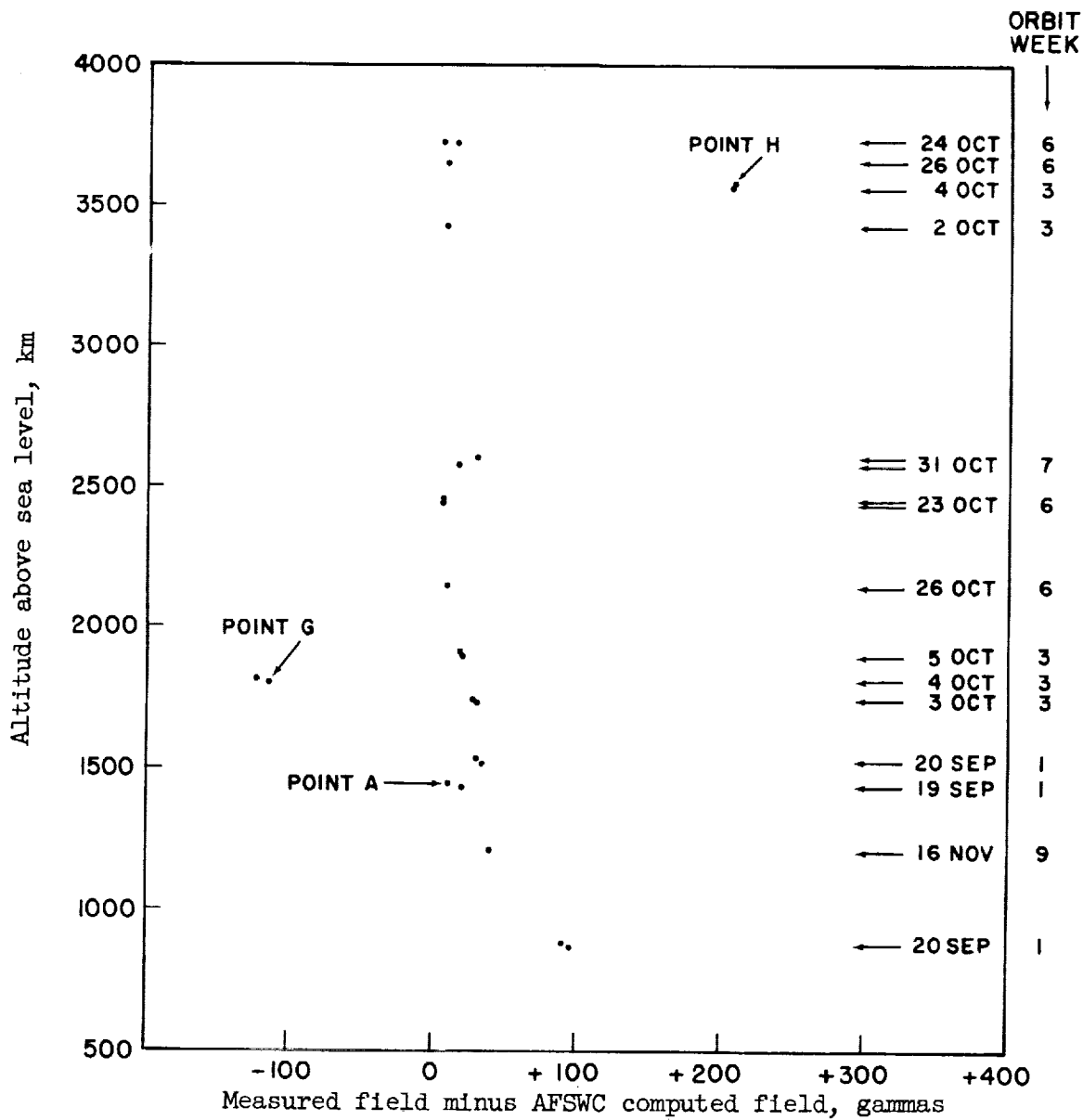
(a) Longitude,  $134^{\circ}$  E to  $140^{\circ}$  E; latitude,  $24^{\circ}$  S to  $30^{\circ}$  S.

Figure 25.- Differences between the measured field and the field computed by Jensen and Whitaker from the U.S.N.H.O. charts as a function of altitude with orbit computation at one-week intervals. (From ref. 36.)



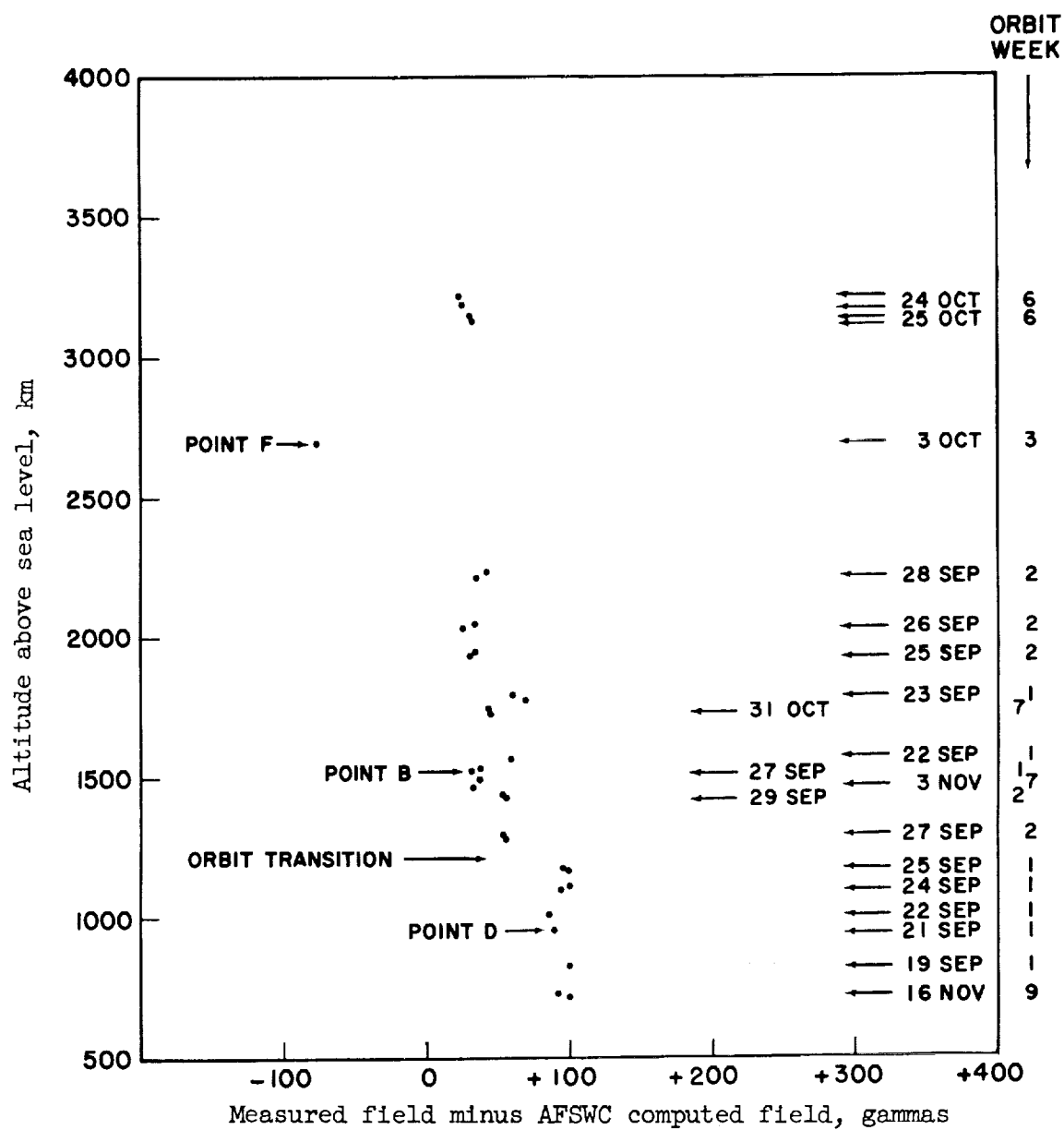
(b) Longitude,  $134^{\circ}$  E to  $140^{\circ}$  E; latitude,  $30^{\circ}$  S to  $33.5^{\circ}$  S.

Figure 25.- Continued.



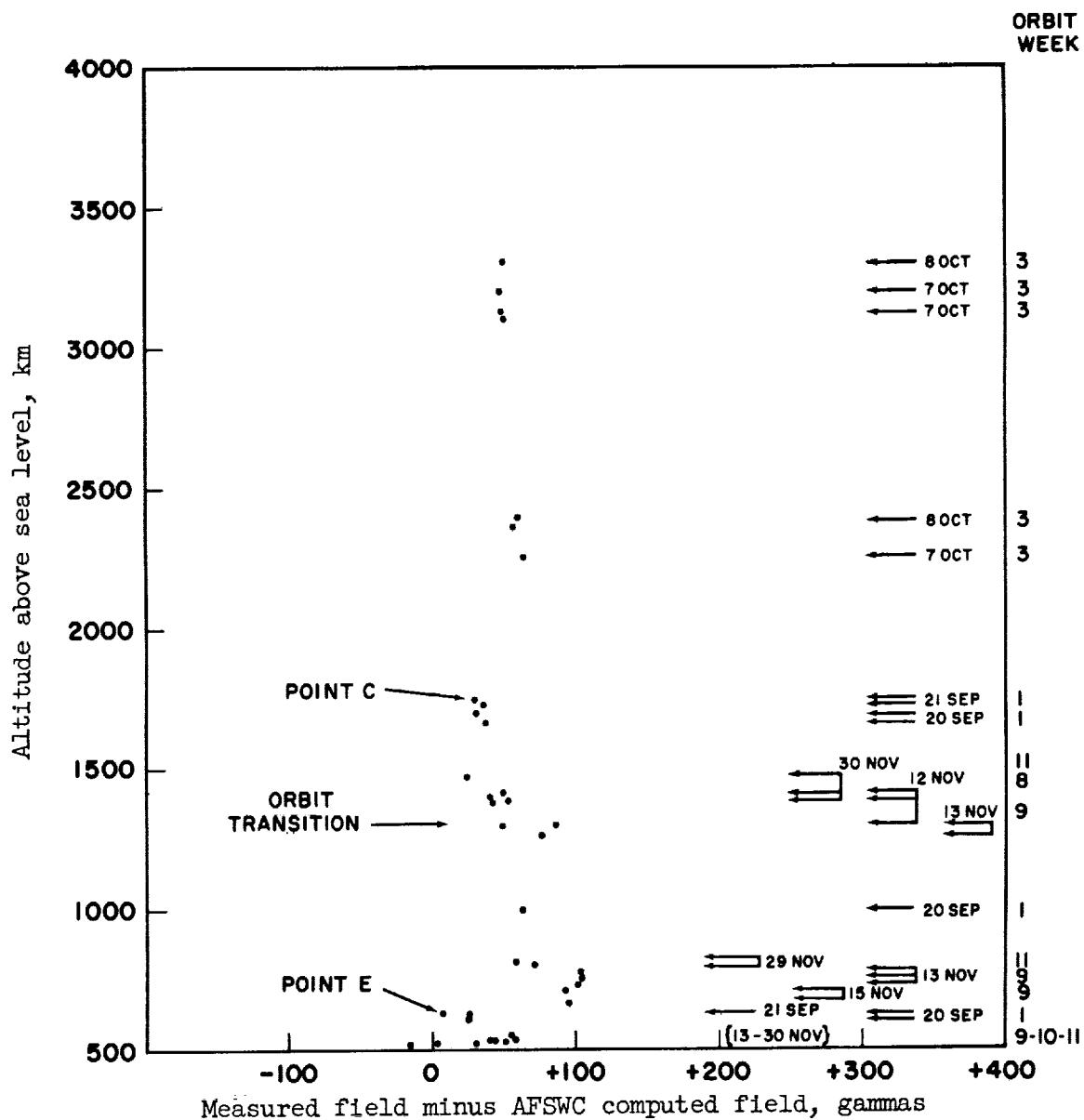
(c) Longitude,  $74^{\circ}$  W to  $80^{\circ}$  W; latitude,  $26^{\circ}$  N to  $30^{\circ}$  N.

Figure 25.- Continued.



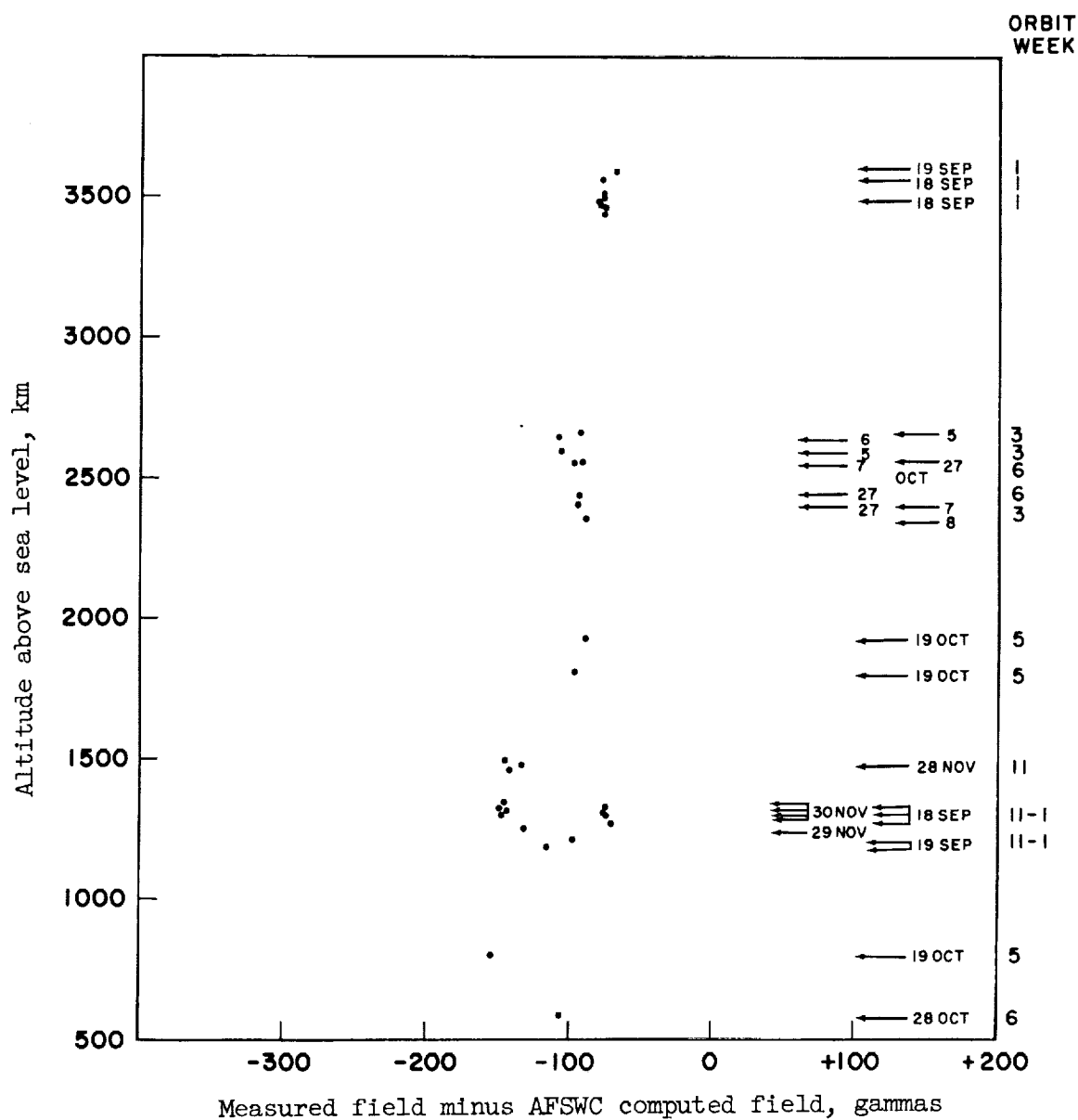
(d) Longitude,  $74^{\circ}$  W to  $80^{\circ}$  W; latitude,  $30^{\circ}$  N to  $33.5^{\circ}$  N.

Figure 25.- Continued.



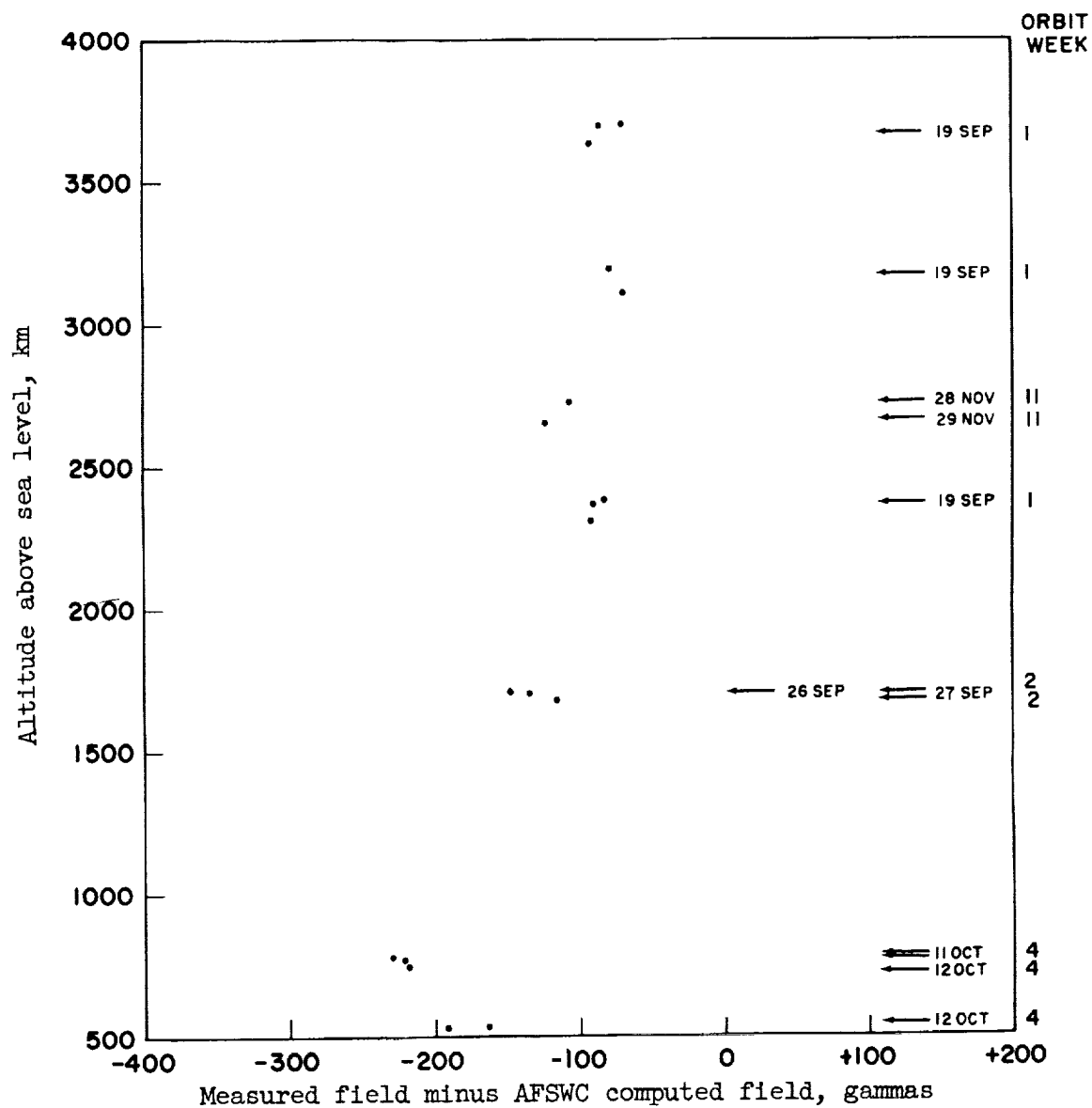
(e) Longitude,  $114^{\circ}$  W to  $120^{\circ}$  W; latitude,  $26^{\circ}$  N to  $33.5^{\circ}$  N.

Figure 25.- Continued.



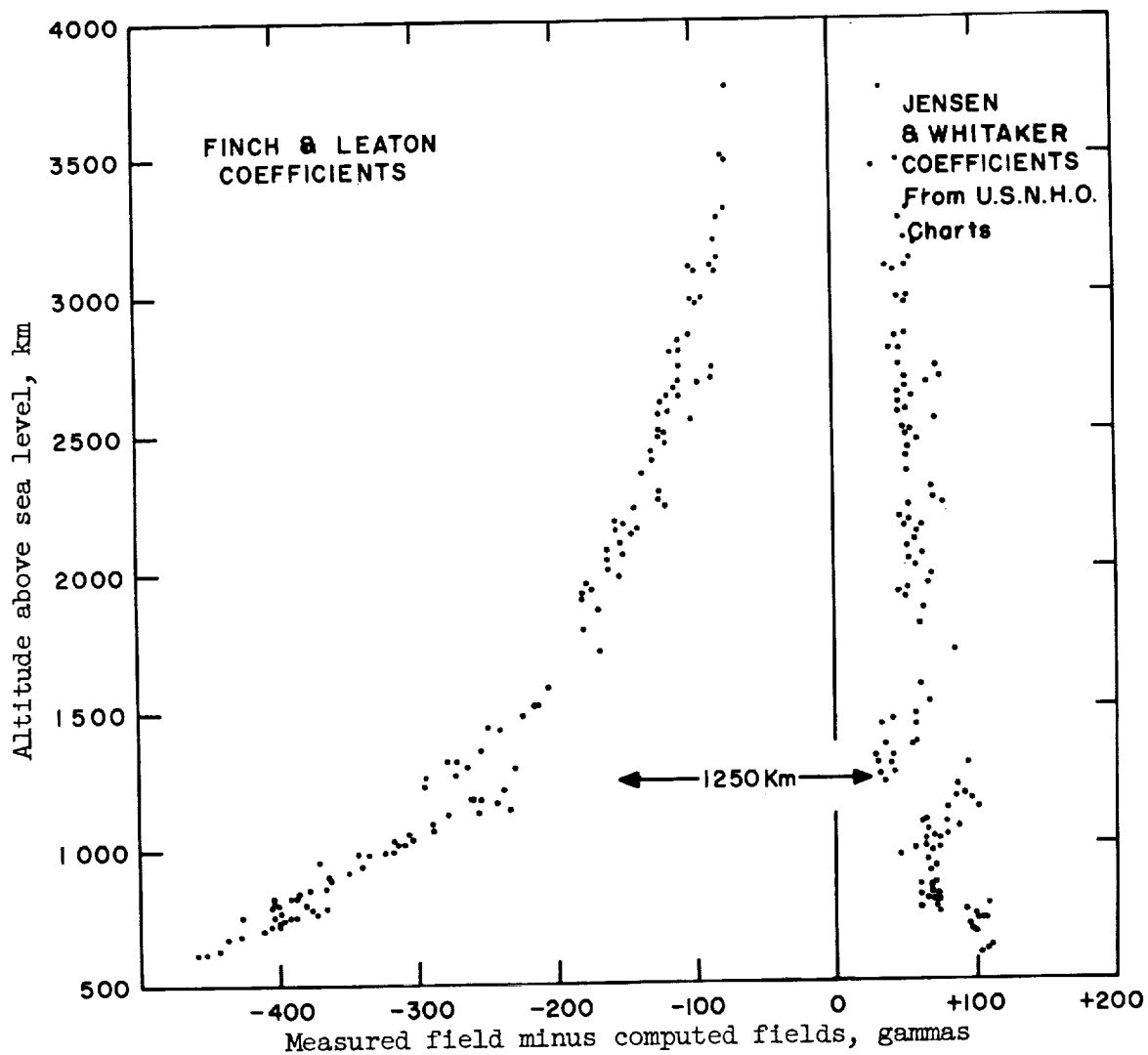
(f) Longitude,  $74^{\circ}$  W to  $82^{\circ}$  W; latitude,  $5^{\circ}$  S to  $20^{\circ}$  S.

Figure 25.- Continued.



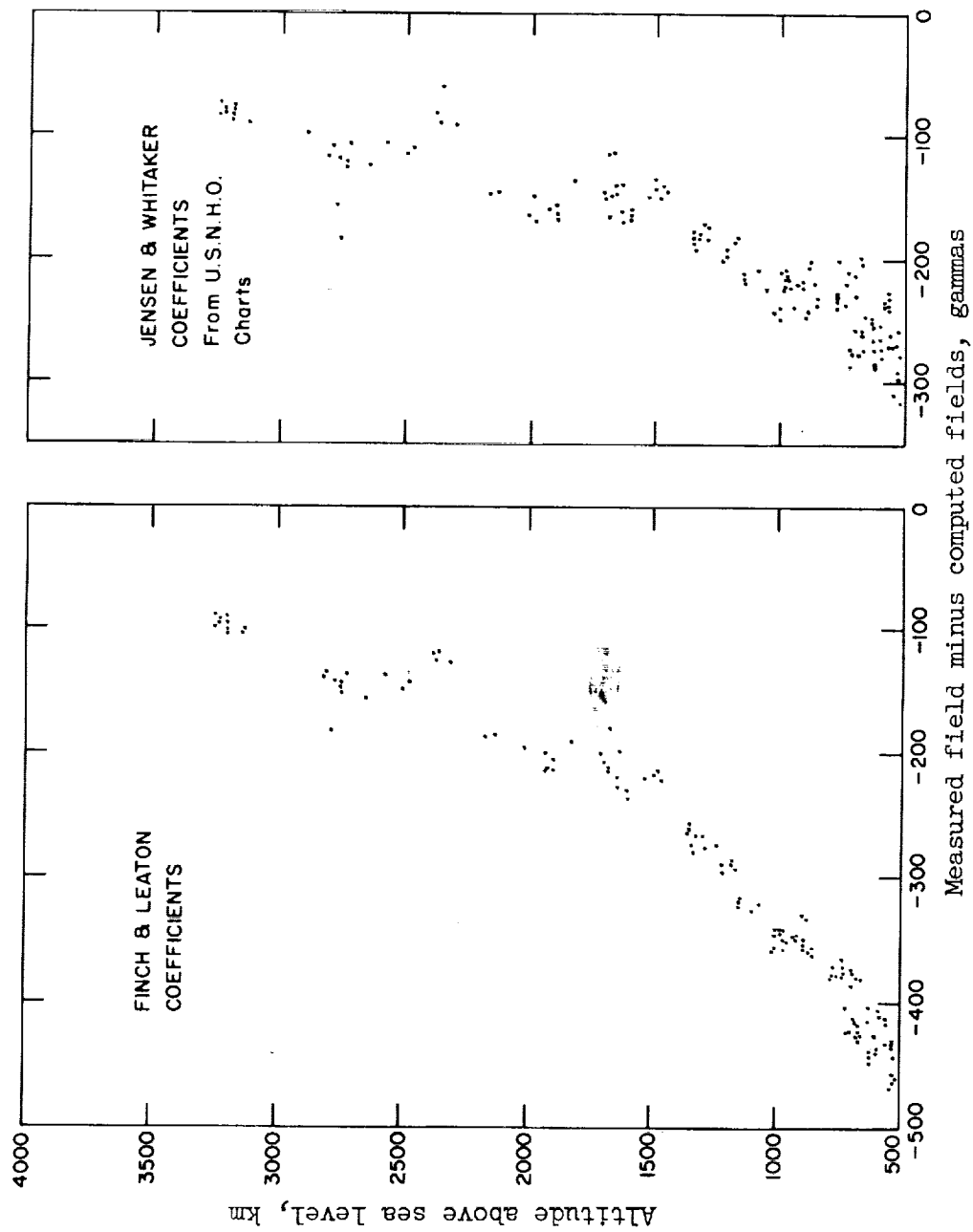
(g) Longitude,  $66^{\circ}$  W to  $74^{\circ}$  W; latitude,  $25^{\circ}$  S to  $33.5^{\circ}$  S.

Figure 25.- Concluded.



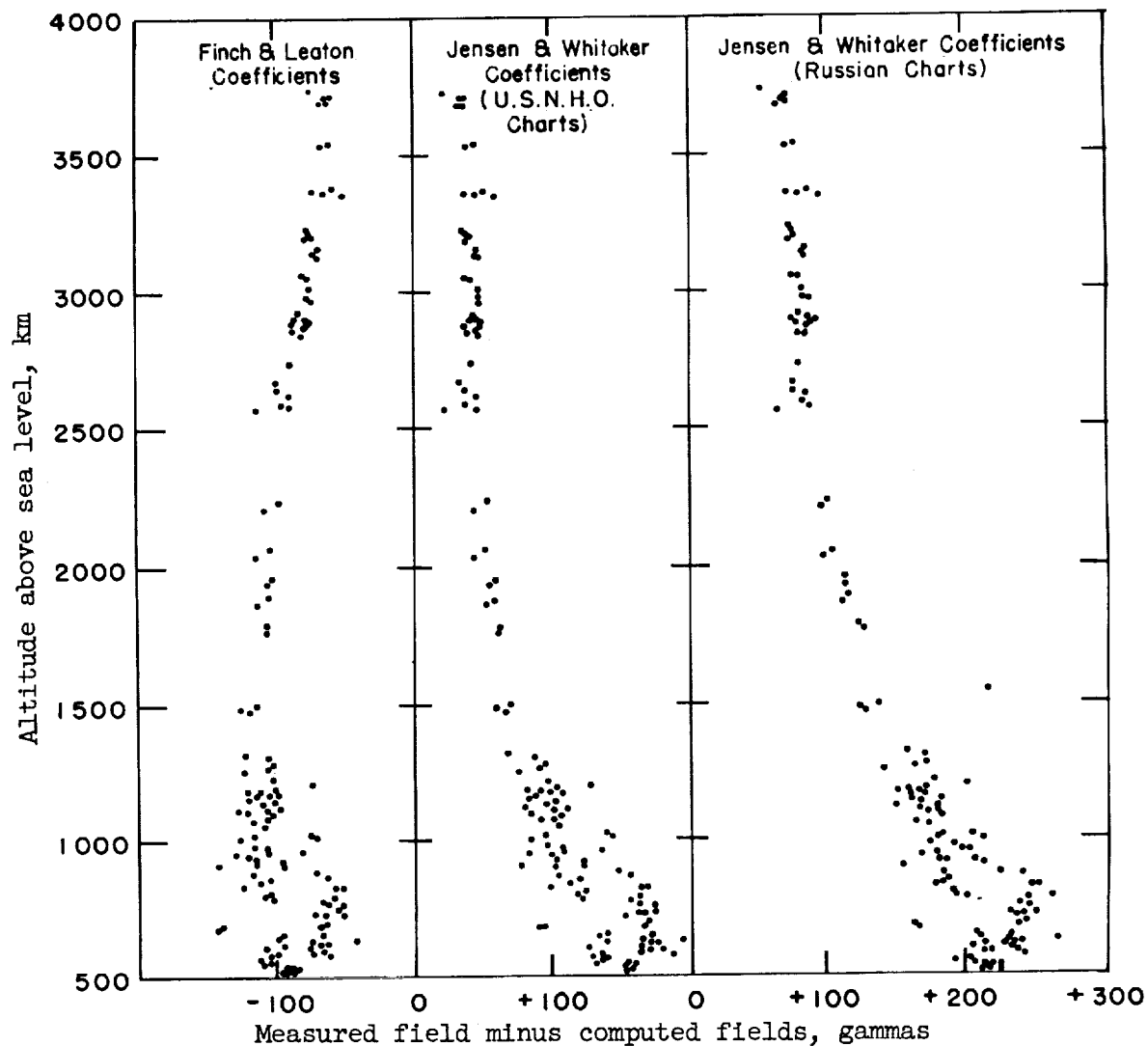
(a) Longitude,  $111^{\circ}$  W to  $121^{\circ}$  W; latitude,  $32^{\circ}$  N to  $33.5^{\circ}$  N.

Figure 26.- Differences between the measured field and the computed fields as a function of altitude with orbit computation at one-week intervals. (From ref. 37.)



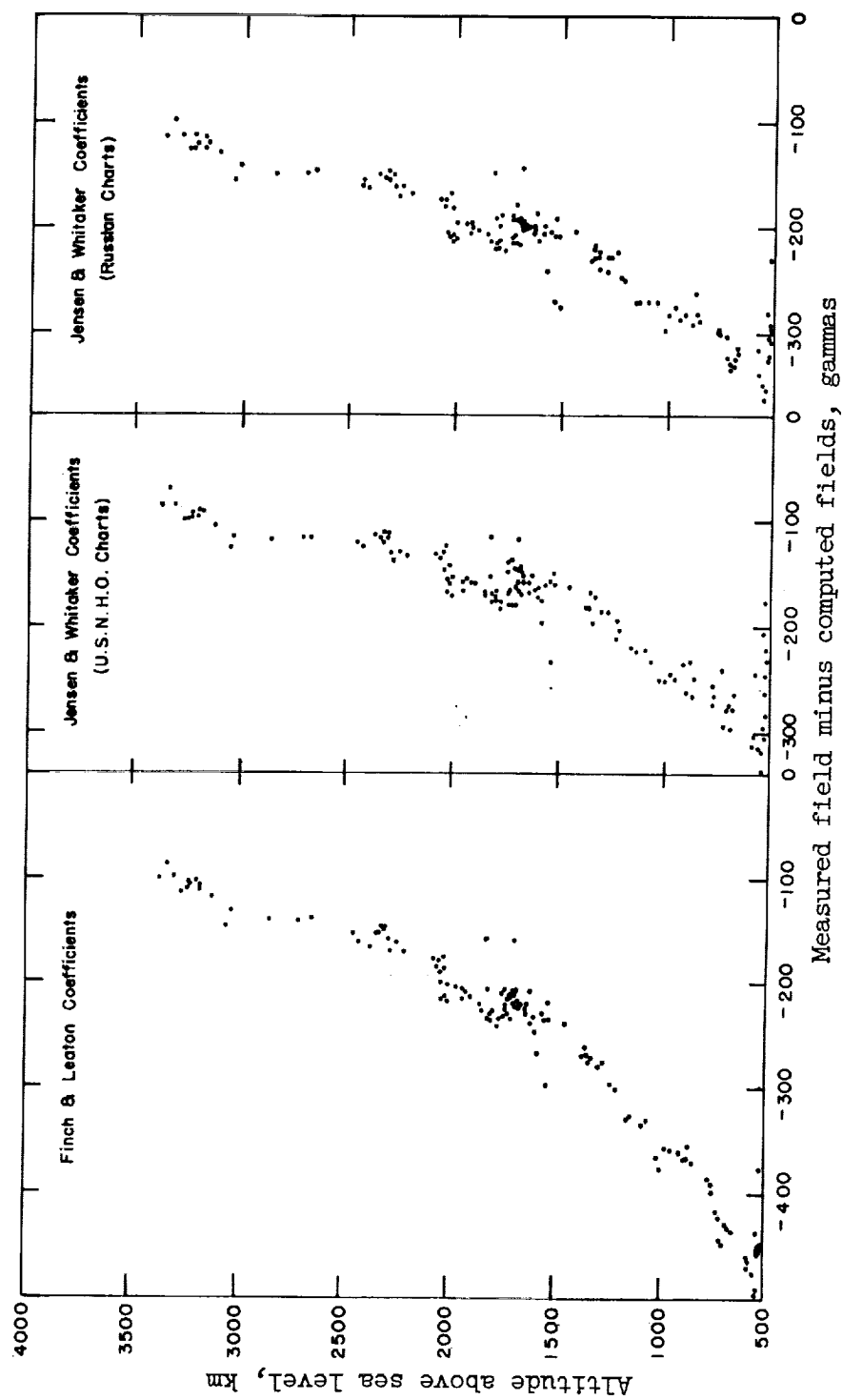
(b) Longitude,  $69^{\circ}$  W to  $74^{\circ}$  W; latitude,  $29^{\circ}$  S to  $33.5^{\circ}$  S.

Figure 26.- Concluded.



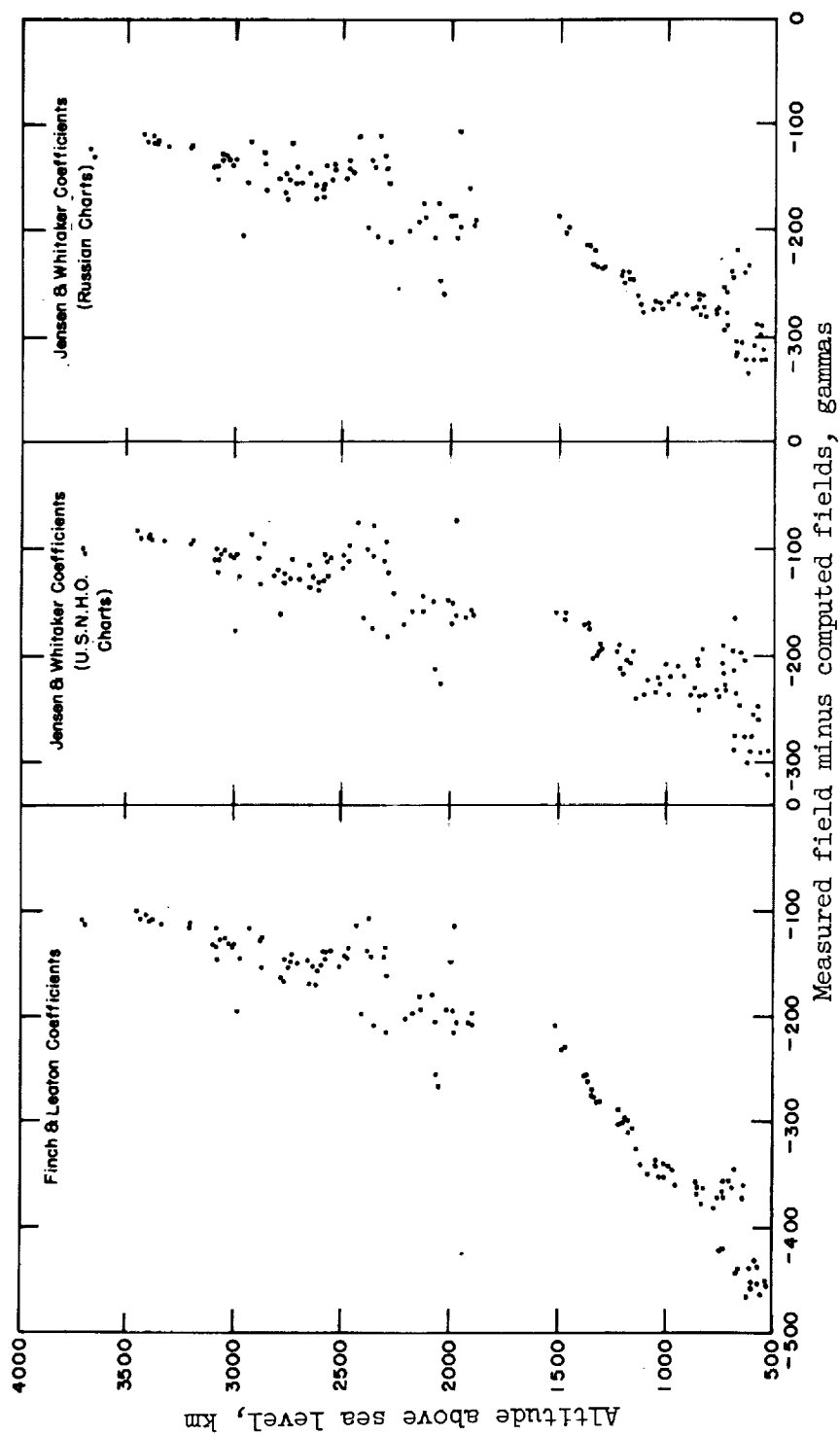
(a) Longitude,  $74^{\circ}$  W to  $79^{\circ}$  W; latitude,  $32^{\circ}$  N to  $33.5^{\circ}$  N.

Figure 27.- Differences between the measured field and the computed fields as a function of altitude with orbit computation at one-month intervals. (From ref. 37.)



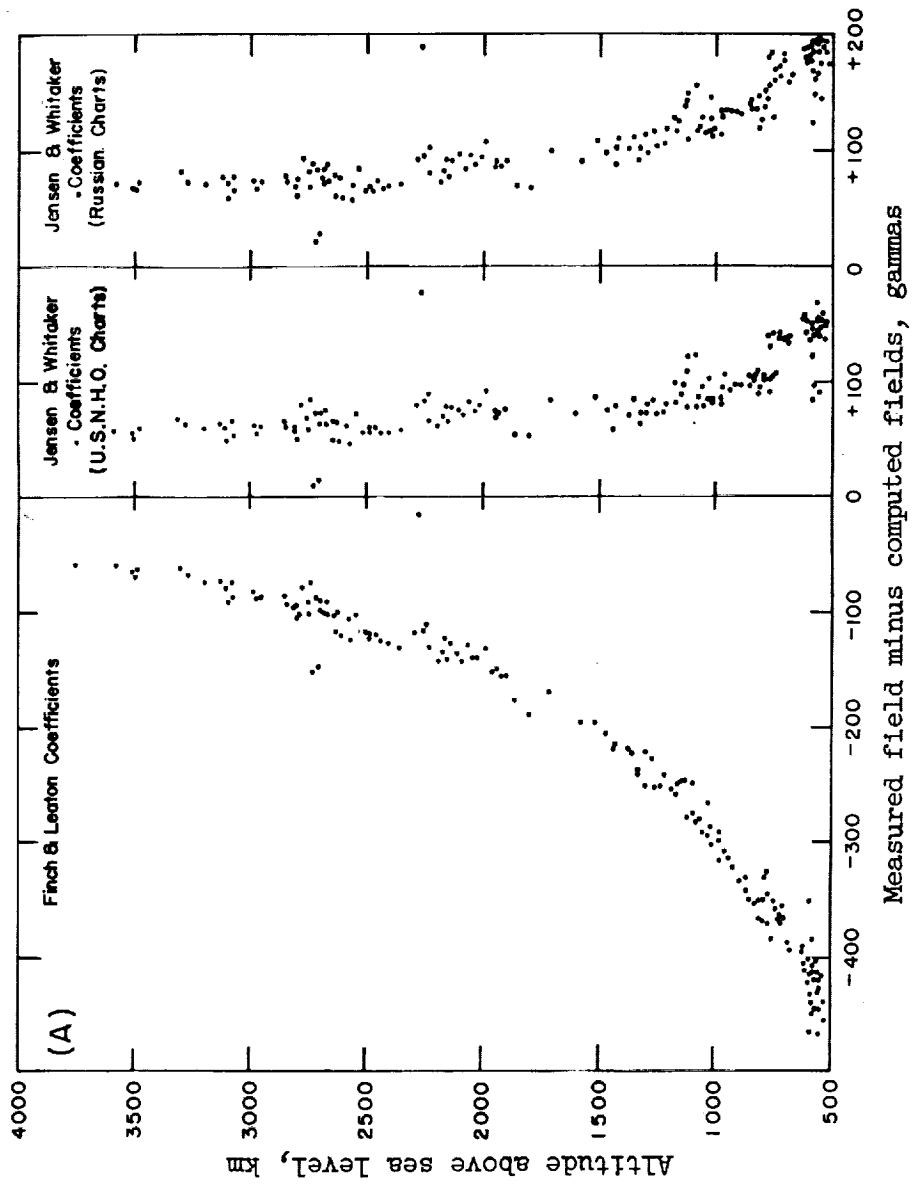
(b) Longitude,  $64^{\circ}$  W to  $74^{\circ}$  W; latitude,  $32^{\circ}$  S to  $33.5^{\circ}$  S.

Figure 27.- Continued.



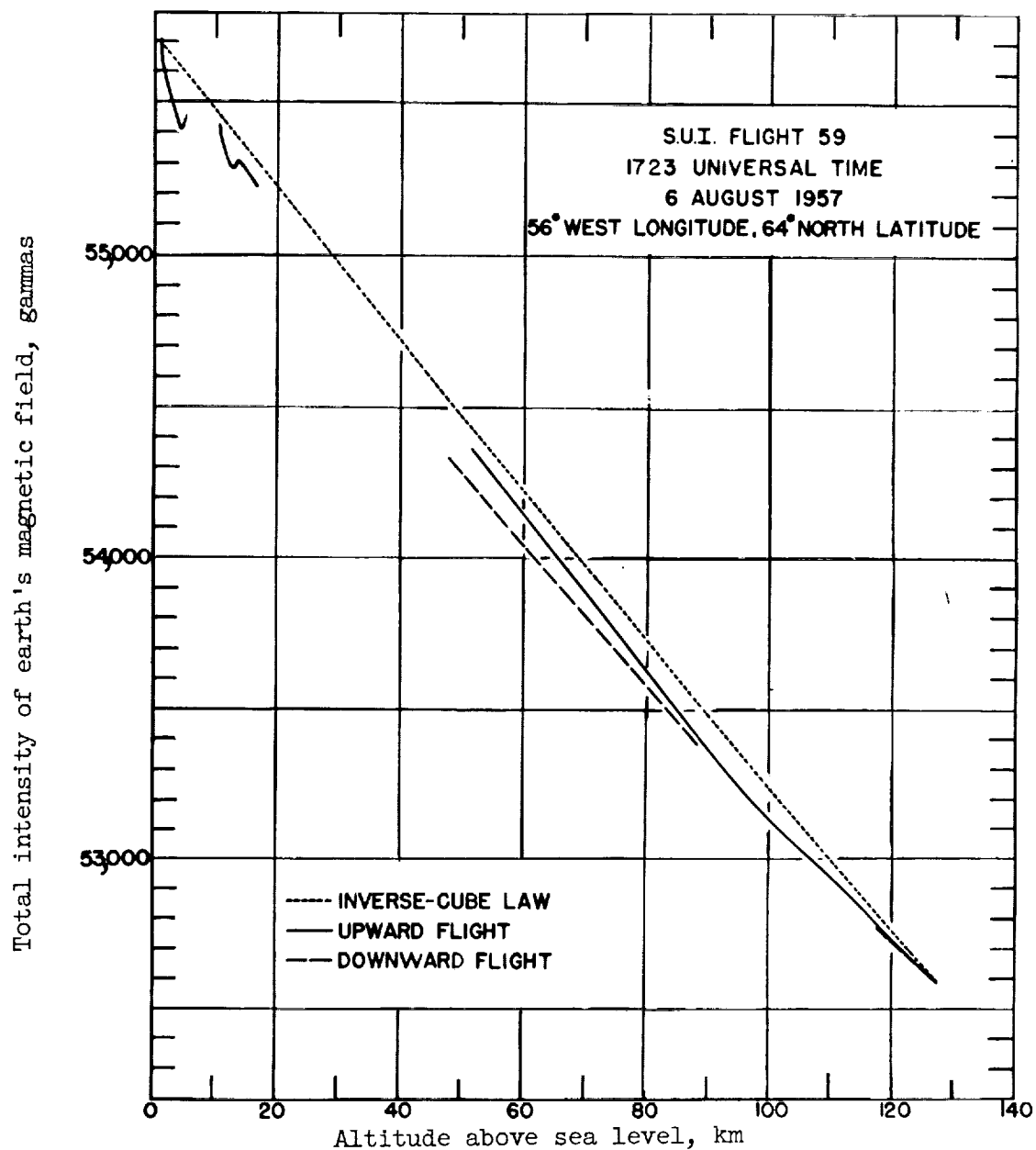
(c) Longitude,  $64^{\circ}$  W to  $74^{\circ}$  W; latitude,  $29^{\circ}$  S to  $32.5^{\circ}$  S.

Figure 27.- Continued.



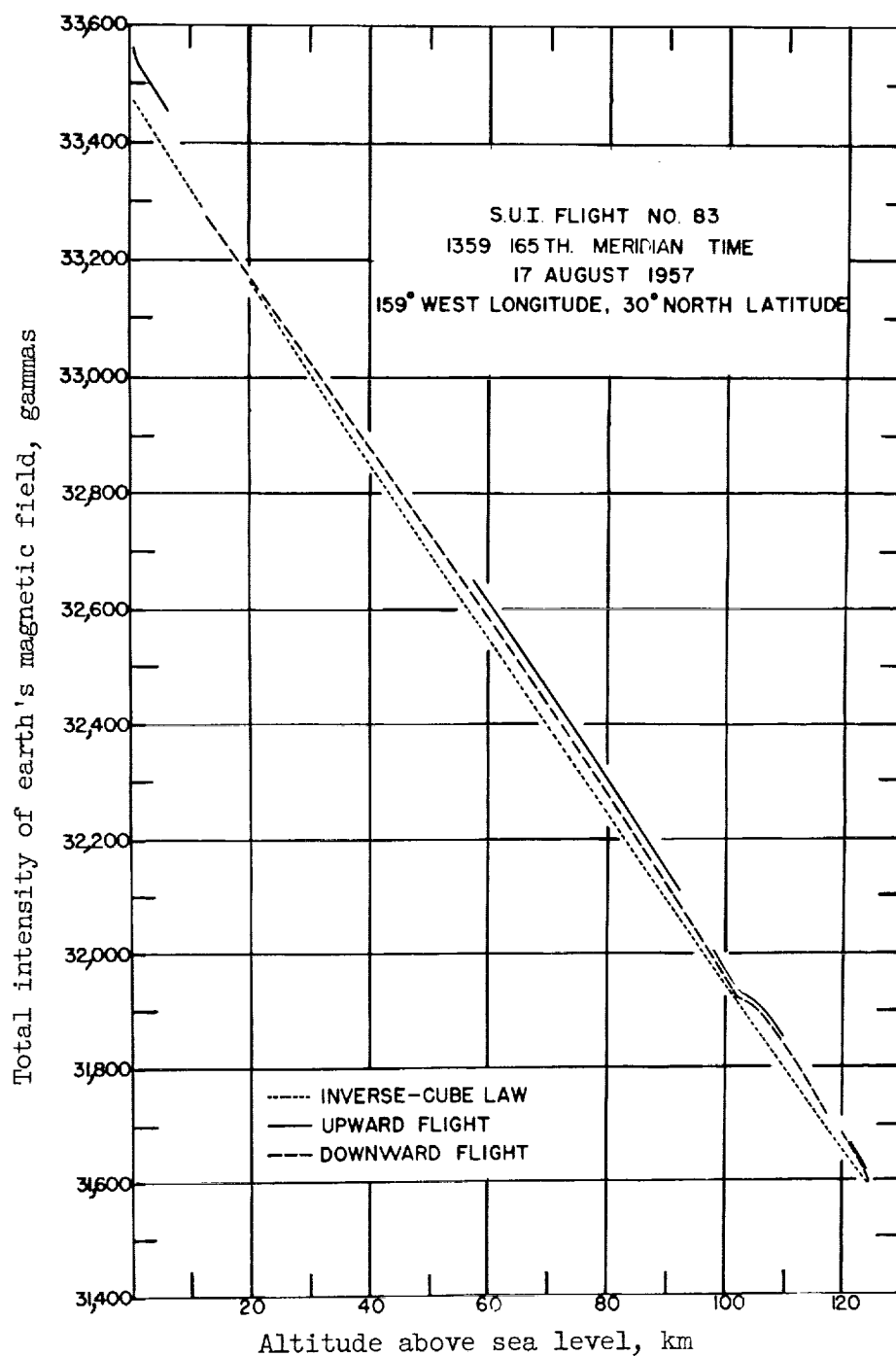
(d) Longitude,  $111^{\circ}$  W to  $121^{\circ}$  W; latitude,  $32^{\circ}$  N to  $33.5^{\circ}$  N.

Figure 27.- Concluded.



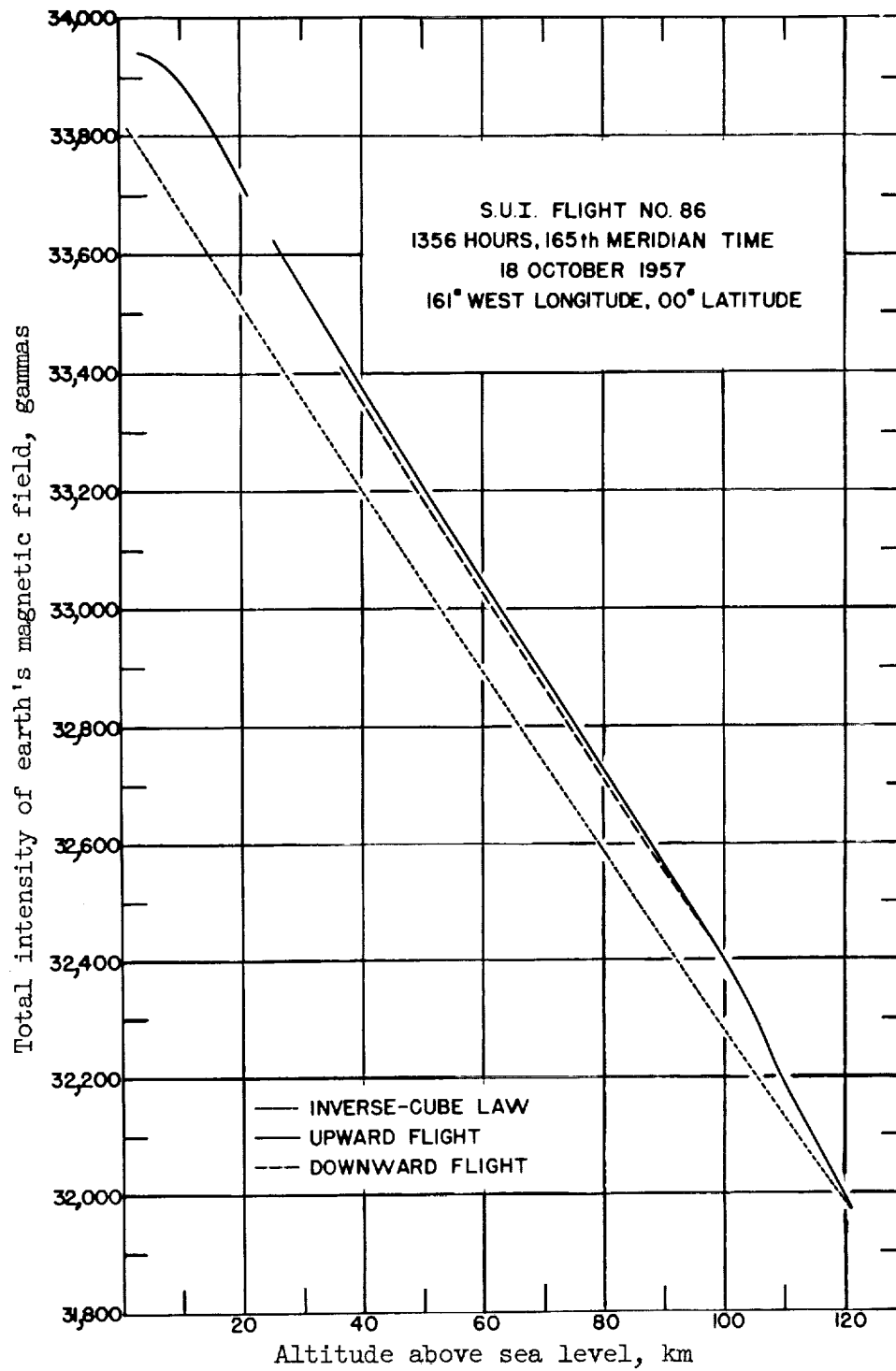
(a) State University of Iowa flight no. 59.

Figure 28.- Measured magnetic-field intensity as a function of altitude compared with the inverse cube law. (From ref. 40.)



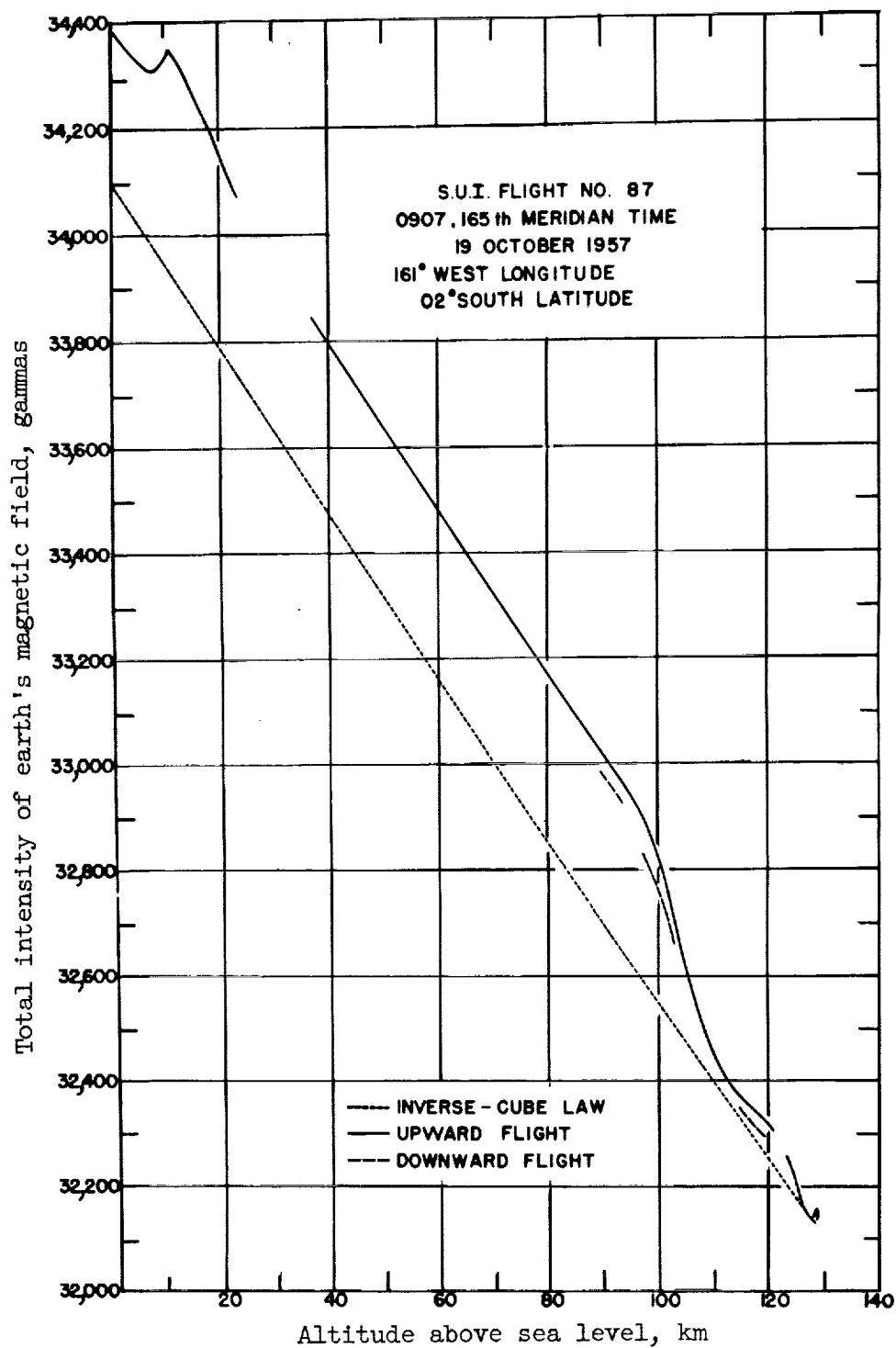
(b) State University of Iowa flight no. 83.

Figure 28.- Continued.



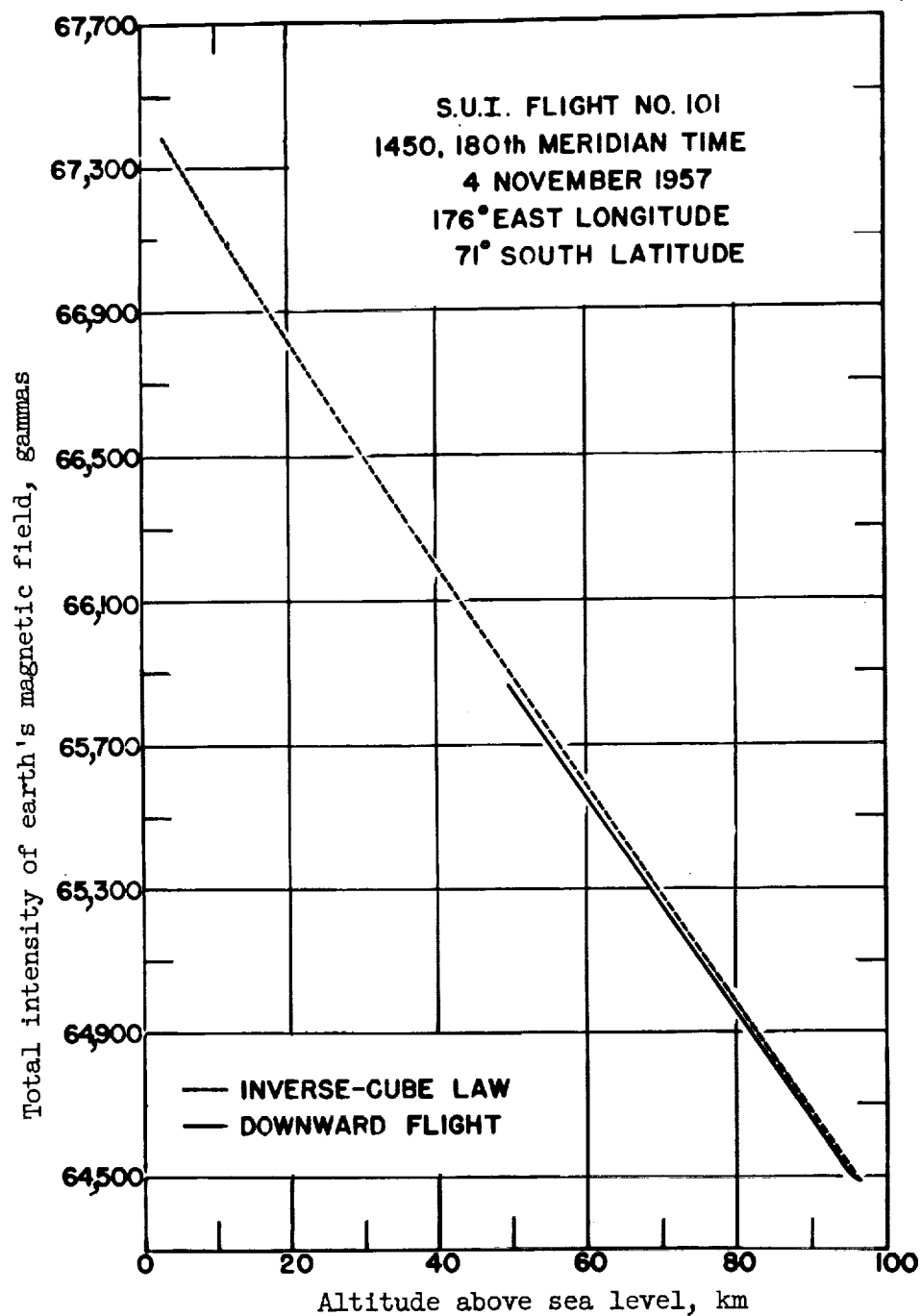
(c) State University of Iowa flight no. 86.

Figure 28.- Continued.



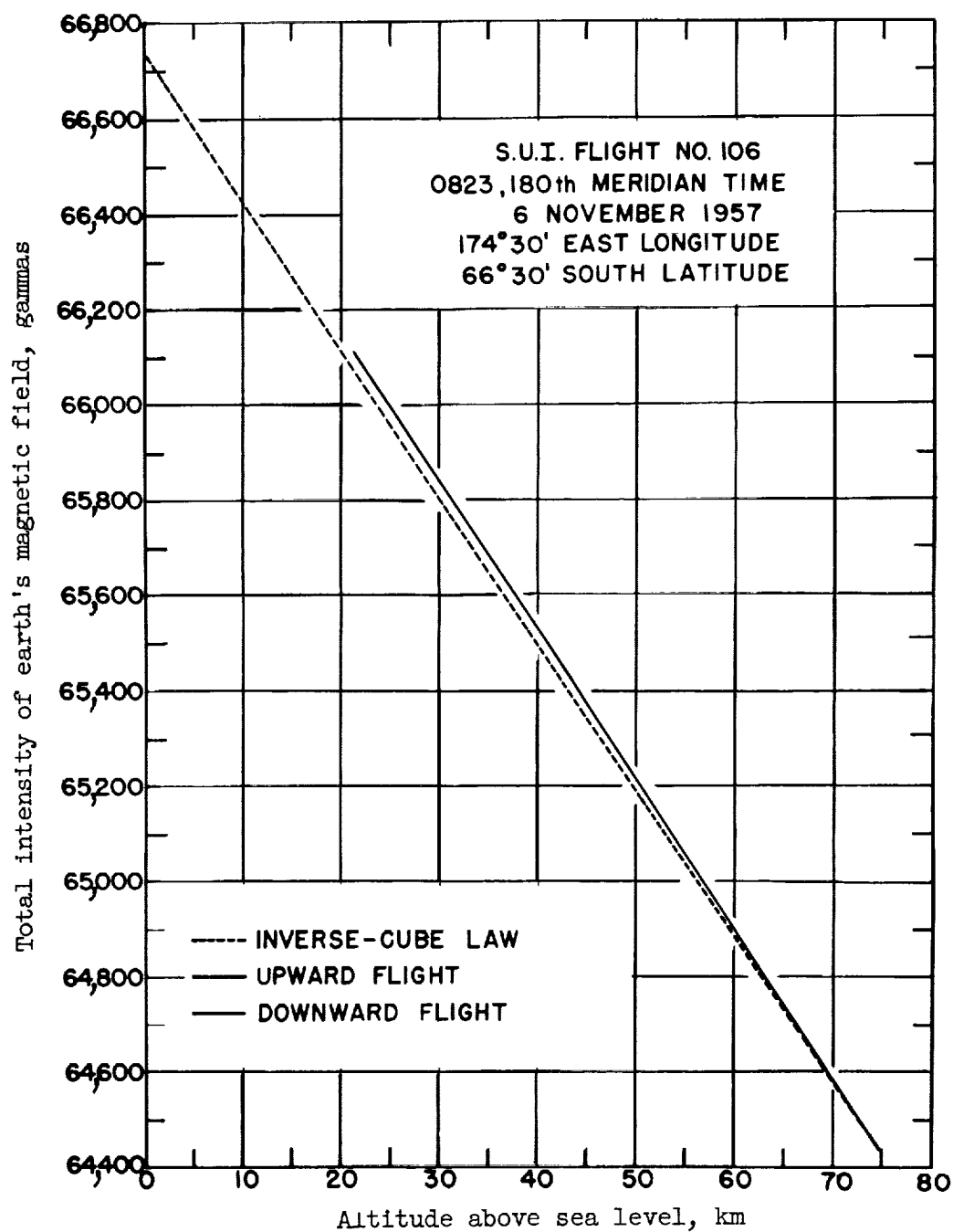
(d) State University of Iowa flight no. 87.

Figure 28.- Continued.



(e) State University of Iowa flight no. 101.

Figure 28.- Continued.



(f) State University of Iowa flight no. 106.

Figure 28.- Concluded.

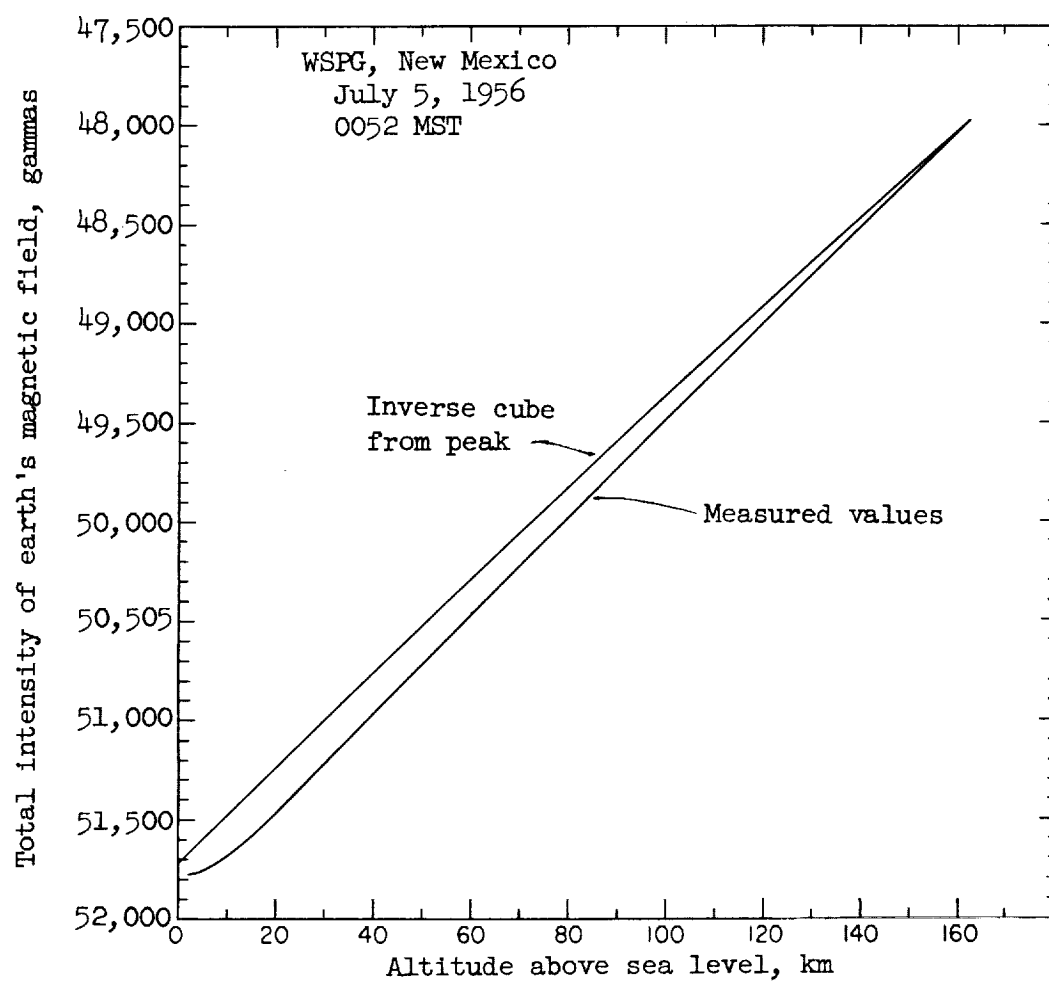
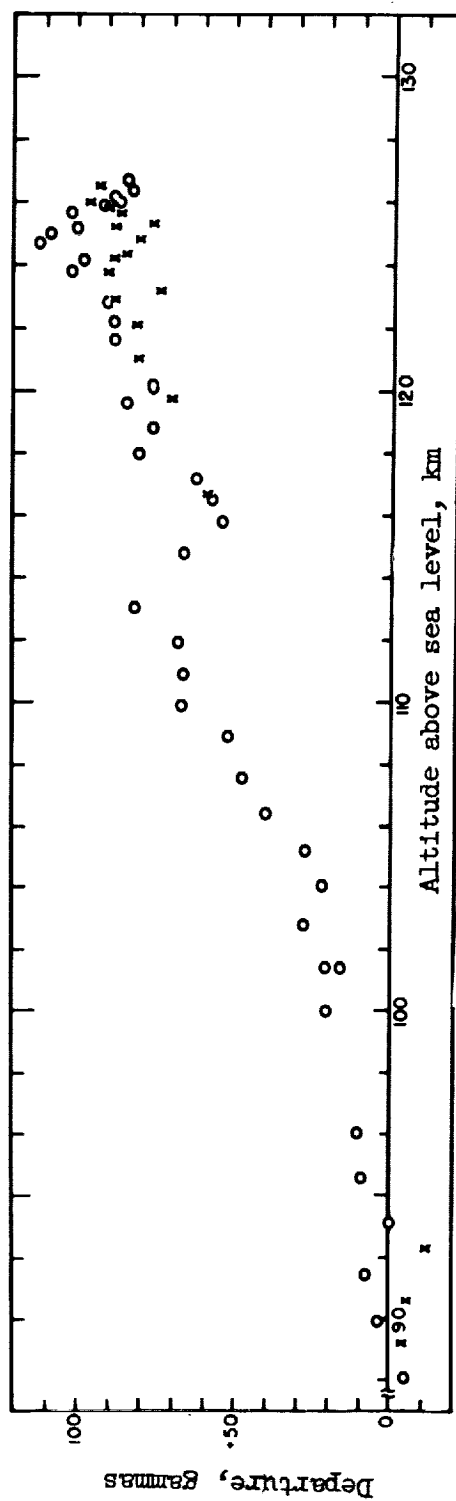
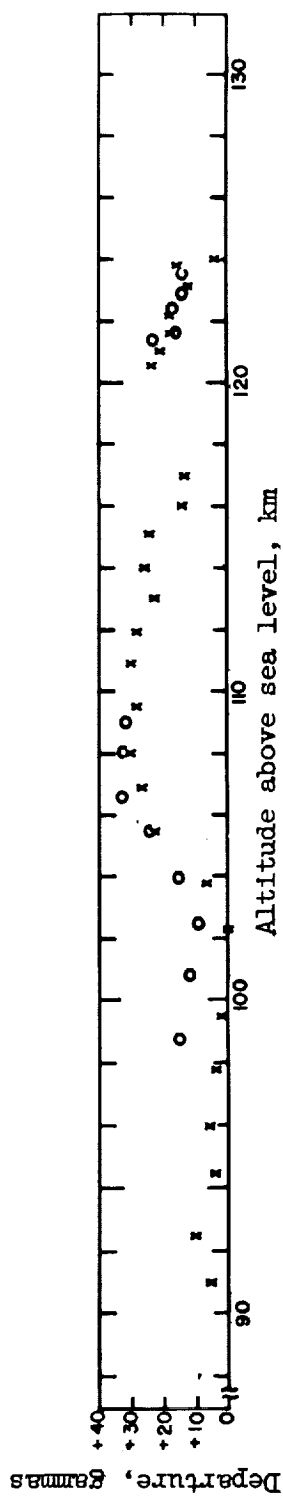


Figure 29.- Magnetic-field intensity as a function of altitude. (From ref. 41.)



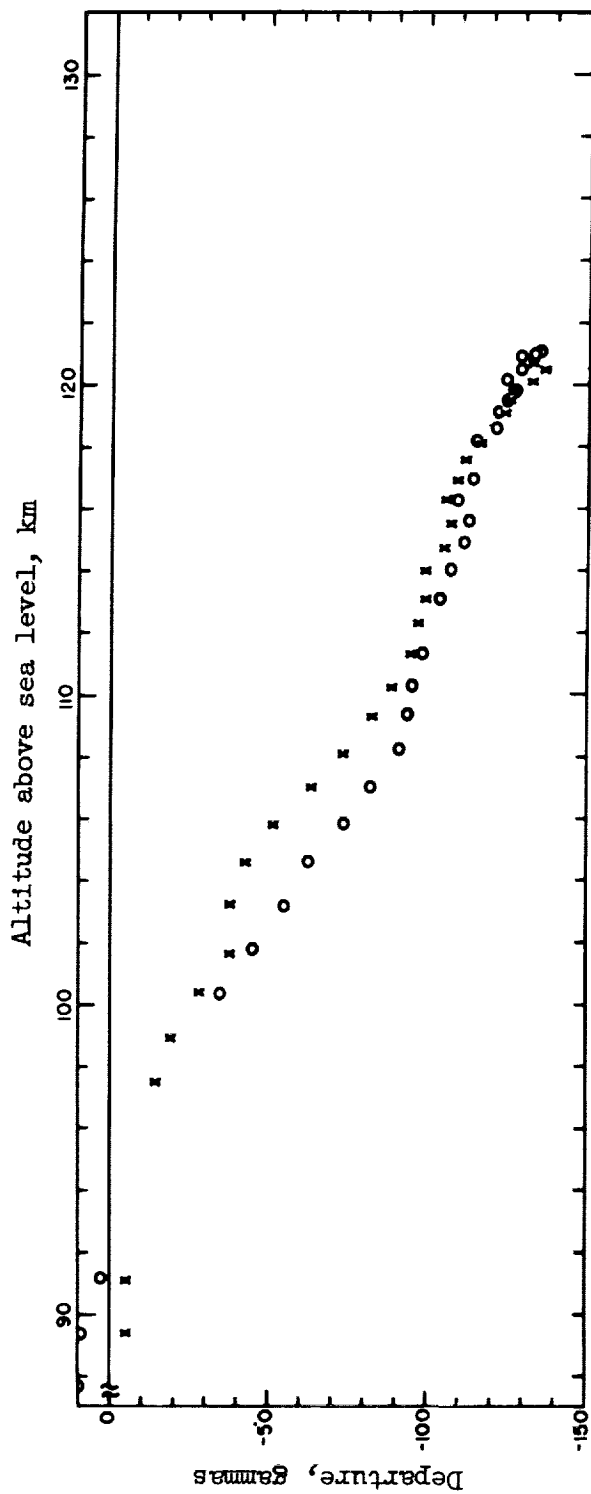
(a) State University of Iowa flight no. 59.

Figure 30.- Departure of flight measurements from inverse cube law as a function of altitude.  
(From ref. 40.)



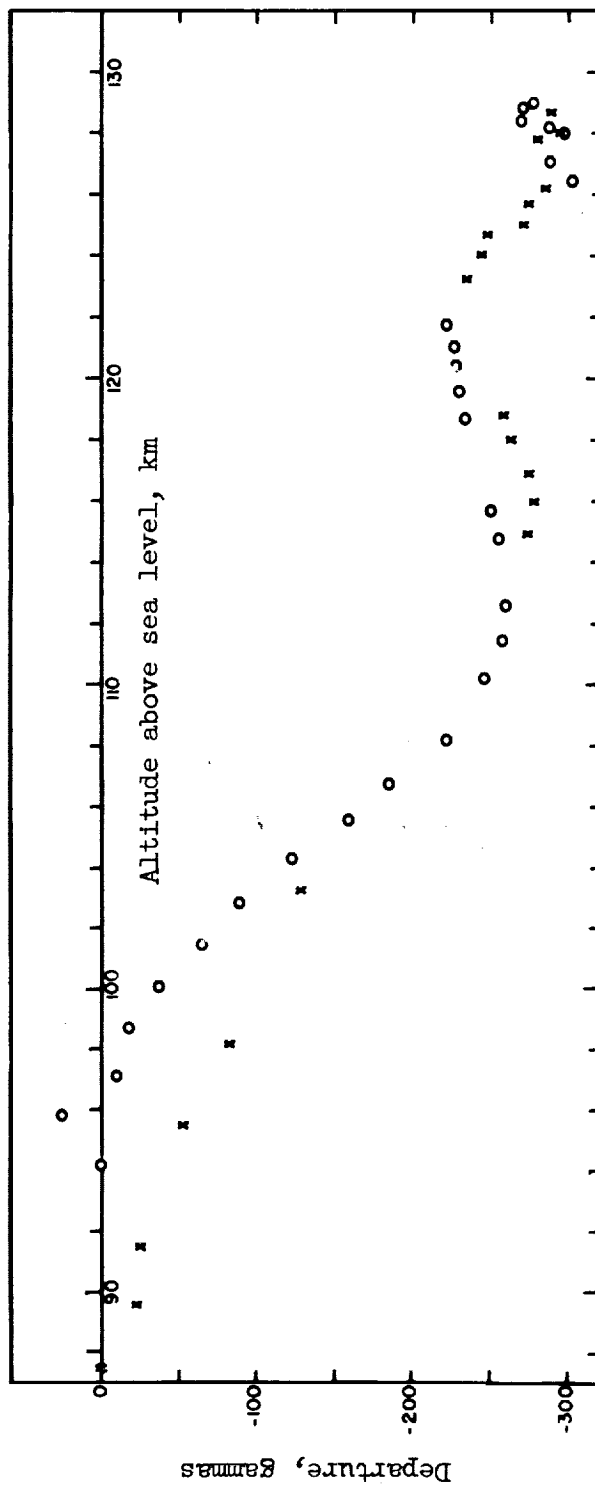
(b) State University of Iowa flight no. 83.

Figure 30.- Continued.



(c) State University of Iowa flight no. 86.

Figure 30.- Continued.



(d) State University of Iowa flight no. 87.

Figure 30.- Concluded.

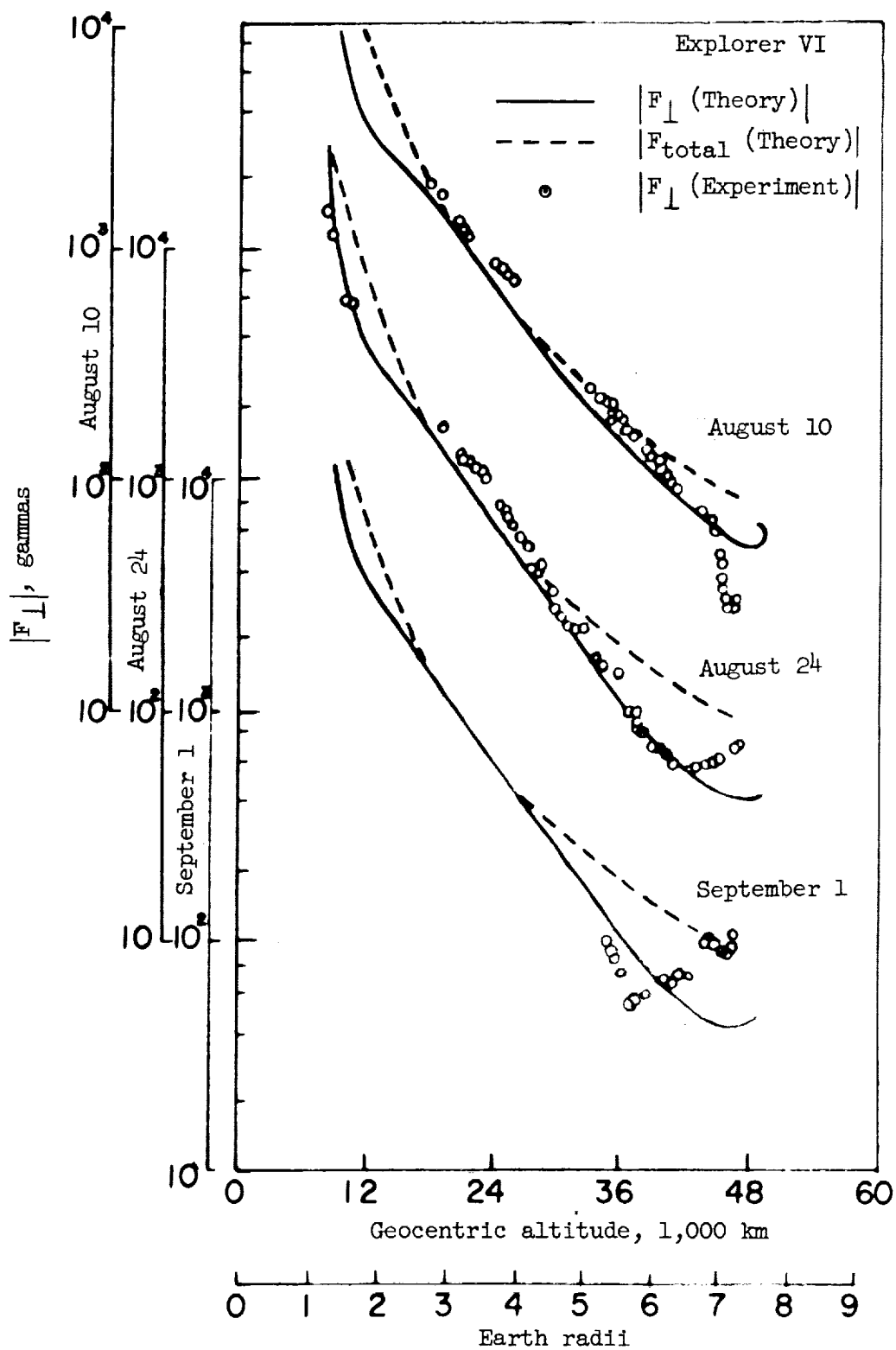


Figure 31.- Magnetic-field intensity in plane perpendicular to the spin axis  $F_{\perp}$  as a function of altitude. (From ref. 42.)

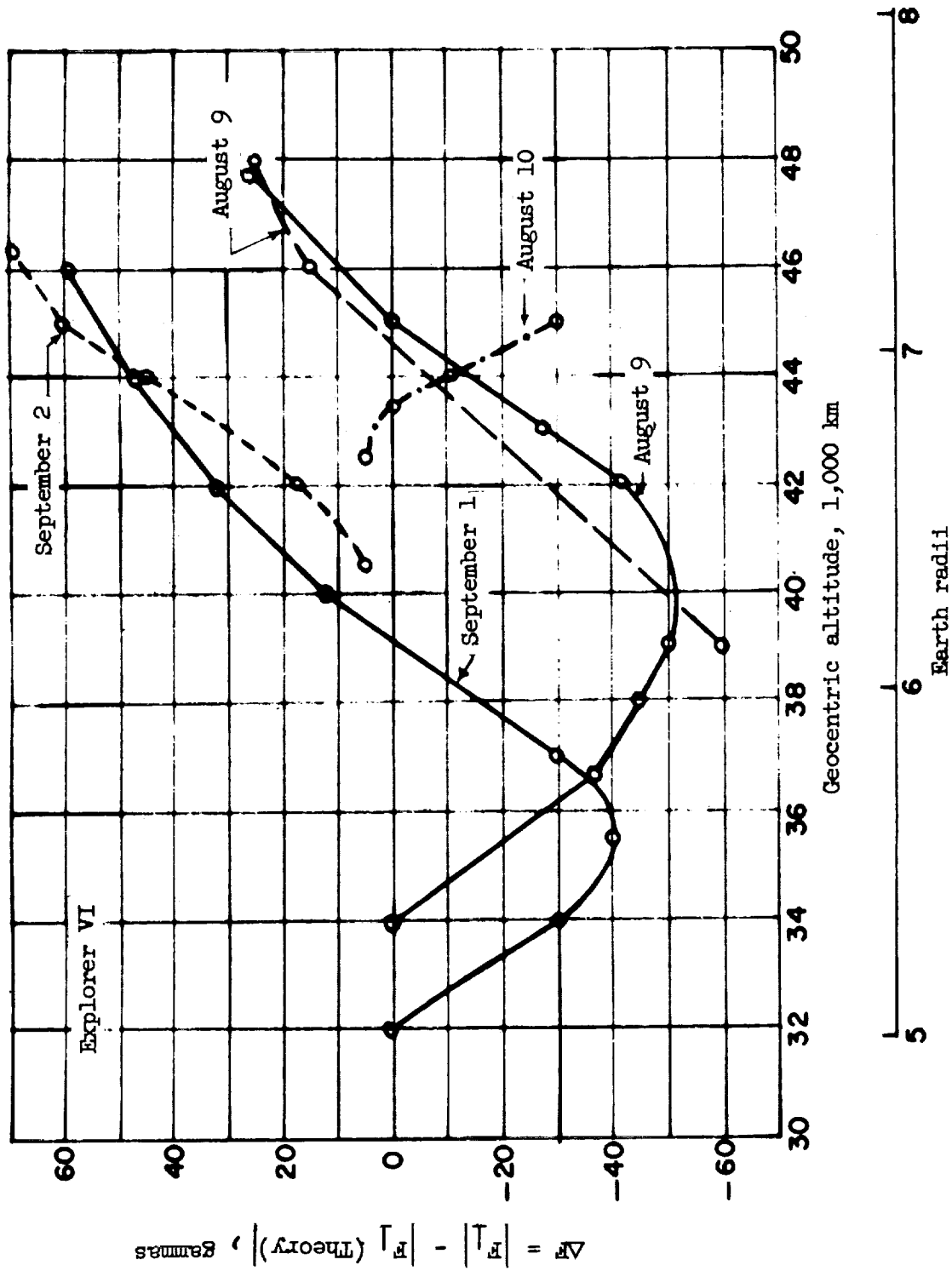


Figure 32.- The difference between the measured and the theoretical values of  $F_1$ .  
(From ref. 42.)

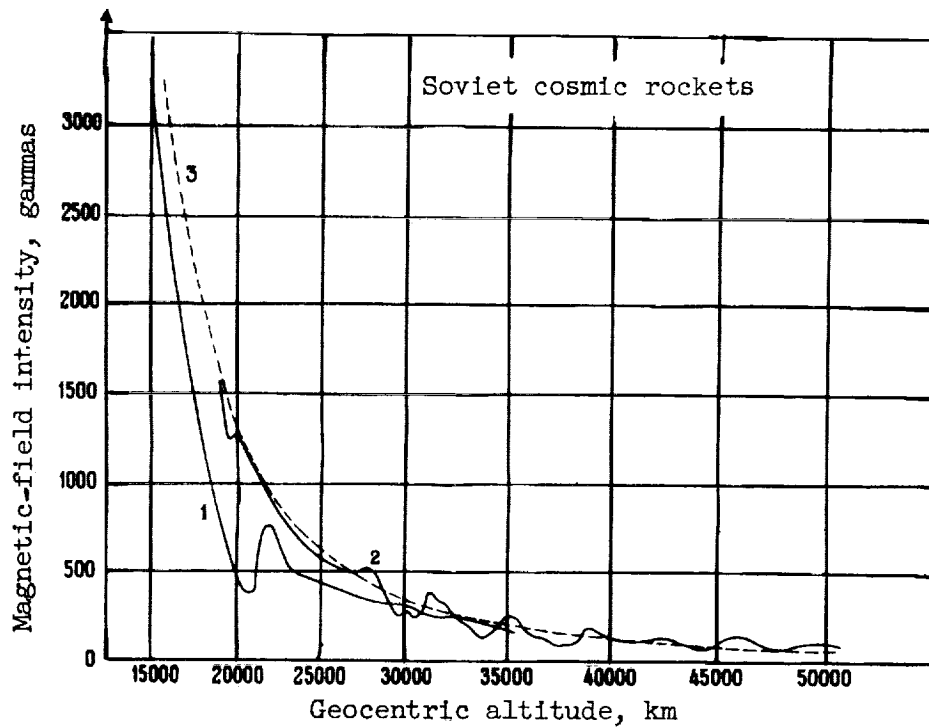


Figure 33.- Magnetic-field intensity as a function of altitude. Curves 1 and 2 represent data obtained during the flight of the first and second Soviet cosmic rockets, respectively. Curve 3 shows the theoretical variation of the magnetic field based on the dipole and quadrupole terms. (From ref. 43.)

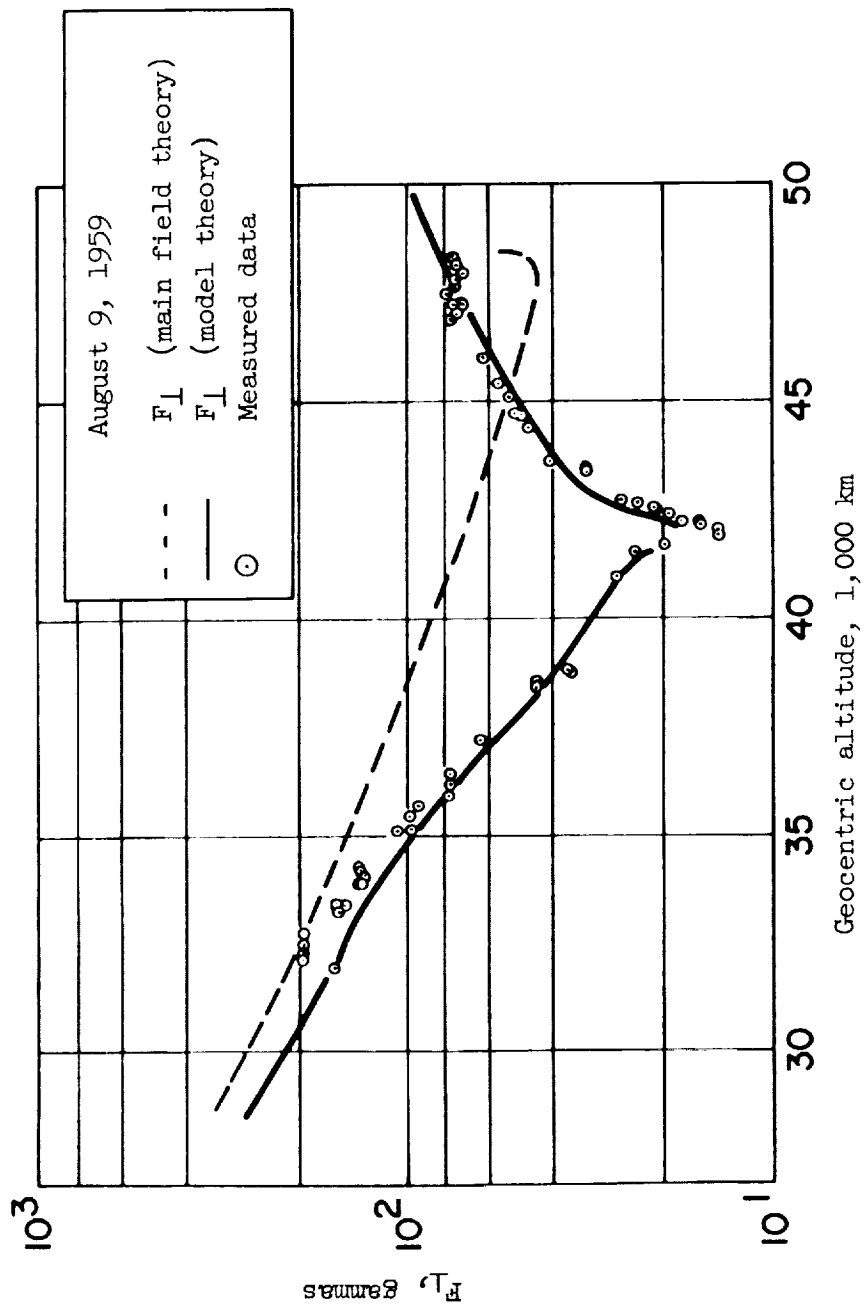


Figure 34.- Comparison between the results of the model calculation and Explorer VI (1959 Delta) data. (From ref. 44.)

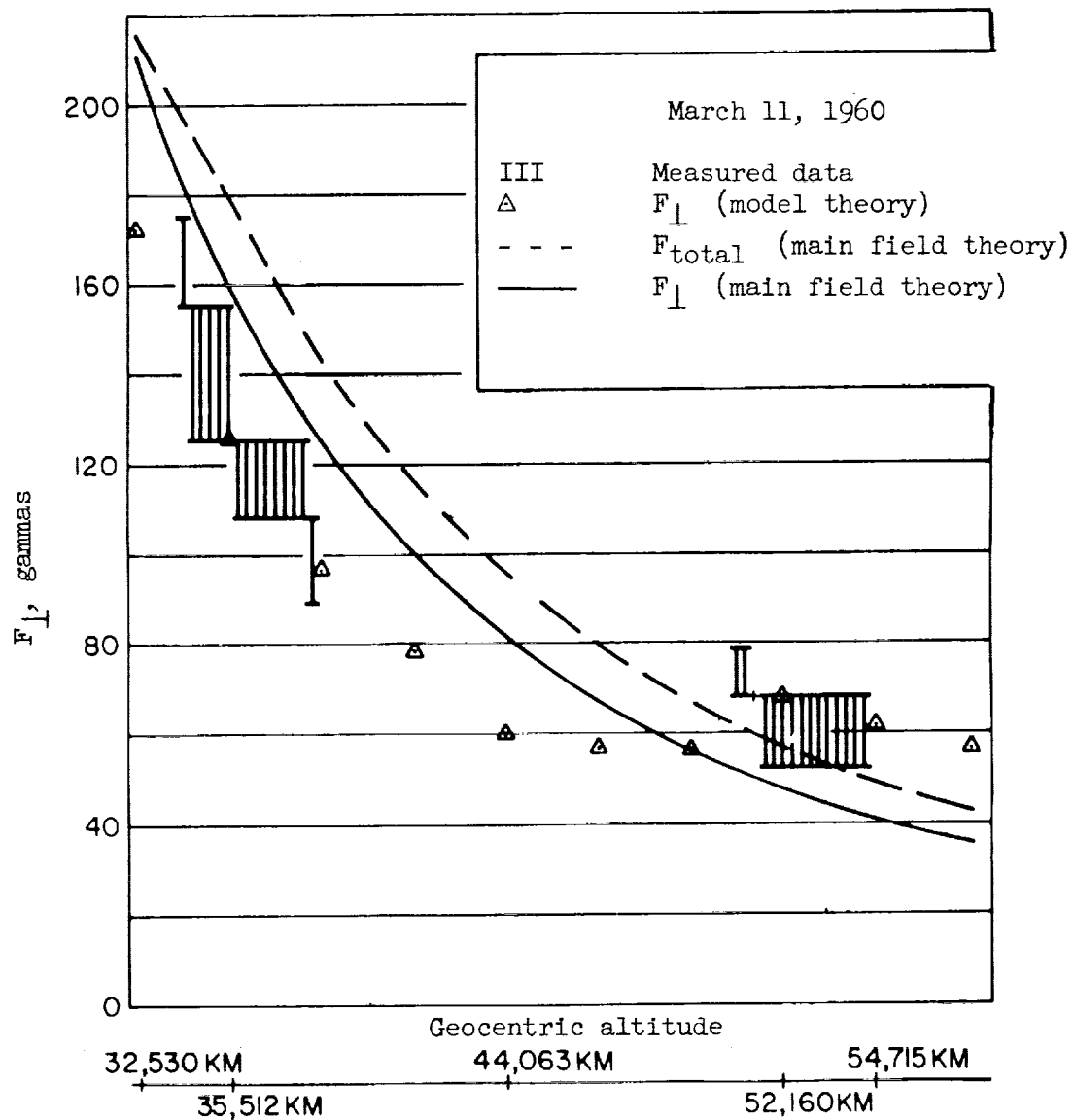


Figure 35.- Comparison between the results of the model calculation and Pioneer V data. (From ref. 44.)

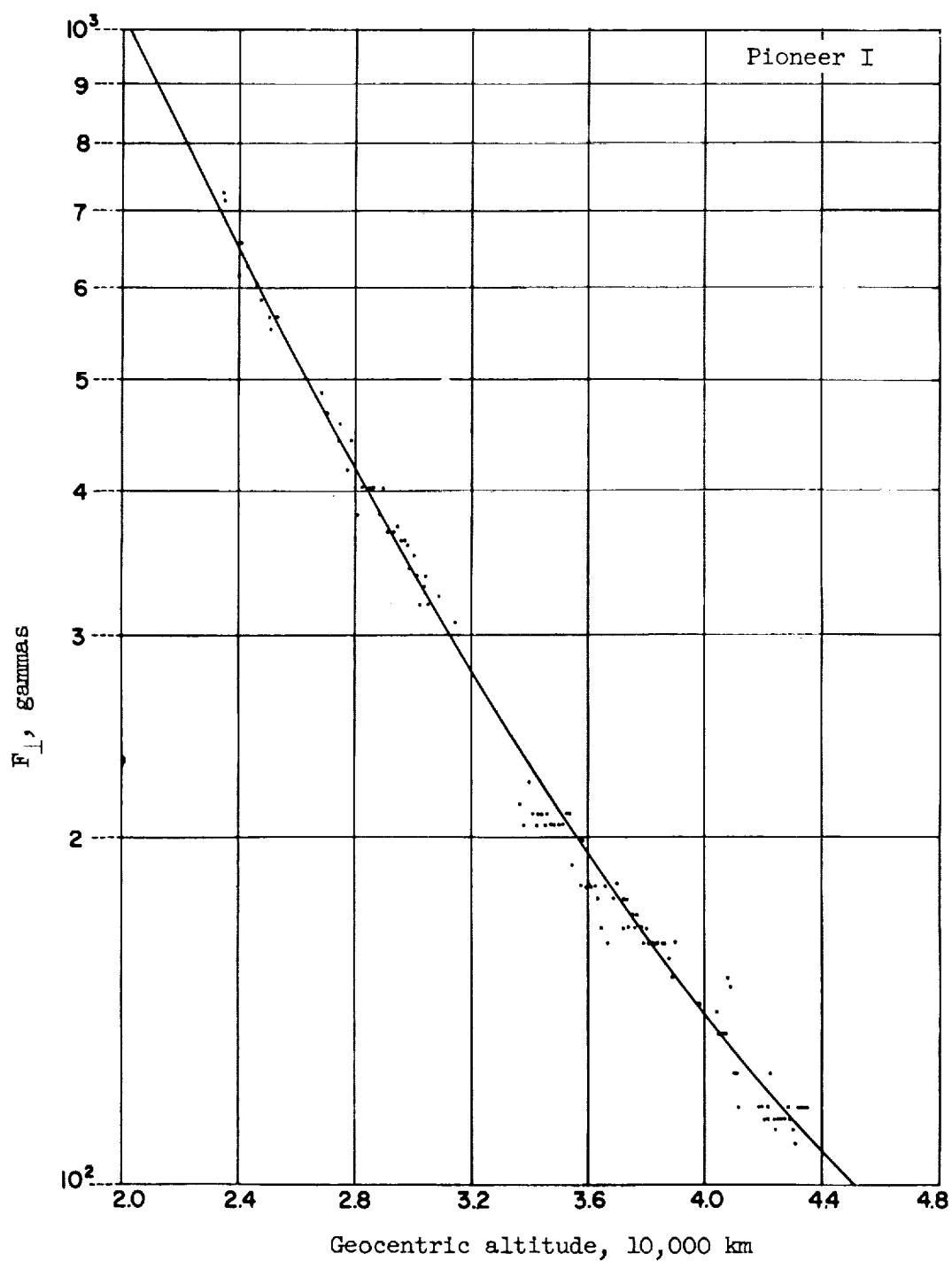


Figure 36.- Magnetic-field intensity in plane perpendicular to the spin axis  $F_{\perp}$  as a function of altitude. The solid curve is the theoretically expected value. (From ref. 47.)

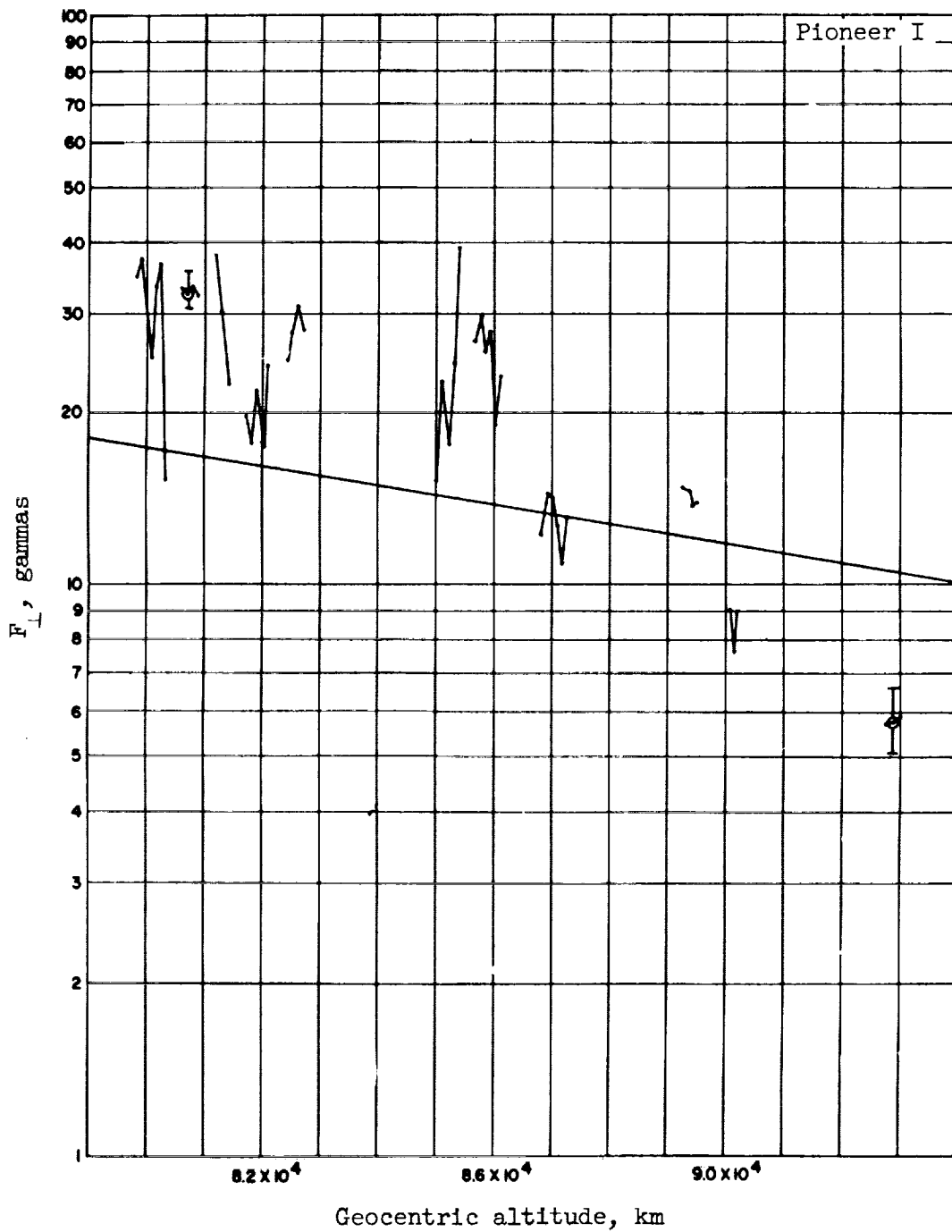
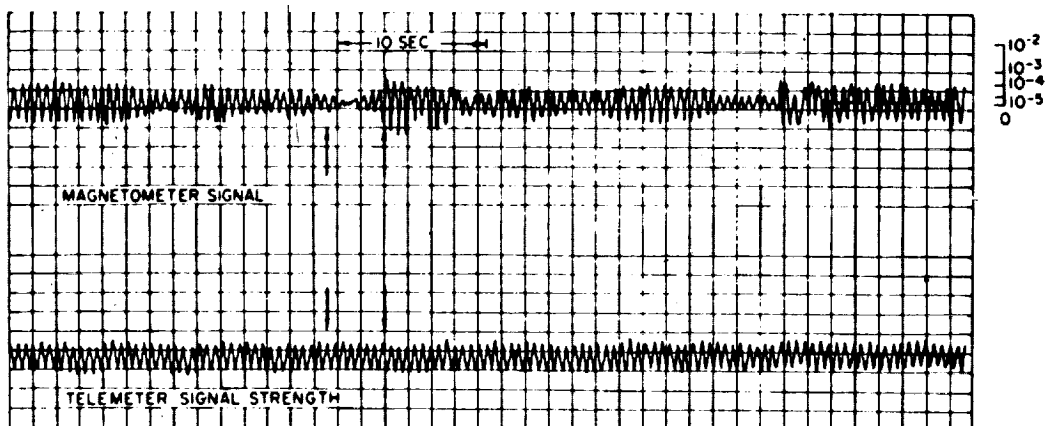
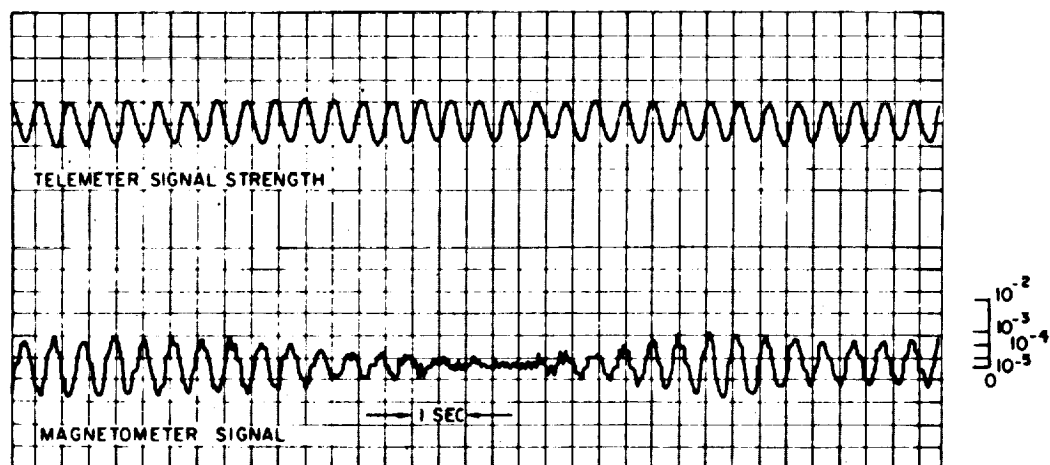


Figure 37.- Magnetic-field intensity in plane perpendicular to the spin axis  $F_{\perp}$  as a function of altitude. The solid curve is the theoretically expected value. (From ref. 47.)



(a) Signal at approximately 86,300 kilometers from the earth's surface.



(b) An expanded section (between arrows) of 38(a) showing clearly the phase change.

Figure 38.- Typical magnetometer and telemeter recording from Pioneer I. Magnetometer signal shows changes in oscillation, level, and phase. Phase change is seen by comparison with telemeter signal. (From ref. 49.)

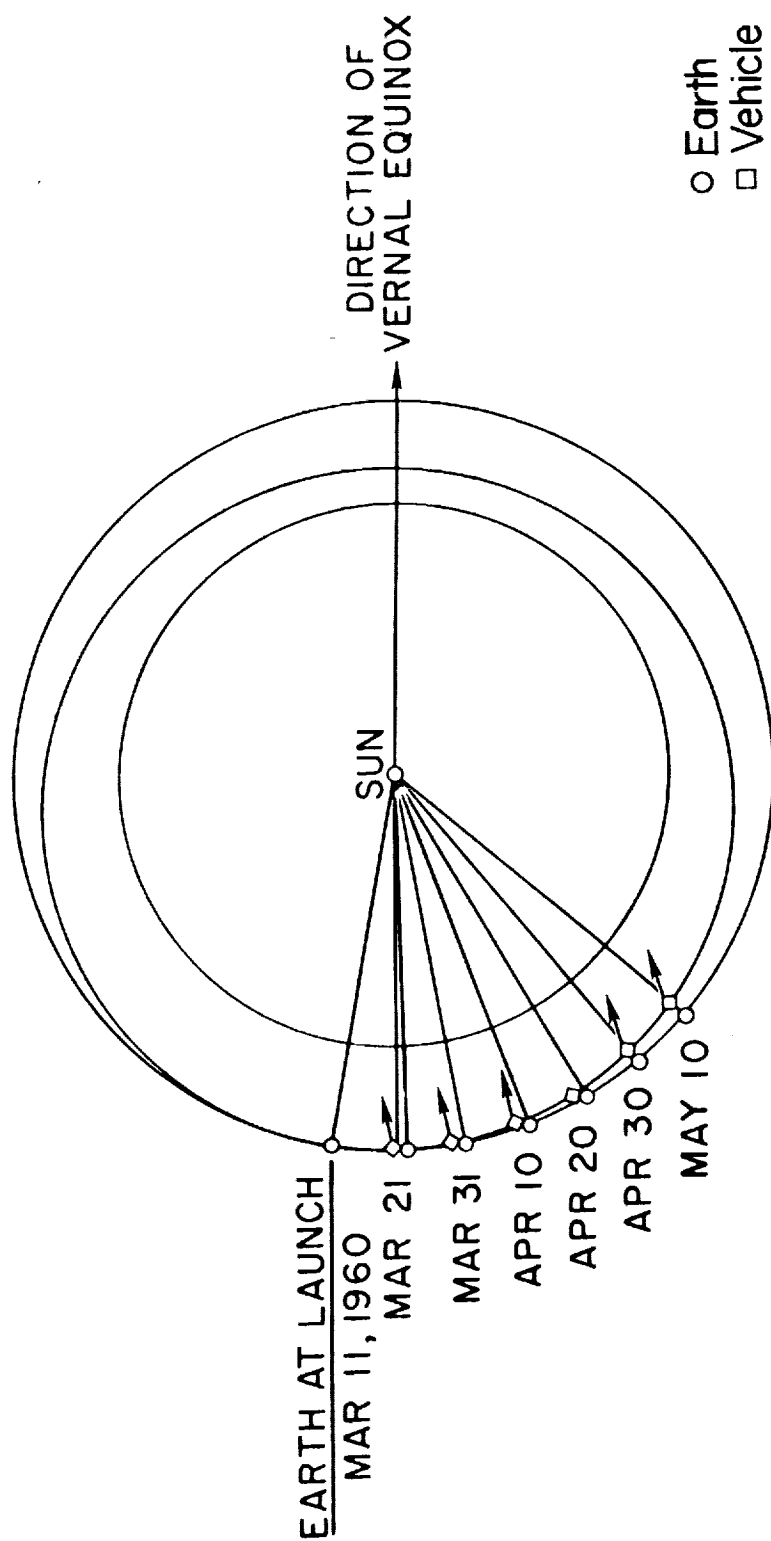


Figure 39.- Ecliptic plane view of Pioneer V orbit with positions shown at 10-day intervals. The arrows show the direction of vehicle spin axis when projected onto the ecliptic plane. (From ref. 53.)

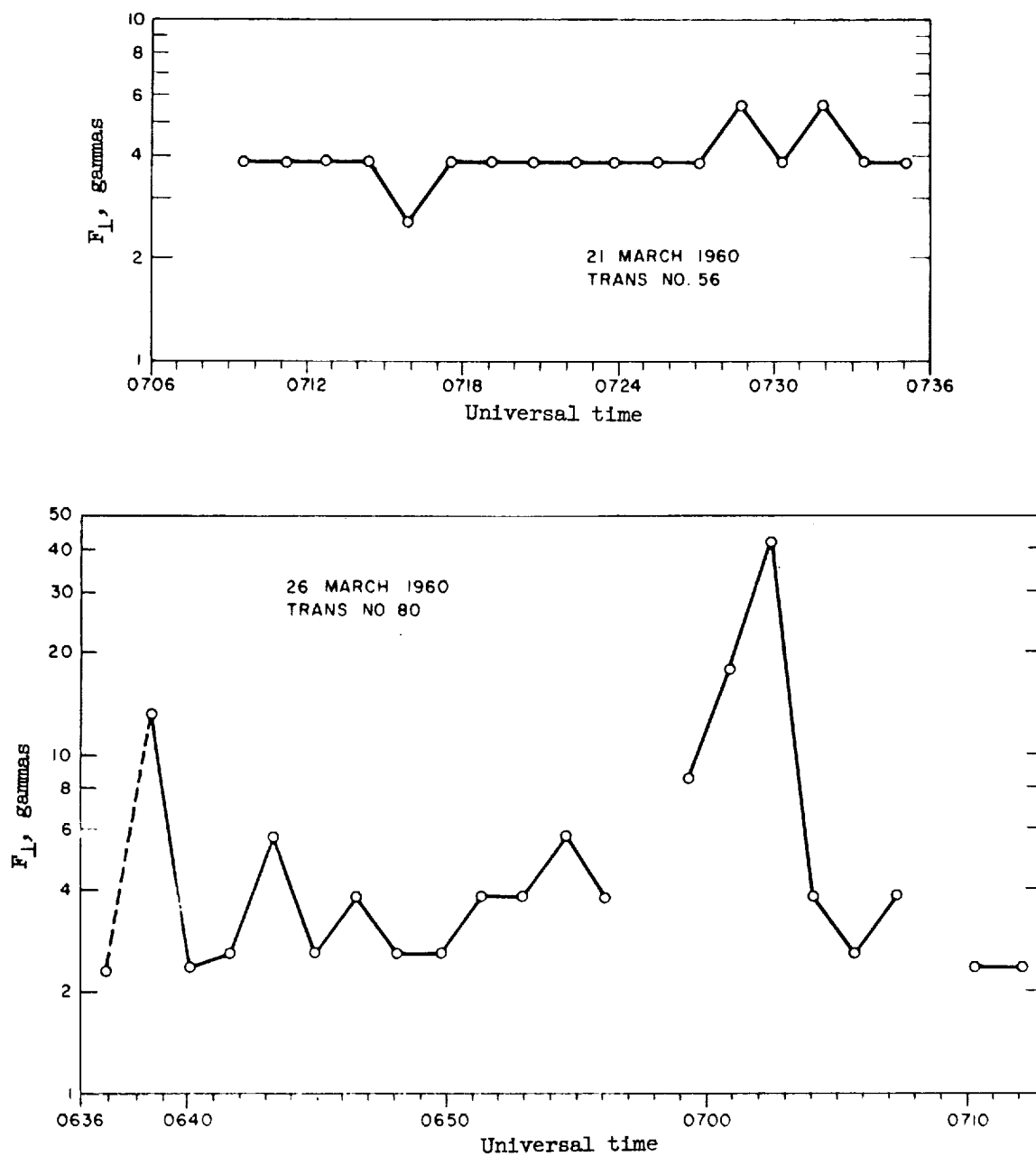


Figure 40.- Typical Pioneer V transmissions of magnetic-field data.  
(From ref. 53.)

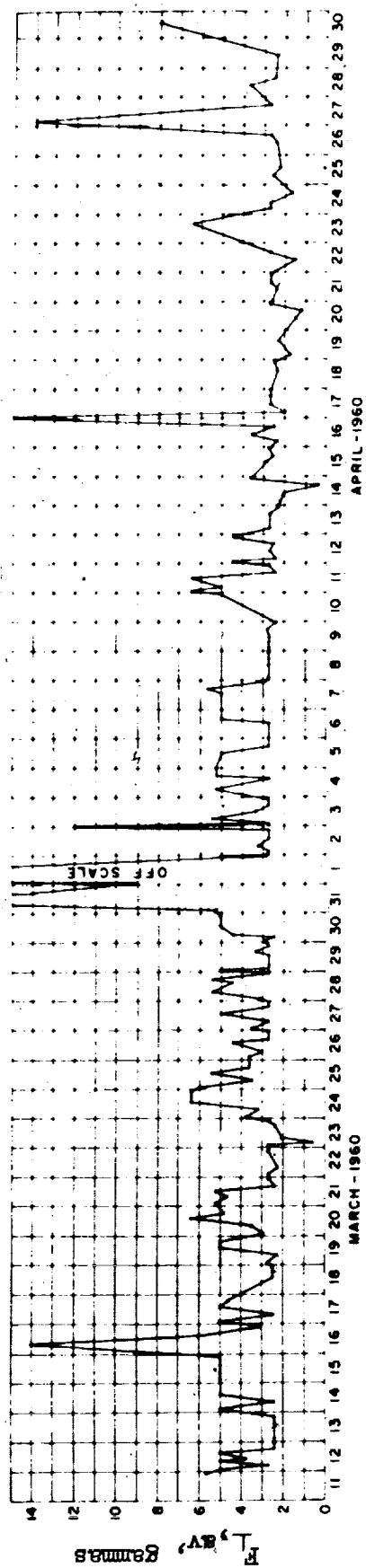


Figure 41.- Values of  $F_L$  averaged over each period of data transmission from Pioneer V as a function of time. The points indicate the times at which measurements were made. (From ref. 52.)

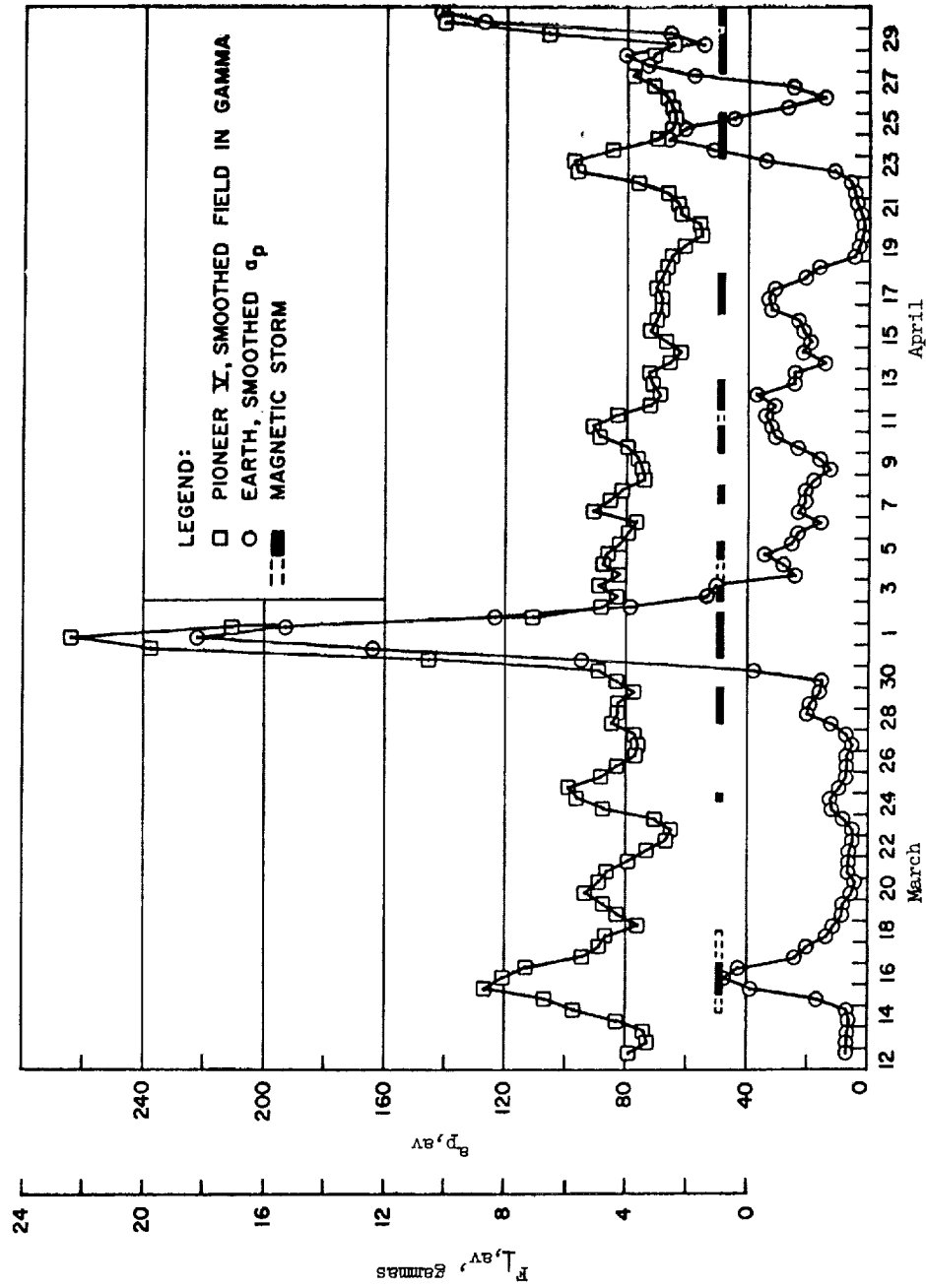


Figure 42.- Comparison of  $F_{L,av}$  from Pioneer V with the averaged 3-hour planetary equivalent amplitude  $a_{p,av}$ . Magnetic-storm occurrences are also shown. (From ref. 54.)

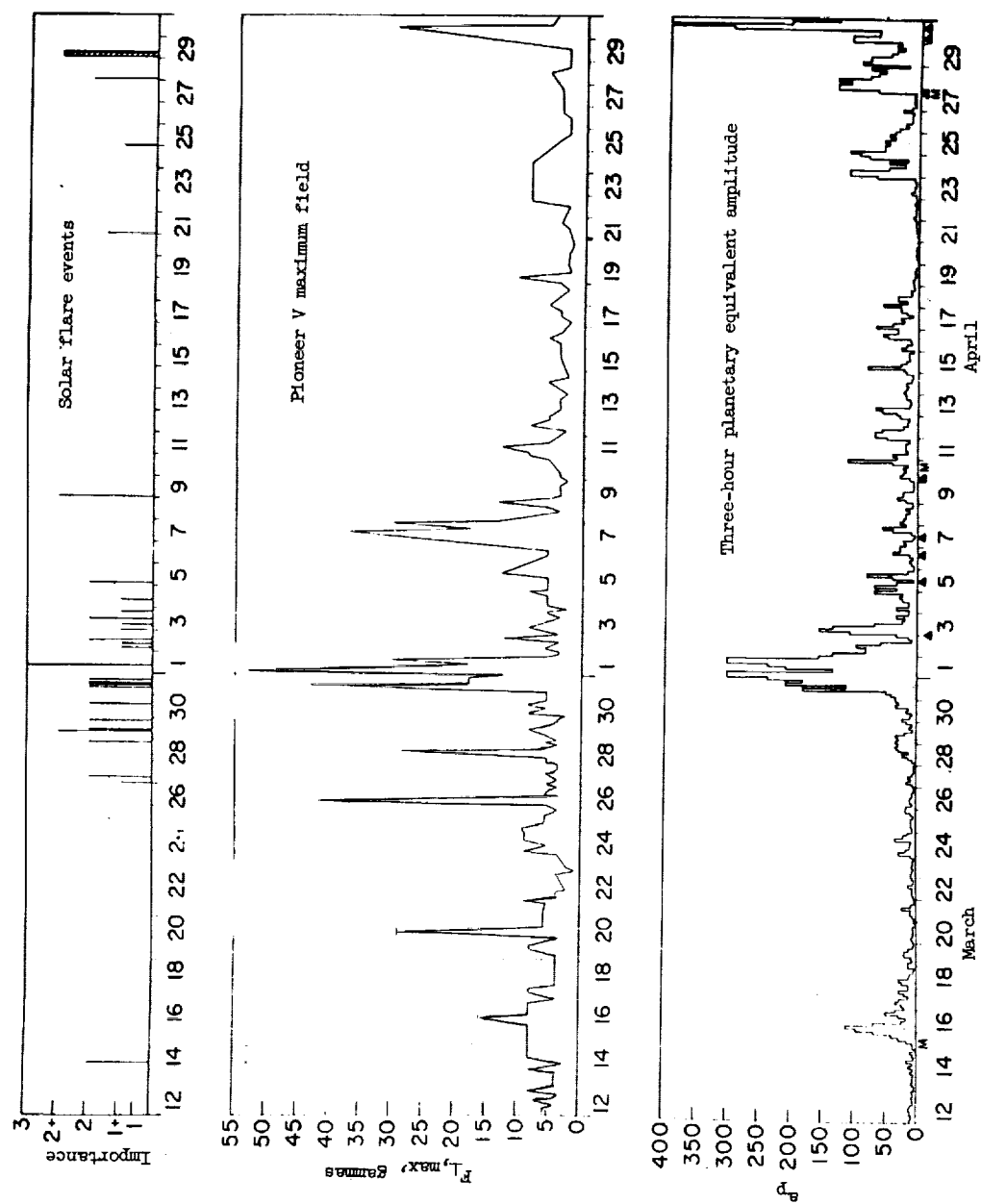


Figure 43.- Comparison of  $F_{1,\max}$  from Pioneer V with the three-hour planetary equivalent amplitude  $a_p$  and the occurrence of solar flares of importance 1+ or greater. (From ref. 53.)

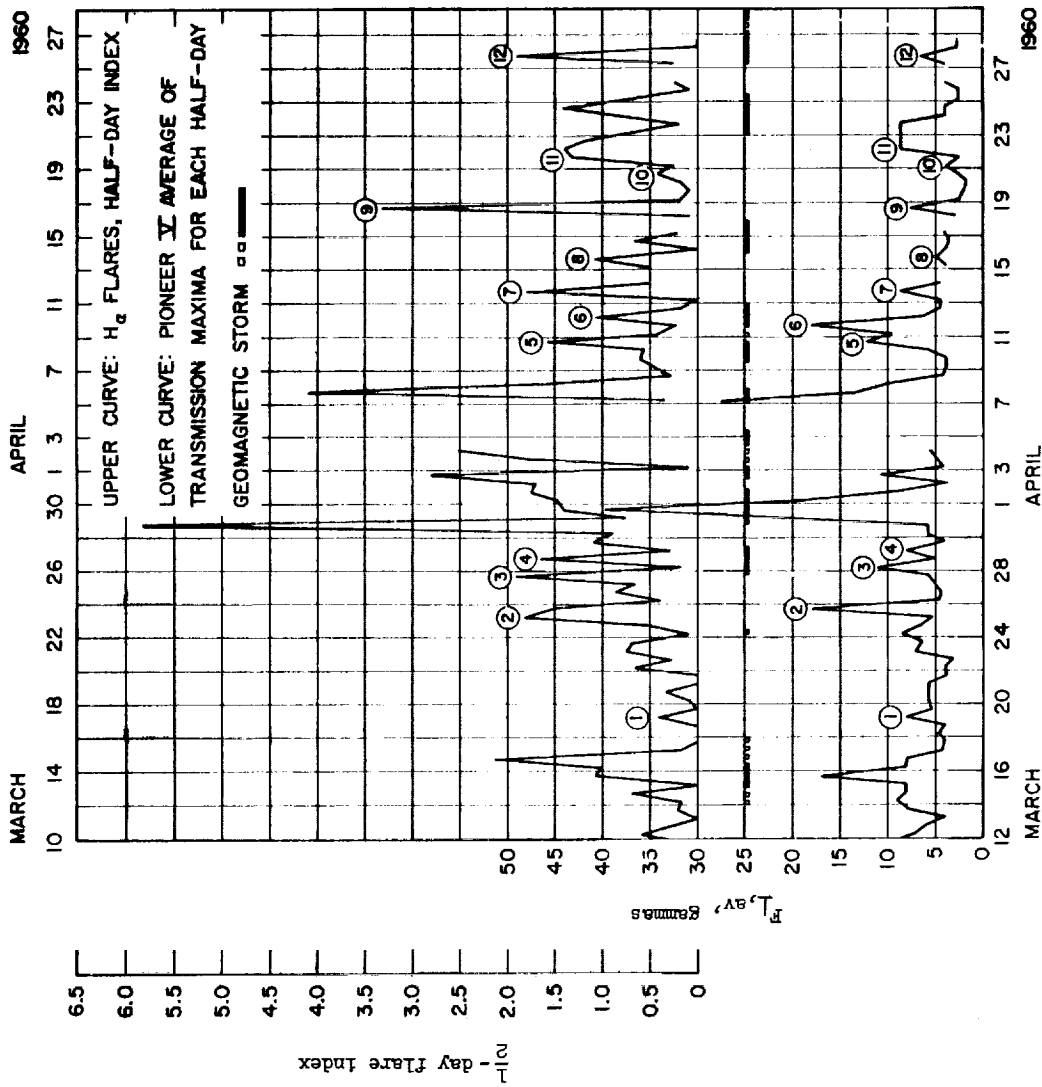


Figure 44.- Comparison of  $\frac{1}{2}$ -day flare index and Pioneer V  $\frac{1}{2}$ -day mean high field. Circled numbers indicate peaks selected as correlated maxima for individual flare identification. Horizontal bars are geomagnetic storms. Note the 2-day shift in solar time scale (top of graph). (From ref. 55.)



<p>NASA TN D-1019 National Aeronautics and Space Administration. GEOMAGNETIC- AND INTERPLANETARY - MAGNETIC-FIELD ENVIRONMENT OF AN EARTH SATELLITE. Edward W. Leyhe. July 1962. 145p. OTS price, \$2.75. (NASA TECHNICAL NOTE D-1019)</p> <p>A general description of the geomagnetic field, based on data accumulated on the earth's surface, is presented to acquaint the reader with the various phases of this subject. The description is then enlarged to include the discoveries of the recent rockets and satellites. Data that will be useful in the design, operation, and utilization of earth satellites and space probes are included.</p>	<p>I. Leyhe, Edward W. II. NASA TN D-1019</p> <p>(Initial NASA distribution: 7, Astrophysics; 21, Geophysics and geodesy; 30, Physics, atomic and molecular; 31, Physics, nuclear and particle; 33, Physics, theoretical.)</p>
<p>NASA TN D-1019 National Aeronautics and Space Administration. GEOMAGNETIC- AND INTERPLANETARY - MAGNETIC-FIELD ENVIRONMENT OF AN EARTH SATELLITE. Edward W. Leyhe. July 1962. 145p. OTS price, \$2.75. (NASA TECHNICAL NOTE D-1019)</p> <p>A general description of the geomagnetic field, based on data accumulated on the earth's surface, is presented to acquaint the reader with the various phases of this subject. The description is then enlarged to include the discoveries of the recent rockets and satellites. Data that will be useful in the design, operation, and utilization of earth satellites and space probes are included.</p>	<p>I. Leyhe, Edward W. II. NASA TN D-1019</p> <p>(Initial NASA distribution: 7, Astrophysics; 21, Geophysics and geodesy; 30, Physics, atomic and molecular; 31, Physics, nuclear and particle; 33, Physics, theoretical.)</p>
<p>NASA TN D-1019 National Aeronautics and Space Administration. GEOMAGNETIC- AND INTERPLANETARY - MAGNETIC-FIELD ENVIRONMENT OF AN EARTH SATELLITE. Edward W. Leyhe. July 1962. 145p. OTS price, \$2.75. (NASA TECHNICAL NOTE D-1019)</p> <p>A general description of the geomagnetic field, based on data accumulated on the earth's surface, is presented to acquaint the reader with the various phases of this subject. The description is then enlarged to include the discoveries of the recent rockets and satellites. Data that will be useful in the design, operation, and utilization of earth satellites and space probes are included.</p>	<p>I. Leyhe, Edward W. II. NASA TN D-1019</p> <p>(Initial NASA distribution: 7, Astrophysics; 21, Geophysics and geodesy; 30, Physics, atomic and molecular; 31, Physics, nuclear and particle; 33, Physics, theoretical.)</p>
<p>NASA TN D-1019 National Aeronautics and Space Administration. GEOMAGNETIC- AND INTERPLANETARY - MAGNETIC-FIELD ENVIRONMENT OF AN EARTH SATELLITE. Edward W. Leyhe. July 1962. 145p. OTS price, \$2.75. (NASA TECHNICAL NOTE D-1019)</p> <p>A general description of the geomagnetic field, based on data accumulated on the earth's surface, is presented to acquaint the reader with the various phases of this subject. The description is then enlarged to include the discoveries of the recent rockets and satellites. Data that will be useful in the design, operation, and utilization of earth satellites and space probes are included.</p>	<p>I. Leyhe, Edward W. II. NASA TN D-1019</p> <p>(Initial NASA distribution: 7, Astrophysics; 21, Geophysics and geodesy; 30, Physics, atomic and molecular; 31, Physics, nuclear and particle; 33, Physics, theoretical.)</p>

